

Aus der Klinik für Strahlentherapie und Radioonkologie  
Geschäftsführender Direktor: Prof. Dr. Sebastian Adeberg  
des Fachbereichs Medizin der Philipps-Universität Marburg

Titel der Dissertation:

**Development, manufacturing and validation of patient-specific 3D range-modulators for the very fast irradiation of moving tumours in particle therapy**

Inaugural-Dissertation zur Erlangung des Doktorgrades der Medizinwissenschaften

(Dr. rer. med.)

dem Fachbereich Medizin der Philipps-Universität Marburg

vorgelegt von

**Yuri Simeonov**

aus Pleven, Bulgarien

Marburg, 2024

Angenommen vom Fachbereich Medizin der Philipps-Universität Marburg am:  
18.03.2024

Gedruckt mit Genehmigung des Fachbereichs Medizin.

Dekanin: Frau Prof. Dr. Denise Hilfiker-Kleiner

Referenten: Frau Prof. Dr. Rita Engenhardt-Cabillic und Herr Prof. Dr. Klemens Zink

1. Korreferent: Herr Prof. Dr. Andreas Schrimpf

## **Main manuscripts published in Peer-Review Journals:**

The present cumulative dissertation contains a compilation of the research results which were published in peer review journals. The main topic was the development of 2D and 3D range-modulators for the purpose of reducing the irradiation time.

- 1. Simeonov Y, Weber U, Schuy C, Engenhardt-Cabillic R, Penchev P, Durante M and Zink K 2021 Monte Carlo simulations and dose measurements of 2D range-modulators for scanned particle therapy *Z. Med. Phys.* **31** 203–14**
- 2. Simeonov Y, Weber U, Schuy C, Engenhardt-Cabillic R, Penchev P, Flatten V and Zink K 2022 Development, Monte Carlo simulations and experimental evaluation of a 3D range-modulator for a complex target in scanned proton therapy *Biomed. Phys. Eng. Express* **8** 035006**
- 3. Holm K M, Weber U, Simeonov Y, Krauss A, Jäkel O and Greilich S 2020 2D range modulator for high-precision water calorimetry in scanned carbon-ion beams *Phys. Med. Biol.* **65** 215003**

The publications are referenced in the text according to the above order with the numbers 1-3. Publications are printed with permission.

## **Conference contributions:**

During the dissertation results were presented at different conferences. The following list shows a selection of these conference contributions:

- DEGRO 25, 2019, Münster, Germany, Poster
- DGMP 50, 2019, Stuttgart, Germany, Poster
- ESTRO 38, 2019, Milan, Italy, Poster
- GSI 1st Meeting of the International Biophysics Collaboration, 2019, Darmstadt, Germany, Oral presentation
- PTCOG 58, 2019, Manchester, United Kingdom, Oral presentation
- AAPM, 2020, Vancouver, Canada, Poster
- DEGRO 27, 2021, online, Poster
- DGMP, 2021, online, Oral presentation
- FRPT, 2021, online, Oral presentation
- Varian Engineering Colloquium 2022, Troisdorf, Germany, Oral presentation as invited speaker
- PTCOG 61, 2023, Madrid, Spain, Poster

## SUMMARY

Particle therapy has established clinically in the last decades as it can deliver dose to the target in a highly precise and conformal manner and has been shown to be especially beneficial and effective for certain types of cancer.

Its application for moving targets, however, is challenging due to the relatively long irradiation time and the resulting “interplay” effects between the scanned beam and the target motion, which lead to dose deterioration. In addition, ultra-high dose rate FLASH irradiation, which is expected to enhance the therapeutic window, cannot be achieved with the conventional active raster scanning method due to the switching time between the single iso-energy layers.

This dissertation presents the concept of static range-modulating devices manufactured by rapid prototyping for the very fast dose application with only one fixed energy and a scanned particle beam. The development of 2D range-modulators (RM) is shown and their application is validated in a research project for high-precision water calorimetry. The concept is extended to a 3D range-modulator (3D RM), optimized and customized to a patient-specific target shape.

The modulators are manufactured with high-quality 3D printers, different materials and printing techniques. The resulting dose distribution is first validated by simulations and then by fast, completely automated and high resolution measurements using a water phantom system.

Overall, an end-to-end process chain is demonstrated, from the RM development to the final dose evaluation. Highly homogeneous dose distributions are achieved with a very good agreement between the predicted and measured data. In the case of the 3D RM, the delivered dose is additionally conformed to both the proximal and distal edge of the target. Most importantly, the modulators manage to deliver the prescribed dose in a fraction of the time required for conventional scanned particle therapy.

The presented work demonstrates the feasibility of using 3D-printed 3D range-modulators in particle therapy. The 3D RM concept combines extremely short irradiation times with a high degree of dose conformity and homogeneity, promising clinically applicable dose distributions for lung and/or FLASH treatment, potentially comparable and competitive to those from conventional irradiation techniques.

## ZUSAMMENFASSUNG

Die Partikeltherapie hat sich in den letzten Jahrzehnten klinisch etabliert, da sie die Dosis hochpräzise und konform im Ziel applizieren kann und sich für bestimmte Krebsarten als besonders wirksam erwiesen hat. Bewegte Tumoren stellen allerdings aufgrund der relativ langen Bestrahlungszeiten eine Herausforderung dar, weil „Interplay“ Effekte zwischen dem gescannten Strahl und der Tumorbewegung zu starken Dosisinhomogenitäten führen können. Außerdem ist die Anwendung des üblichen Multi-Energy Rasterscanning-Verfahren für FLASH-Bestrahlung aufgrund der Umschaltzeiten zwischen den einzelnen Energieschichten nicht möglich.

In dieser Dissertation wird das Konzept statischer, durch Rapid Prototyping hergestellter Reichweitenmodulatoren, vorgestellt. In Kombination mit einer einzigen Energie und einem gescannten Feld können solche Modulatoren die Bestrahlungszeit deutlich senken. Es wird die Entwicklung von 2D Modulatoren gezeigt und ihre Anwendung in einem Forschungsprojekt für hochpräzise Wasserkalorimetrie validiert. Zudem wird das Konzept auf einen 3D-Reichweitenmodulator ausgeweitet, der für eine patientenspezifische Tumorform optimiert und angepasst ist.

Die Modulatoren werden mit hochqualitativen 3D-Druckern, verschiedenen Materialien und Druckverfahren hergestellt. Die resultierende Dosisverteilung wird zunächst durch Simulationen und dann durch schnelle, automatisierte und hochaufgelöste Messungen mit einem Wasserphantom validiert.

Insgesamt wird eine komplette Prozesskette demonstriert, von der Modulatorentwicklung bis zur abschließenden Dosisauswertung. Die simulierten und gemessenen Dosisverteilungen stimmen sehr gut überein und weisen hohe Homogenität auf. Im Falle des 3D RM wird die applizierte Dosis zusätzlich sowohl an die proximale als auch an die distale Kante des Tumors angepasst. Vor allem aber gelingt es, mit den Modulatoren die verschriebene Dosis in einem Bruchteil der Zeit zu applizieren, die für das konventionelle Rasterscan Verfahren benötigt wird.

Die vorgestellte Arbeit demonstriert die mögliche Verwendung von 3D-gedruckten 3D Modulatoren in der Partikeltherapie. Das 3D RM Konzept kombiniert extrem kurze Bestrahlungszeiten mit hoher Dosiskonformität und -homogenität und verspricht aber gleichzeitig klinische Dosisverteilungen für die Lungen- und/oder FLASH-Behandlung, die mit denen konventioneller Bestrahlungstechniken vergleichbar und konkurrenzfähig sind.

# Contents

Summary.....	III
Zusammenfassung .....	IV
List of Figures.....	VII
Abbreviations .....	X
1. Introduction .....	1
1.1. Cancer therapy.....	1
1.2. Interaction of charged particles with Matter.....	2
1.3. Proton therapy and beam delivery .....	4
1.3.1. Passive Scattering .....	4
1.3.2. Pencil beam scanning .....	6
1.3.3. The moving target challenge .....	7
1.3.4. Hybrid beam delivery: 3D range-modulator .....	8
1.3.5. FLASH therapy .....	11
1.4. The Monte Carlo code FLUKA.....	12
2. Aim and motivation.....	14
3. Summary of the published results .....	16
3.1. Publication 1 .....	16
3.1.1. Summary of publication 1 .....	16
3.1.2. Contribution.....	21
3.2. Publication 2 .....	22
3.2.1. Summary of publication 2 .....	22
3.2.2. Contribution.....	30
3.3. Publication 3 .....	31
3.3.1. Summary of publication 3 .....	31
3.3.2. Contribution.....	37
4. Discussion.....	38

5. Conclusion and outlook .....	44
6. References .....	47
7. Published Articles.....	53
Appendix .....	95
Verzeichnis der akademischen Lehrenden .....	95
Danksagung .....	96



## LIST OF FIGURES

Figure 1. Depth dose curves of monoenergetic photons, protons and carbon ( $^{12}\text{C}$ ) ions. Photons have an exponential dose decrease with maximum at shallow depths in the order of several cm. Particles, on the other hand, show an inverted dose profile with finite range and sharply defined dose maximum.....	3
Figure 2. Schematic representation of the passive scattering (a) and pencil beam scanning (b) methods for the irradiation of tumors in particle therapy. Image from (Ishikawa <i>et al</i> 2019) .....	5
Figure 3. An exemplary 5 cm SOBP in water for a 151 MeV proton beam. ....	6
Figure 4. A single pyramid-shaped pin optimized for a 5 cm SOBP in water for 150.68 MeV/u monoenergetic proton beam (a). Frontal view of the middle slice from a 3D range modulator for a spherical target with a diameter of 5 cm. The pins have different heights to laterally modulate and conform the dose to the proximal target edge.....	8
Figure 5. Example of a beam-modulating pyramid-like object with only 4 weights, corresponding to 4 different material thicknesses and partial areas (a). A pin form with $\Delta z \approx 3\text{mm}$ and larger, visible steps (b) and a pin form with $\Delta z < 0.5\text{mm}$ (c).....	9
Figure 6. Principle of depth modulation by a 3D range-modulator with both distal and proximal conformity for a spherical target. Monte Carlo simulated X-Z midplane profile (a) and center line depth dose distribution (b). $^{12}\text{C}$ , $E = 400.41\text{ MeV/u}$ . Figure taken from (Simeonov <i>et al</i> 2017) – Figure 4. ....	10
Figure 7. Comparison between the original and improved pin profile. The main difference is in the pin base (groove) and the pin tip (a). A single pyramid-shaped pin optimized for a 5 cm SOBP in water for 150.68 MeV/u monoenergetic proton beam (b). Figure taken from (Simeonov <i>et al</i> 2021) – Figure 2.....	16
Figure 8. The manufactured <b>polymer RM</b> (a) and the <b>steel RM</b> (b) with a protection wall around and positioning bars. Figure taken from (Simeonov <i>et al</i> 2021) – Figure 4. ....	17
Figure 9. Schematic drawing of the dose measurement setup. Panel (a) shows the 2D polymer RM, which was positioned 40 cm in front of the isocenter and irradiated with an undeflected beam. The dose was measured with the PTW Peakfinder. Panel (b) shows the 2D steel RM, which was positioned 30 cm in front of the isocenter and irradiated with a scanned $3.2\text{ cm}^2$ rectangular field. The dose was measured with the newly developed WERNER system using the PTW Octavius 1000P. All measurements were conducted with a 150.68 MeV/u proton beam. Figure taken from (Simeonov <i>et al</i> 2021) – Figure 7. ....	18
Figure 10. <b>Polymer RM:</b> A comparison between the measured and simulated SOBP. Both depth dose distributions are normalized to one in the middle of the SOBP. Figure taken from (Simeonov <i>et al</i> 2021) – Figure 8. ....	19
Figure 11. <b>Steel RM:</b> Centre line SOBP (a), isodose lines comparison of a X-Z midplane profile (b) and the corresponding local gamma index for 2%/2 mm acceptance criteria (c). Three lateral X profiles (d)–(f), plotted at 6 cm, 10 cm and 14 cm respectively. The vertical red lines in (a) denote the depths, at which the X profiles were plotted. Figure taken from (Simeonov <i>et al</i> 2021) – Figure 10.....	20

Figure 12. One slice of the patient CT with the original (inner blue contour) and a 4 mm extended PTV, used for the development of the modulator (outer red contour). Figure taken from (Simeonov <i>et al</i> 2022) – Figure 1. ....	22
Figure 13. 3D view of the lung target (a), a single 50 mm pin (b), a 3D view of the optimized modulator (c) and the corresponding manufactured prototype (d). The prototype has positioning bars defining the isocenter, used for alignment with the in-room lasers and side walls for better stability and usability. Figure taken from (Simeonov <i>et al</i> 2022) – Figure 2. ....	23
Figure 14. Number of particles in each scan spot before (a) and after the optimization (b) expressed as a scaling factor. Additionally, the scan path is plotted with a solid line and the isocenter is denoted with a red cross mark. Figure taken from (Simeonov <i>et al</i> 2022) – Figure 3. ....	24
Figure 15. The aluminum 3D RM with a side wall and positioning bars. Figure taken from (Simeonov <i>et al</i> 2022) – Figure 5. ....	25
Figure 16. A schematic drawing of the dose measurement setup (a) and a picture of the measurement session (b). The 3D range-modulator was positioned 25 cm in front of the water phantom. The dose was measured with the PTW Octavius 1000P. Figure taken from (Simeonov <i>et al</i> 2022) – Figure 6. ....	25
Figure 17. Isodose lines of the measured (solid line) and simulated (dashed line) dose distribution (a)-(b). The corresponding 1D profiles in panel (c) and (d) were plotted at 15 cm depth, denoted as a vertical dotted line in the panel above. Additionally, the measured (thick lines) and simulated (thin lines) dose is overlaid on top of the raw CT data (e). The blue line denotes the PTV contour. <b>Note:</b> The modulator was developed on the basis of the homogeneous “water” CT, not the heterogeneous one shown here. Figure taken from (Simeonov <i>et al</i> 2022) – Figure 7. ....	26
Figure 18. A lateral X profile (a) and three depth dose distributions (b)-(d). Additionally, 2D isodose line figures are included to denote the exact position, at which the 1D profiles were plotted. Figure taken from (Simeonov <i>et al</i> 2022) – Figure 8. ....	27
Figure 19. The dose distributions (simulated dose in the upper panel, measured dose in the middle panel) and the resulting GI (lower panel) for one transversal (a) and one sagittal (b) slice. 99 % of the evaluated voxels were found to pass the dose and distance agreement criteria. Figure taken from (Simeonov <i>et al</i> 2022) – Figure 9. ....	28
Figure 20. DVH calculated inside the PTV target for both the measured and simulated dose and the resulting statistical information. Figure taken from (Simeonov <i>et al</i> 2022) – Figure 10. ....	29
Figure 21. A center line depth dose distribution (a); Comparison between the isodose lines of the measured (solid line) and simulated (dashed line) dose distribution (b). Results are from the <b>aluminum</b> modulator. Figure taken from (Simeonov <i>et al</i> 2022) – Figure 11. ....	29
Figure 22. Oblique view of the 2D RM with 3x3 mm <sup>2</sup> pin base area and detailed view of 4x4 pins. ....	32
Figure 23. Comparison of the depth dose distributions of 2D RMs with different pin base areas. Measured with the Peakfinder. Figure taken from (Holm <i>et al</i> 2020) – Figure 5. ....	33

Figure 24. SOBP sensitivity on the tilting ( $0.5^\circ$ ,  $1^\circ$  and  $2^\circ$ ) of the 2D RM as a function of its pin base ( $2 \times 2 \text{ mm}^2$ ,  $3 \times 3 \text{ mm}^2$ ,  $4 \times 4 \text{ mm}^2$ ). Figure taken from (Holm *et al* 2020) – Figure 6..... 34

Figure 25. EBT3 film measurements of the lateral dose distributions in front of the calorimeter (top), at a 5 cm depth in water inside the calorimeter (middle) and at a 10 cm depth in water (bottom), which corresponds to the middle of the SOBP and the calorimetric measurement position. Measurements were performed with the  $3 \times 3 \text{ mm}^2$  (left) and the  $4 \times 4 \text{ mm}^2$  (right) pin base area 2DRM in the beam path. Standard deviations were calculated inside the inner red square, indicated in the lower right picture. Figure taken from (Holm *et al* 2020) – Figure 7..... 35

Figure 26. Results of the field characterization measurements using the Octavius water phantom setup: Comparison of the depth dose distribution measured with the Octavius and the Peakfinder (left). Lateral dose distributions for different depths across the x- (middle) and the y-axes (right). The results shown are for measurements performed with the original  $3 \times 3 \text{ mm}^2$  pin base area 2D RM. Figure taken from (Holm *et al* 2020) – Figure 8..... 36

## ABBREVIATIONS

<b>CAD</b>	Computer Aided Design
<b>CT</b>	Computed Tomography
<b>DICOM</b>	Digital Imaging and Communications in Medicine
<b>DKFZ</b>	Deutsches Krebsforschungszentrum
<b>DVH</b>	Dose-Volume Histogram
<b>ESS</b>	Energy Selection System
<b>FLUKA</b>	FLUktuierende Kaskade
<b>GI</b>	Gamma Index
<b>GSI</b>	GSI Helmholtzzentrum für Schwerionenforschung Darmstadt
<b>IEC</b>	International Electrotechnical Commission
<b>IMPT</b>	Intensity modulated proton therapy
<b>MC</b>	Monte Carlo
<b>MIT</b>	Marburg Ion-Beam Therapy Center
<b>MU</b>	Monitor Unit
<b>PB</b>	Pencil Beam
<b>PBS</b>	Pencil Beam Scanning
<b>PTB</b>	Physikalisch-Technische Bundesanstalt
<b>QA</b>	Quality Assurance
<b>RM</b>	Range-Modulator
<b>SLM</b>	Selective Laser Melting
<b>SOBP</b>	Spread-Out Bragg Peak
<b>SS</b>	Scan Spot
<b>TPS</b>	Treatment Planning System
<b>WERNER</b>	WatER column for 2D ionization chamber array detectors
<b>WET</b>	Water Equivalent Thickness
<b>WHO</b>	World Health Organization

# 1. INTRODUCTION

## 1.1. Cancer therapy

Cancer is a major health problem causing millions of deaths each year. The World Health Organization (WHO) estimates that cancer was responsible for roughly 10 million deaths in 2020, making it the second leading cause of death worldwide. Breast, lung and prostate are the most prevalent types of cancer, with lung cancer being the leading cause of cancer death (Sung *et al* 2021).

The primary treatment options are surgery, chemotherapy, radiotherapy or a combination of them (Baskar *et al* 2012). Radiotherapy is especially important in cases where surgery is not possible. It uses ionizing radiation to kill cancer cells by damaging their DNA and preventing them from dividing and growing. Conventional external radiotherapy makes use of high-energy photons to deliver a lethal dose to the tumour. Healthy tissue surrounding the target is also irradiated, which can cause severe side effects and limits the maximum dose, which can be administered. Therefore, maximising the dose in the tumour, while sparing the surrounding normal tissues, especially critical organs such as the heart, spinal cord, etc., is one of the main challenges towards an effective and safe treatment.

Although conventional radiation therapy with high-energy X-rays has long established for the treatment of cancer, photons exhibit some unfavourable physical properties. First of all, photons deposit the maximum energy in the first few centimetres near the surface of the body and not at the optimal depth for the specific tumour. Moreover, their range is not finite and therefore unnecessary low dose is accumulated in the healthy tissue behind the distal edge of the target (Linz 2012).

Particle therapy with protons and heavier ions (e.g. carbon and helium ions), on the other hand, takes advantage of the more favourable physical properties of heavy charged particles, which deposit most of their energy at a specific depth in the tissue (the so-called Bragg peak) before coming to a complete stop (Durante *et al* 2017, Schlegel *et al* 2018). These characteristics enable the delivery of higher dose to the target in a highly precise and conformal manner for a potentially better tumour control rate and overall outcome for patients.

Proton therapy has established clinically in the last decades and has been shown to be especially beneficial and effective for certain types of cancer, such as brain tumours and pediatric cancer.

Carbon ions have higher biological effectiveness than protons or photons and the damage to cancer cells per unit dose of radiation is higher, which is especially relevant in the case of more aggressive or resistant tumours (Kraft 2000, Weber and Kraft 2009).

This work focuses mainly on simulations and irradiation with protons, however, the fundamental principle is the same for carbon ions.

## 1.2. Interaction of charged particles with Matter

When a charged particle penetrates an absorber, its Coulomb electric field interacts with the orbital electrons and the nuclei of atoms along its path (Podgorsak 2016). As the energy transfer in each of these interactions is generally small the particle undergoes a large number of interactions before its kinetic energy is completely absorbed (Andreo *et al* 2017). The loss of energy due to interactions with the shell electrons is defined as collision energy loss, whereas interactions with the absorber's nuclei cause radiation loss. Collision energy loss is the dominant process for heavy charged particles at high energies in the therapeutic range, radiation energy loss plays virtually no role (Paganetti 2012). The collision energy loss per unit path length is defined as the linear collision stopping power  $S$  or mass collision stopping power  $S/\rho$  and described by the Bethe-Bloch equation:

$$\frac{S_{col}}{\rho} = 4\pi N_A \frac{Z}{A} \left( \frac{e^2}{4\pi\epsilon_0} \right)^2 \frac{z^2}{m_e v_0^2} \left\{ \ln \frac{2m_e c^2}{I} + \ln \beta^2 - \ln (1 - \beta^2) - \beta^2 \right\} \quad (1)$$

where  $N_A$  is the Avogadro constant,  $Z$  and  $A$  are the nuclear charge and mass number of the target material,  $z$  is the charge of the projectile,  $e$  is the elementary charge,  $m_e$  is the mass of the electron,  $\beta = v/c$  is the ratio of particle velocity to the speed of light and  $I$  is the mean ionization potential.

The mass collision stopping power is inversely proportional to the square velocity of the heavy charged particle  $v_0$ . Therefore, and in contrary to photons, whose depth dose distribution decreases exponentially as they pass through matter, charged particles have the advantage that their energy loss increases with decreasing kinetic energy (Figure 1).

The energy loss increase results in the characteristic inverse depth dose profile with maximum energy deposition, Bragg peak (BP), at the end of the range. The sharp, narrow BP can be positioned precisely in the tumour. However, it is not clinically applicable because the dose distribution is not homogeneous over the entire target volume. Therefore, the beam must be scattered both transversely and longitudinally, which can be achieved by passive scattering or active raster scanning.

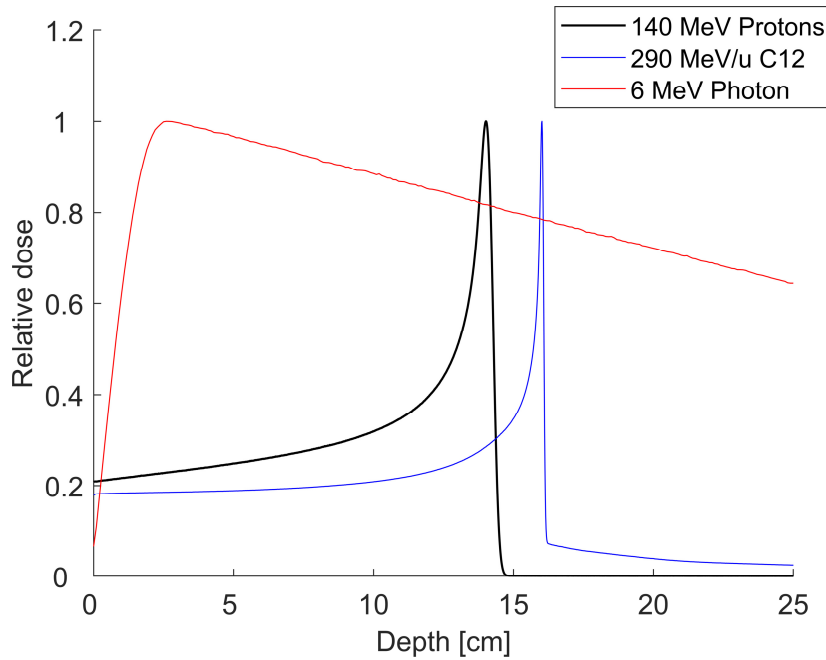


Figure 1. Depth dose curves of monoenergetic photons, protons and carbon ( $^{12}\text{C}$ ) ions. Photons have an exponential dose decrease with maximum at shallow depths in the order of several cm. Particles, on the other hand, show an inverted dose profile with finite range and sharply defined dose maximum.

An additional process that must be considered for heavy particles such as  $^{12}\text{C}$  ions is fragmentation. In this process, a primary particle collides with a target nucleus and a projectile fragment with a low nuclear charge number is formed, which then continues to travel at almost the same speed and direction. These projectile fragments have a smaller energy loss and therefore a longer range, which leads to additional dose contribution (fragmentation tail) behind the BP maximum. Due to fragmentation, the beam composition changes with increasing depth, the number of primary ions decreases and the number of fragments increases.

When traveling through matter, charged particles are scattered laterally in addition to the energy loss they suffer. This mainly occurs due to elastic Coulomb collisions with the target nuclei, but also due to the fragmentation processes mentioned above. The angular deflection from a single scattering event is very small. Therefore, the observed

broadening of a narrow beam with increasing depth in the absorber material is the result of many individual scattering events. The resulting angular distribution is approximately Gaussian.

Molière developed a comprehensive model for describing multiple Coulomb scattering (Molière 1948). The resulting angular distributions agree very well with experimental measurements (Gottschalk *et al* 1993). Highland parameterized the theory developed by Molière for the case of small deflection angles (Highland 1975). Accordingly, the width  $\theta_0$  of a Gaussian angular distribution is calculated as follows:

$$\theta_0 = \frac{14.1 \text{ MeV}}{pv} Z_P \sqrt{\frac{L}{L_R}} \left[ 1 + \frac{1}{9} \log_{10} \left( \frac{L}{L_R} \right) \right] \quad (2)$$

where  $p$  is the momentum,  $v$  the velocity,  $Z_P$  is the atomic number of the projectile,  $L$  is the thickness of the target and the radiation length  $L_R$  is a material-specific constant that can be taken from the literature (Tsai 1974). The Highland parametrization formula is fast and convenient. However, in cases, where a detailed and very accurate particle transport description is needed, e.g. Monte Carlo simulations (see Chapter 1.4. ), more sophisticated models are utilized. For example, in the particle transport code FLUKA an improved multiple scattering model, based on Molière theory, has been developed and implemented (Ferrari *et al* 1992).

### 1.3. Proton therapy and beam delivery

#### 1.3.1. Passive Scattering

Passive beam application was the first method developed and is still used (Figure 2a). To cover the entire target volume homogeneously the beam must be scattered laterally. This is achieved either by a single or in most cases by a double scattering system. Additional patient-specific hardware is necessary to adjust the dose individually for each patient. For example, a bolus compensates for the tissue inhomogeneities and the curvature of the patient surface and is designed in such a way that the modulated Bragg peak matches the distal edge of the target volume.



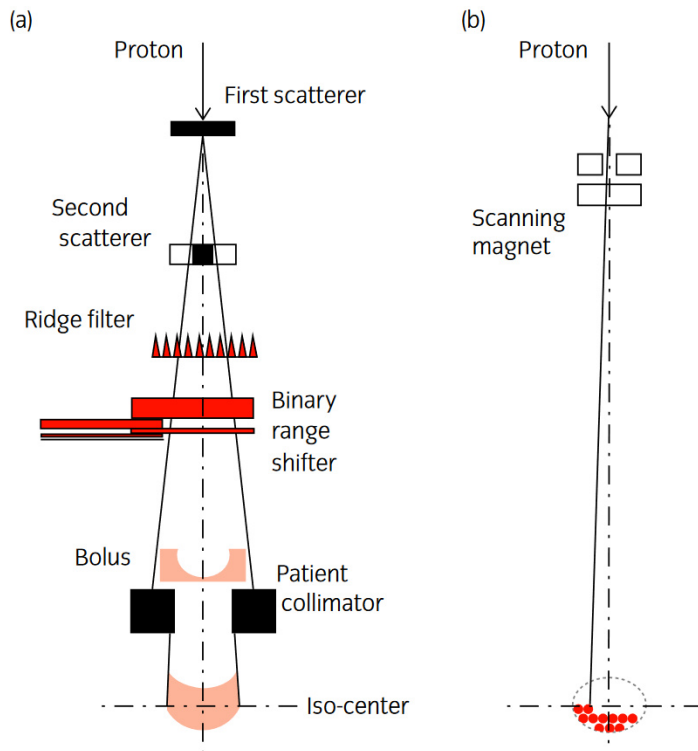


Figure 2. Schematic representation of the passive scattering (a) and pencil beam scanning (b) methods for the irradiation of tumors in particle therapy. Figure taken from (Ishikawa *et al* 2019)

A collimator is used to adapt the treatment field to the lateral contour of the target volume. In addition, when using a cyclotron where the energy cannot be actively varied, the narrow depth dose profile of the monoenergetic particle beam from the accelerator must be broadened in depth by a modulator, which can be achieved by a rotating wheel with different thicknesses known as a range modulation wheel (Koehler *et al* 1975) or a plate with periodically arranged wedge-shaped structures known as a ridge filter (Chu *et al* 1993, Schaffner *et al* 2000). In both cases, the modulator is optimized to give a predefined homogeneous depth dose profile, the so-called spread-out Bragg peak (SOBP, Figure 3). To adapt the energy and shift the modulated Bragg peak to the desired radiological depth in cyclotron facilities, an additional "range shifter" is needed. It typically consists of a number of homogeneous plates of different thicknesses that can be inserted into the beam path.

The major disadvantage of the passive beam application is that the dose distribution can only be conformed to the distal edge of the tumour, but not to the proximal. Therefore, a significant portion of the high dose area is deposited in the healthy tissue in front of the target volume. In addition, due to the scattering system and the collimator, which laterally cuts off a large part of the particles, the efficiency of the passive irradiation method is poor and varies between ~5 % and ~40 %, depending on the complexity of the scattering

foils (Paganetti 2016, Jolly *et al* 2020). This becomes especially relevant in cases where very short treatment times and high dose rates at the isocenter are desirable.

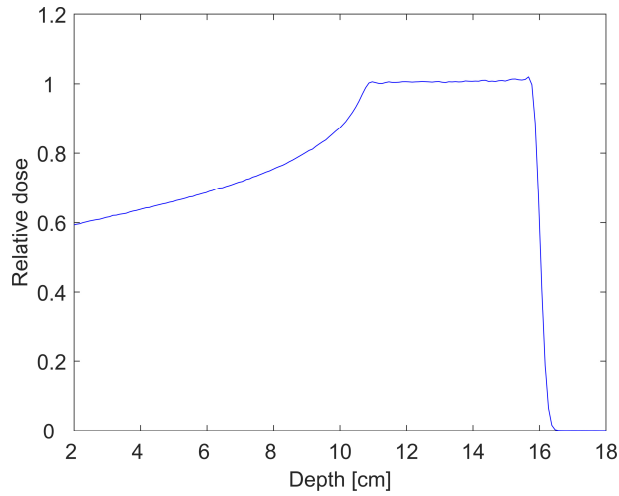


Figure 3. An exemplary 5 cm SOBP in water for a 151 MeV proton beam.

### 1.3.2. Pencil beam scanning

The pencil beam scanning technique (PBS) has established as the state-of-the-art beam delivery in proton therapy. The narrow pencil beam (PB) is deflected by magnetic dipoles to irradiate the whole tumour laterally (Figure 2b), whereas the depth dose distribution is controlled either by varying the energy in the synchrotron or the thickness of the range shifter in cyclotron facilities. The typical clinically available energy range is 48-220 MeV/u for protons and 86-420 MeV/u for carbon ions, which corresponds approximately to a water equivalent depth of 20-300mm. The exact number of particles at each PB position (scan spot, SS), is calculated by the treatment planning system. When all scan spots of an iso-energy layer are irradiated, the next energy is chosen and this process repeats until all layers and thus the whole tumour volume are irradiated (Haberer *et al* 1993, Blattmann *et al* 1990). The raster scan method enables highly homogeneous dose distributions conformed to both the distal and proximal edges of the tumour, thus minimizing the integral dose in healthy tissue.

However, PBS requires a large number of different energies, which comes at the cost of increased treatment time. Typical energy switching times are in the order of several seconds even though faster facilities are also available (Safai *et al* 2012, Furukawa *et al* 2010). Therefore, a typical treatment plan can have a cumulative dead time of a minute or even more depending on the facility.

### 1.3.3. The moving target challenge

The irradiation of moving targets, e.g. lung tumours in the chest area, is generally challenging. Especially the PBS technique and the resulting dose distribution is very sensitive to target movement as the irradiation time of a multi-energy layer plan is relatively long and the scanned beam spatiotemporal pattern interferes with the target motion. These interference effects, also called "interplay effects", can lead to large under- and overdosage in the healthy tissue and the tumour itself (Bert *et al* 2008, Lambert *et al* 2005).

In the case of passive scattering, on the contrary, interplay effects are reduced to a great extent or not observed at all as the irradiation is quasi-instantaneous (Paganetti 2012). However, this comes at the cost of missing proximal dose conformity with extra unnecessary dose in the normal tissue. Moreover, the beam quality deterioration and neutron production in the predominantly high-Z materials in the beam path (e.g., scattering foils) increase the integral dose to the healthy tissue.

There are different target motion-mitigation approaches. One method, called "gating", relies on the continuous monitoring of the tumour movement. The beam is switched on automatically only during a certain predefined breathing phase, ensuring that the tumour is in the right position (Rietzel and Bert 2010).

Another method is the so-called "beam tracking", where the beam follows the tumour movement in real time. This method requires very precise monitoring of tumor motion and a very fast adaptive scanning system with response times below 1ms (Paganetti 2012).

Rescanning is one of the simplest methods to counterfight the target motion. In this case the optimized plan is delivered multiple times with only a fraction of the prescribed dose. The underlying assumption is that the motion-induced hot and cold spots will average and cancel out with enough plan repetitions and the resulting total mean dose will be more or less homogeneous.

The aforementioned methods have some drawbacks. Gating and rescanning, for example, prolong the treatment time significantly, which in turn may lead to positioning uncertainties due to patient movements. The beam tracking method is very complex and involves a great deal of technical effort.

### 1.3.4. Hybrid beam delivery: 3D range-modulator

A feasible approach to mitigate the aforementioned moving-target challenges and to achieve a conformal, homogeneous dose distribution with very short irradiation times is by using a 3D range-modulator (3D RM) irradiated with only one single energy (Sakae *et al* 2000, 2001, 2003, Ishizaki *et al* 2009, Simeonov *et al* 2017). It can be denoted as a hybrid beam delivery technique due to the combination of active lateral scanning with a passive dose modulation in depth. The 3D RM consists of two seamlessly integrated parts: a conventional range compensator to adjust the dose to the distal edge of the target and a fine static ridge/ripple filter (Weber and Kraft 1999). The ripple filter has a novel pyramid-shaped base structure (Weber and Kraft 1999, Ringbæk *et al* 2014). These structures (pins) have well-defined, optimized shapes to create homogenous SOBPs by the weighted superposition of BPs from particles flying through different material thicknesses. In addition, the pins have different laterally-dependent heights to conform the dose distribution also to the proximal target edge (Figure 4). Modern rapid prototyping techniques can be utilized to manufacture the modulators (Ju *et al* 2014, Lindsay *et al* 2015, 2016).

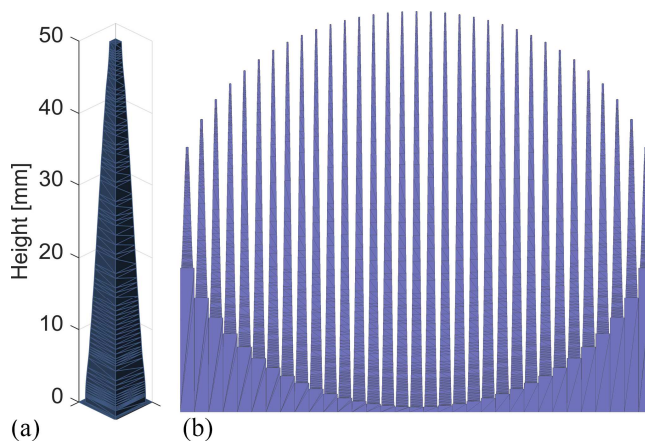


Figure 4. A single pyramid-shaped pin optimized for a 5 cm SOBP in water for 150.68 MeV/u monoenergetic proton beam (a). Frontal view of the middle slice from a 3D range modulator for a spherical target with a diameter of 5 cm. The pins have different heights to laterally modulate and conform the dose to the proximal target edge.

The depth dose distribution  $D(z)$ , resulting from the pin modulation is described as follows:

$$D(z) = \sum_{i=1}^N w_i * B(z + \Delta z * i) \quad (3)$$

$B(z)$  is the original pristine BP and  $\Delta z$  defines the distance between the BPs of the different energies. The weight factor  $w_i$  ( $i$  being the index for the single BPs) is introduced to scale each BP and adjust its individual contribution to the SOBP (Weber and Kraft 1999, Gardey et al 1999, Akagi et al 2003). In order to obtain a SOBP with high degree of homogeneity, the weights  $w_i$  must be optimized. As they determine directly the geometrical shape of the final pin some constraints might be necessary to produce a more favourable, “printer-friendly” form that can also be manufactured easily and reproducibly.

Figure 5a illustrates schematically the relationship between the mathematically optimized weights and the resulting geometrical form of the beam-modulating structure. The underlying principle lies in the fact that the larger the partial area of the material thickness  $\Delta z * i$ , the more particles will fly through it. Consequently, the weight  $w_i$  of each BP is proportional to the partial area. A direct conversion of all weights to partial areas will deliver a “stair-shaped” pin form if  $\Delta z$  is in the order of several millimeters (Figure 5b).

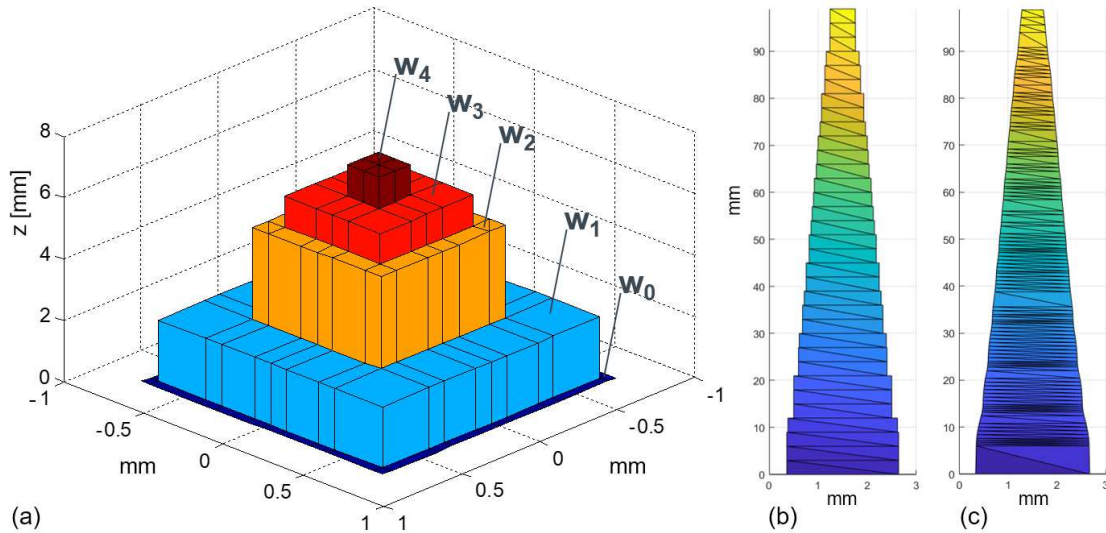


Figure 5. Example of a beam-modulating pyramid-like object with only 4 weights, corresponding to 4 different material thicknesses and partial areas (a). A pin form with  $\Delta z \approx 3\text{mm}$  and larger, visible steps (b) and a pin form with  $\Delta z < 0.5\text{mm}$  (c).

An alternative to the optimization of discrete weights is to use a fit polynomial/power function with a set of parameters that must be optimized. The advantage of this method is that the oscillations of the single weights and therefore the oscillations (waves) in the pin shape are reduced (Simeonov et al 2017). Both the fit function optimization and the discrete weight optimization with very high resolution (very small  $\Delta z$ ) will deliver a smoother pin contour (Figure 5c). The modulating properties of both pin shapes in Figure 5 are, however, completely identical and they are equally suitable for manufacturing.

A 3D RM, consisting of many of these pins, can be optimized for the shape of complex targets and creates a static, highly homogeneous field. In contrast to conventional passive scattering, the dose is conformed both to the distal and proximal target edge, thus reducing unnecessary exposure of healthy tissue (Figure 6). As only one energy is used and consequently energy-switching times are eliminated, a very fast treatment can be achieved so that the patient can potentially hold his breath during the complete irradiation, thus avoiding interplay effects.

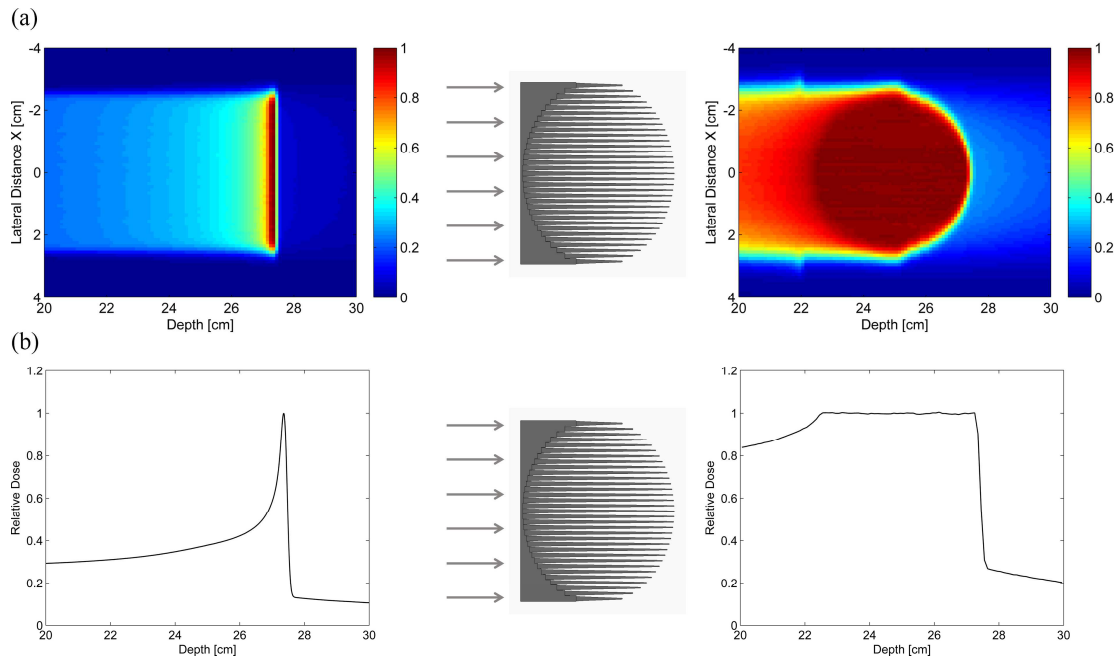


Figure 6. Principle of depth modulation by a 3D range-modulator with both distal and proximal conformity for a spherical target. Monte Carlo simulated X-Z midplane profile (a) and center line depth dose distribution (b).  $^{12}\text{C}$ ,  $E = 400.41 \text{ MeV/u}$ . Figure taken from (Simeonov *et al* 2017) – Figure 4.

### 1.3.5. FLASH therapy

In recent years, interest in the so-called "FLASH" particle therapy has been growing. Several studies (Favaudon *et al* 2014, Durante *et al* 2018, Vozenin *et al* 2019, Adrian *et al* 2019, Hughes and Parsons 2020, Diffenderfer *et al* 2020, 2022) indicate that ultra-fast irradiation (in the order of ms) with dose rates over 40 Gy/s may increase the therapeutic window by reducing adverse effects in normal tissue. High-intensity accelerators and fast, reliable dose delivery and monitoring systems are some of the requirements to achieve FLASH therapy (Romano *et al* 2022). While the biological mechanisms behind the FLASH irradiation are not yet well understood, different models have been proposed to define the dose rate and quantify the flash effect (Water *et al* 2019, Folkerts *et al* 2020, Krieger *et al* 2022).

The commercially available beam delivery techniques reach their limits when it comes to achieving a full irradiation in the order of milliseconds for larger, clinically relevant target volumes. The main bottleneck in PBS is the large cumulative energy-layer switching time. The conventional passive scattering method, on the other hand, has very low efficiency, i.e., number of useful protons that reach the patient behind the (double) scattering foils and does not meet the very high dose rate requirement at the isocenter plane necessary for FLASH.

A relatively simple approach to overcome the energy switching time limitation in PBS is to use one single energy in a transmission mode with the BP outside (behind) the patient (van Marlen *et al* 2021, Schwarz *et al* 2022). Assuming an isochronous cyclotron (Strijckmans 2001), as it is the only clinical system in particle therapy where Flash capabilities for clinical target volumes have been demonstrated, it is necessary to use the maximum available energy. The reason for this is simple: smaller energies are modulated by introducing a degrader in the beam path, which deteriorates the beam quality in terms of angular and energy spread. An energy selection system (ESS) must then be used to restore the beam quality, which results in large beam losses. Most of the particles do not pass the ESS, do not reach the isocenter and consequently, the high current requirements for FLASH are not fulfilled.

Using transmission beam delivery at the highest energy, it should be possible to improve the lateral conformity as the lateral beam penumbra at the target depth is sharper compared to conventional BP-based IMPT. Moreover, using the plateau dose region results in better robustness with lower sensitivity to setup and range uncertainties.

On the other hand, the advantage of the higher dose of the BP is lost and the overall integral dose deposition in healthy tissue is large due to the lack of distal dose conformity (Rothwell *et al* 2022). In addition, multiple beams are required to increase the dose in the target, which by itself prolongs the total treatment time and might introduce additional uncertainties.

Another way to approach the challenge of fast irradiation in the order of milliseconds would be by using the aforementioned 3D range-modulator, optimized for a single energy and individual tumour shape. Just as in the case of moving targets, 3D range-modulators seem as a promising and viable solution for FLASH treatments in particle therapy. This hybrid beam delivery method might be the most practical way to adapt existing facilities and implement FLASH treatment with dose distributions similar in homogeneity and conformity to active PBS (Jolly *et al* 2020, Diffenderfer *et al* 2022, Weber *et al* 2022).

#### 1.4. The Monte Carlo code FLUKA

A 3D RM is a complex 3D object composed of a large number of very fine structures. Predicting the complex polyenergetic field behind it and the resulting dose distribution is nontrivial, especially for a treatment planning system (TPS) with analytical dose calculation algorithms. Therefore, in this work Monte Carlo (MC) methods were utilized to simulate the dose distribution from all modulators.

The term “Monte Carlo” refers to a class of computational techniques that involve the use of random sampling from given probability distributions to evaluate complex mathematical expressions or models. These techniques have been widely used in fields such as physics, chemistry, engineering and finance. The origins of Monte Carlo calculations can be traced back to the 1940s, when Stan Ulam and John von Neumann developed the technique as part of the Manhattan Project.

The MC transport code FLUKA is a general-purpose tool for calculating particle transport and interactions with matter (Ferrari *et al* 2005, Battistoni *et al* 2006, Böhlen *et al* 2014, Battistoni *et al* 2015). FLUKA has been extensively benchmarked and used by many research groups and has proven as a reliable simulation tool (Sommerer *et al* 2006, Parodi *et al* 2007, 2012, Battistoni *et al* 2016, Baumann *et al* 2021). It can be used for a variety of different tasks, including activation calculations, dosimetry, radiation protection, etc. Combinatorial geometry logic or a voxel-based geometry can be used to build complex shapes. The distribution package includes a number of user-routine



templates. They can be additionally customized and linked to the original code, so that special cases can be also handled.

The simulation of a range-modulator in FLUKA is an example of such a special case, where additional modifications were needed (Simeonov *et al* 2017). Firstly, the complex geometric shape of the modulators, consisting of many very fine structures, cannot be described with the FLUKA Combinatorial Geometry logic. For this reason, a custom routine was implemented based on the Möller and Trumbore ray-tracing algorithm (Möller and Trumbore 2005). This routine searches for the intersection points of each particle with the modulator, calculates the total material thickness the particle will travel in the modulator and shifts it correspondingly inside a homogenous slab along its original trajectory.

In order to compare the simulated dose distribution with measurements from a clinical facility, an additional routine for intensity modulated raster scanning was developed and implemented. Thus, it is possible to irradiate the modulator with single Gaussian scan spots while varying the number of particles in each scan spot. The raster file, which contains the energy, the coordinates of the individual scan spots and their partial particle number, can be loaded by both FLUKA and the accelerator.

## 2. AIM AND MOTIVATION

The main purpose of this dissertation is to establish and validate a process chain for the development, manufacturing and dose verification of patient-specific 3D range-modulators and thus bring the 3D RM dose delivery method one step closer to a potential clinical application.

The modulators are meant to be printed with advanced and quickly evolving rapid-prototyping techniques. The manufacturing accuracy and more importantly the preservation of the correct height-dependent partial pin area are of crucial importance in order to obtain the exact homogeneous dose distribution the RMs are optimized for. Therefore, the first objective is to optimize and improve the design of the fine single modulator structures (pins). So called 2D RMs, consisting of pins with the same height, are used to verify the improvements and homogeneity of the resulting dose distribution and thus demonstrate the feasibility of the proposed depth dose modulation and manufacturing workflow. As the dose distribution from 2D modulators is not as complex as from patient-specific 3D RMs, they are better suited to identify in a systematic way dose deviations coming explicitly from manufacturing artefacts and trace them back. Thus it would be possible to quickly iterate between different pin shapes to find an optimum solution and improve the manufacturing process.

In addition to the more “conventional” PolyJet manufacturing with photopolymer resin, an alternative technique, the selective laser melting (SLM), should be investigated. SLM uses metal powder and a laser to selectively melt and fuse the powder layer by layer, thus producing very well-bonded and high density structures.

Using the aforementioned rapid prototyping techniques, different 2D modulators should be manufactured with polymer resin and metal alloys and investigated with both MC simulations and measurements. The 2D modulator is a static element that can be positioned in a flexible way relatively close to the target and its SOBP width and shape can be customized arbitrarily, making it an excellent and flexible solution for different research projects in particle therapy facilities. Hence, in a next step, the usability, modulating properties, etc. of 2D RMs should be investigated in practical research applications in the framework of collaborations with different institutions.

Finally, a 3D RM should be developed for a complex, moving patient-specific target. The information necessary for the 3D modulator design, such as the water equivalent

thickness (WET) and depth of the tumour and its distal edge can be calculated from anonymized DICOM CT patient data using ray tracing techniques.

The modulation properties of the 3D RM can be verified using the established MC simulation package FLUKA. For this purpose, the patient DICOM data must be imported in FLUKA as a voxelised phantom and the relationship between the DICOM, FLUKA and IEC coordinates systems must be established. Previously developed in-house algorithms allow importing the 3D RM and calculating the particle transport through its fine, complex structures. Based on the results of the MC simulations, the design of the modulator and the particle fluence needed to irradiate it should be improved and optimized in an iterative process, taking into account the clinically optimal dose distribution.

To validate the simulation results, the 3D RM should be manufactured with high-quality 3D printing techniques with both polymer resin and aluminum and the resulting dose distributions should be measured at a particle therapy facility. It is desirable and important that the dose distribution of a modulator should be verified reliably and quickly during experiments, as well as in a time constrained clinical environment. For this purpose, the water phantom system WERNER developed in-house at the GSI, can be utilized as it can perform fast, completely automated and high resolution dose measurements. In a final step, the measured dose is analysed and compared with the FLUKA simulations.

### 3. SUMMARY OF THE PUBLISHED RESULTS

#### 3.1. Publication 1

##### Monte Carlo simulations and dose measurements of 2D range-modulators for scanned particle therapy

##### 3.1.1. Summary of publication 1

In Publication 1 (Simeonov *et al* 2021) the concept of the 2D range-modulator is introduced. It is a static device that can generate a quasi-instantaneous spread-out Bragg peak and can be positioned at a relatively close distance to the target. It has multiple advantages, such as fast dose delivery, fast manufacturing, flexibility in the SOBP shape and width, etc. In addition, potential inhomogeneities in the resulting dose distribution can be used to identify and even quantify manufacturing issues and artefacts. Based on this knowledge, improvements in the pin shape can be implemented and therefore the 2D RM can be considered as an important, preliminary step towards a patient-specific 3D RM.

The aim of this work was to develop, improve, simulate, manufacture and measure a 2D RM and thus validate the complete workflow process chain.

To begin with, the weights of a 5 cm SOBP, resulting from a 150.68 MeV/u monoenergetic proton beam simulated with FLUKA, were optimized and converted to a continuous stepless pyramid-shaped pin profile (Figure 7).

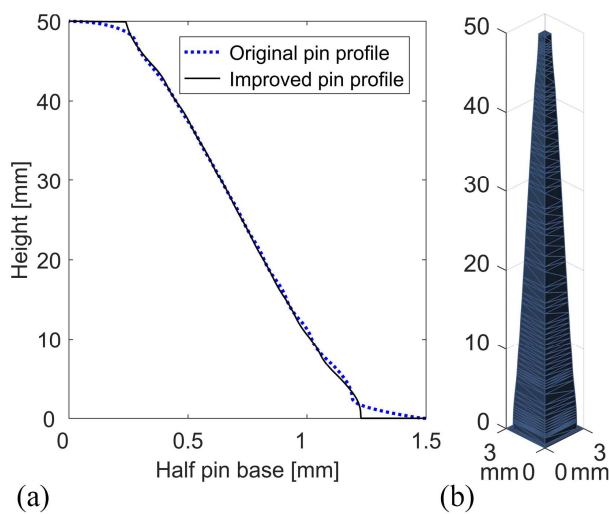


Figure 7. Comparison between the original and improved pin profile. The main difference is in the pin base (groove) and the pin tip (a). A single pyramid-shaped pin optimized for a 5 cm SOBP in water for 150.68 MeV/u monoenergetic proton beam (b). Figure taken from (Simeonov *et al* 2021) – Figure 2.

Several improvements were introduced to the pin shape in comparison with (Simeonov *et al* 2017). A more favourable aspect ratio and thus higher mechanical stability were achieved by increasing the base side from 1.5 mm to 3 mm. In addition, the groove between adjacent pins and the pin tip area were also optimized to be slightly wider, as these areas were found to be particularly susceptible to deviations during the 3D printing process. These changes, although small, significantly improved the manufacturing of the 3D printed pins, as confirmed by test prototypes.

Two 2D RMs were manufactured using the improved pin form. The first one, referred to as the “polymer RM,” is made of a PMMA-like photopolymer (RIGUR RGD450, 1.2 g\*cm<sup>-3</sup> density) and consists of 27x27 periodically positioned adjacent pins. It was manufactured using PolyJet technique with a Stratasys Objet30 Pro 3D-printer. The second RM, referred to as the “steel RM,” is made of stainless steel (316L alloy with 7.95 g\*cm<sup>-3</sup> density) and consists of 19x19 pins. It was manufactured with selective laser melting technique (Kruth *et al* 2005, Konda Gokuldoss *et al* 2017) using a TRUMPF TruPrint 1000 SLM machine. The metal alloy was considered worth investigating as it can further improve the aspect ratio of the pins, the mechanical stability and overall robustness.

Both RMs have a 1 mm thick base plate and 3 mm thick side walls for pin protection. Positioning bars were also added to accurately align the modulators in the treatment field with the lasers during dose measurements (Figure 8).

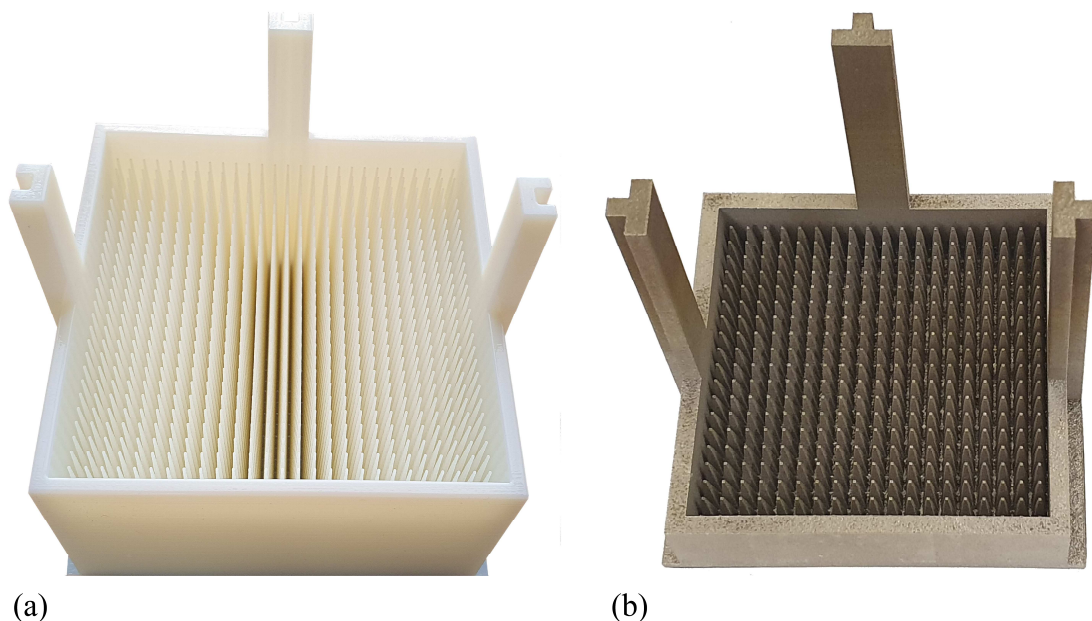


Figure 8. The manufactured **polymer** RM (a) and the **steel** RM (b) with a protection wall around and positioning bars. Figure taken from (Simeonov *et al* 2021) – Figure 4.

In a first step, both modulators and their resulting depth dose distributions were validated with MC FLUKA simulations. An in-house developed routine was used to model the shape of the modulators.

A direct comparison between MC simulations and measurements from particle therapy facilities with pencil beam scanning (PBS) required an implementation of an intensity-modulated raster scanning in the FLUKA 'Source.f' user routine. The information needed for the simulation, such as energy, beam spot size, x/y coordinates of the scan spots, etc., is contained in a raster file, which can be loaded by both FLUKA and the accelerator. All simulations were run on several hundred processors from an in-house CPU cluster with enough primary particles, so that the statistical uncertainty was below 0.3 % in the homogeneous SOBP region.

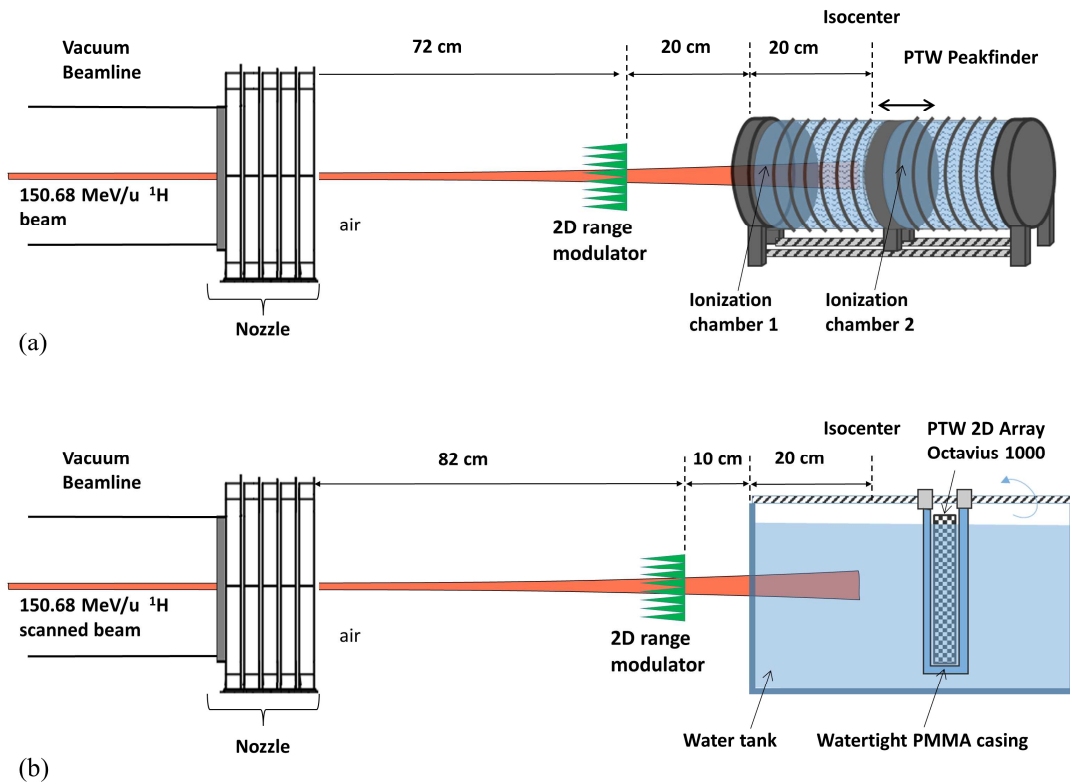


Figure 9. Schematic drawing of the dose measurement setup. Panel (a) shows the 2D polymer RM, which was positioned 40 cm in front of the isocenter and irradiated with an undeflected beam. The dose was measured with the PTW Peakfinder. Panel (b) shows the 2D steel RM, which was positioned 30 cm in front of the isocenter and irradiated with a scanned 3.2 cm<sup>2</sup> rectangular field. The dose was measured with the newly developed WERNER system using the PTW Octavius 1000P. All measurements were conducted with a 150.68 MeV/u proton beam. Figure taken from (Simeonov *et al* 2021) – Figure 7.

The next step was to validate the simulations with dose measurements at the Marburg Ion Beam Therapy Center (MIT). The polymer RM was irradiated with an undeflected 150.68 MeV/u proton pencil beam with a FWHM of 11.1 mm at the isocenter and the dose was measured with the variable depth water column PTW Peakfinder (Figure 9a).

The steel RM was irradiated with the same monoenergetic beam and a field size of 32 x 32 mm<sup>2</sup>. Instead of the PTW Peakfinder, the WERNER system (Schuy *et al* 2020) in combination with the 2D ionization chamber array PTW Octavius 1000P was used to obtain a full, high-resolution 3D dose measurement (Figure 9b). For this purpose, the same raster plan was irradiated multiple times and after each repetition the Octavius detector moved automatically to the next position. The acquired 2D dose distributions at each depth were post-processed to reconstruct a complete 3D dose data set.

Finally, the measured dose was compared to the simulated one. Figure 10 shows the laterally integrated SOBP of the polymer RM measured with the PTW Peakfinder. An excellent agreement can be observed with 1.4 % maximum dose deviation and 0.59 % relative standard deviation in the SOBP region (10.7 cm to 15.7 cm).

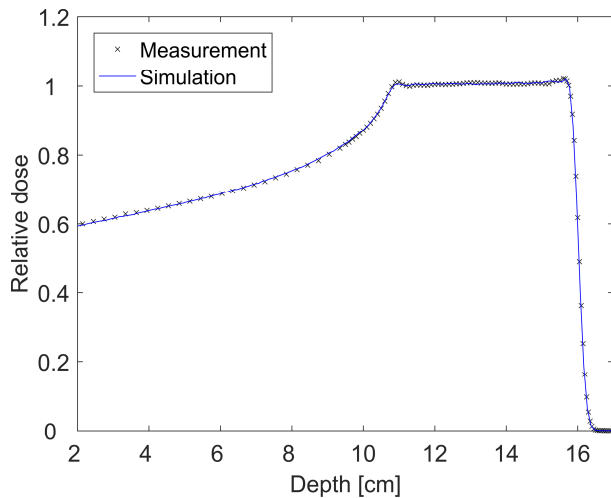


Figure 10. **Polymer RM:** A comparison between the measured and simulated SOBP. Both depth dose distributions are normalized to one in the middle of the SOBP. Figure taken from (Simeonov *et al* 2021) – Figure 8.

The dose from the steel RM is depicted in Figure 11. The center line SOBP in panel (a) has a very good agreement in the proximal region with a slightly increasing deviation up to 4 % towards the distal edge. In addition, a X-Z midplane profile with its corresponding Gamma Index, GI (Low *et al* 1998) and three lateral profiles at different depths are plotted. Apart from the small distal edge discrepancies, which are the result of sub-

optimal manufacturing process from the SLM printer, there is a very good agreement with the FLUKA simulations.

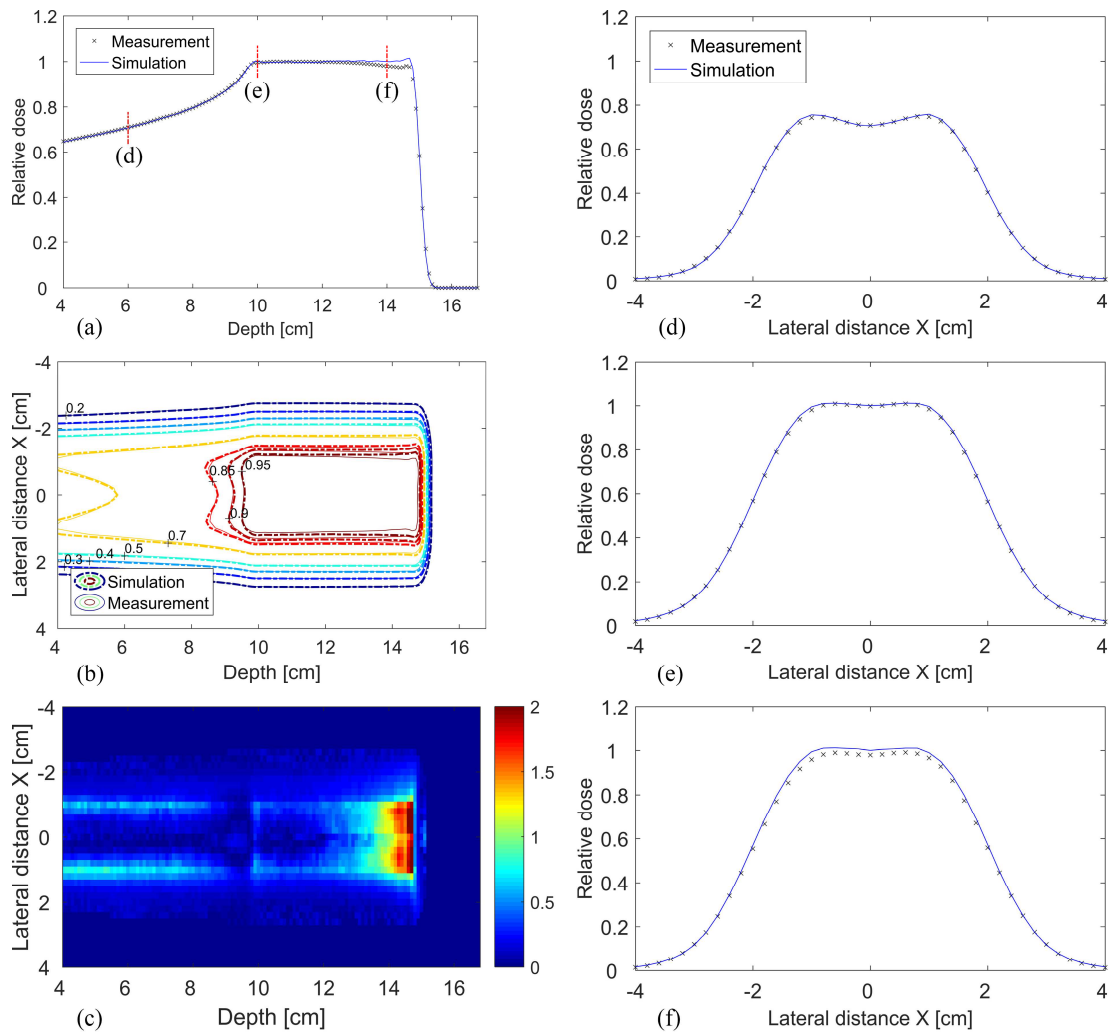


Figure 11. **Steel RM**: Centre line SOBP (a), isodose lines comparison of a X-Z midplane profile (b) and the corresponding local gamma index for 2%/2 mm acceptance criteria (c). Three lateral X profiles (d)–(f), plotted at 6 cm, 10 cm and 14 cm respectively. The vertical red lines in (a) denote the depths, at which the X profiles were plotted. Figure taken from (Simeonov *et al* 2021) – Figure 10.

Publication 1 introduced the 2D RM as a static, modulating device and verified the measured dose distribution of the revised and improved pin shape using two different modulators. The measurements exhibit excellent agreement with the MC simulations, particularly in the case of the polymer RM. All in all, an end-to-end process chain has been shown, encompassing the development and MC simulations of the modulator, its manufacturing and subsequent dose measurements. We have demonstrated the feasibility of high-quality 2D RMs, which can create highly homogeneous SOBPs, thus paving the way for more complex 3D RMs, which will be the scope of Publication 2.



### 3.1.2. Contribution

Y. Simeonov wrote the manuscript and executed most of the study. He developed, optimized the modulators and printed the polymer one. Y. Simeonov conducted all Monte Carlo simulations and developed the necessary user routines. He took part in the dose measurements and analysed the final results.

U. Weber came up with the original idea of 2D/3D modulators manufactured by rapid prototyping and their advantage in the scope of very fast moving target irradiation and potential FLASH treatment. He supported the project and contributed with his expertise to all steps of the workflow process chain.

C. Schuy developed the water phantom system WERNER. U. Weber and C. Schuy took part in the dose measurements and were responsible for the post processing of the raw measured data.

P. Penchev contributed with very helpful technical ideas and programmatic skills, among other things developing routines in the Matlab environment and for the CPU cluster used for the simulations.

R. Engenhardt-Cabillic supervised the work and supported the clinical assessment with her expertise.

K. Zink took part in the dose measurements, supervised the work and helped with the physical assessment.

M. Durante revised the manuscript.

All authors revised this manuscript, substantively.

### 3.2. Publication 2

#### Development, Monte Carlo simulations and experimental evaluation of a 3D range-modulator for a complex target in scanned proton therapy

##### 3.2.1. Summary of publication 2

Publication 2 (Simeonov *et al* 2022) extends the concept of the generic 2D range-modulator to a 3D range-modulator for a complex tumour. Using only one single energy, the 3D RM is a feasible application technique for the very fast treatment of patient-specific tumours resulting in homogeneous and highly conformal dose distribution. It overcomes the problem of the dead time between the energy layers and does not suffer from the large beam losses typical for the conventional passive scattering technique.

The purpose of this work was to develop, simulate, manufacture and measure a 3D RM for a complex patient-specific target contour in a scanned proton therapy beam and thus validate the complete workflow process chain.

In a first step, a pin database was pre-calculated with a 150.68 MeV/u monoenergetic beam by optimizing many single pins with different heights (10 - 60 mm in 10 mm steps) for a homogenous SOBP, using the pin profile improvements and methods presented in Publication 1 (Simeonov *et al* 2021). A right lung target with a complex, irregular contour from an anonymized patient CT was chosen for the development of the modulator (Figure 12). The contour was expanded by 4 mm to ensure better, more homogeneous target coverage.

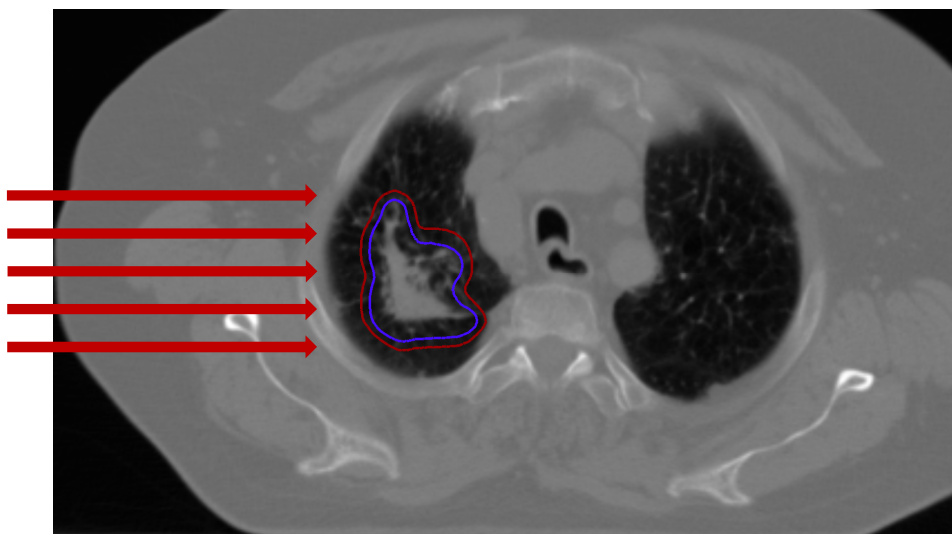


Figure 12. One slice of the patient CT with the original (inner blue contour) and a 4 mm extended PTV, used for the development of the modulator (outer red contour). Figure taken from (Simeonov *et al* 2022) – Figure 1.

For the purpose of reducing complexity, the density of all CT voxels was set to water. The necessary information, such as pin height and thickness of the base material under each pin, was derived by ray-tracing from a single right coplanar beam, utilizing a Matlab implementation of the Siddon algorithm ‘matRad\_siddonRayTracer’ (Wieser *et al* 2017). Based on this information, pins were sampled and interpolated from the database thus creating a first version of the 3D RM (Figure 13c). A lateral margin in the form of some extra pins was added around the modulator in order to improve the lateral edge dose homogeneity. In addition, positioning bars, defining the isocenter and walls for better stability were built on the modulator.

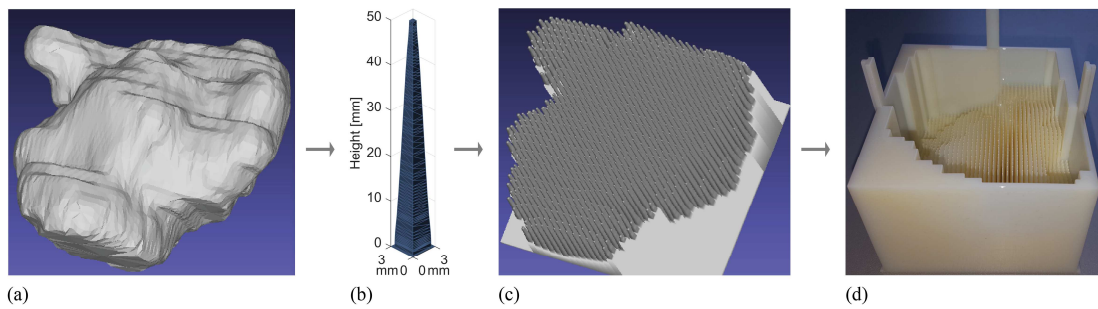


Figure 13. 3D view of the lung target (a), a single 50 mm pin (b), a 3D view of the optimized modulator (c) and the corresponding manufactured prototype (d). The prototype has positioning bars defining the isocenter, used for alignment with the in-room lasers and side walls for better stability and usability. Figure taken from (Simeonov *et al* 2022) – Figure 2.

The next step was to investigate the modulating properties by MC FLUKA simulations. Therefore, the CT was converted to a binary voxel-based file format (.vxl) and imported into FLUKA. The CT was rotated and translated to the same right coplanar beam angle and isocenter position as during the ray-tracing calculation. The previously developed beam model, already used in (Simeonov *et al* 2021), which combines the “SOURCE.f” user routine for the raster scanning and the “USRMED.f” user routine for the modulator implementation, was utilized to simulate the resulting dose distribution (Simeonov *et al* 2017). A raster plan was created by assigning a scan spot to each pin. The initial weights in each scan spot were calculated by summing the optimization weights (the modulating partial areas, see Figure 5 for reference) of its corresponding pin (Figure 14a). These initial weights were used only for the first simulation. A procedure was developed and implemented in order to optimize these weights and improve the dose homogeneity. For this purpose, the source routine and the in-house CPU cluster were customized in such a way that the 3D dose distribution of each scan spot from the raster plan is simulated and

scored separately. All 3D dose files (each corresponding to one scan spot from the raster plan) were subsequently imported into an in-house developed Matlab environment, mapped on the CT grid and assigned an initial weighting factor. Then the weighted sum of all dose distributions was calculated and optimized inside the original PTV contour in an iterative process by minimizing the difference to a prescribed dose value. Mathematically, this optimization is similar to the aforementioned Equation (3) in that the weighted dose sum is optimized for homogeneity. The result of this optimization was a new set of scan spot weights, which were used for the final simulation (Figure 14b). All simulations were run on several hundred processors from an in-house CPU cluster with enough primary particles, so that the statistical uncertainty was below 0.3 % in the homogeneous SOBP region.

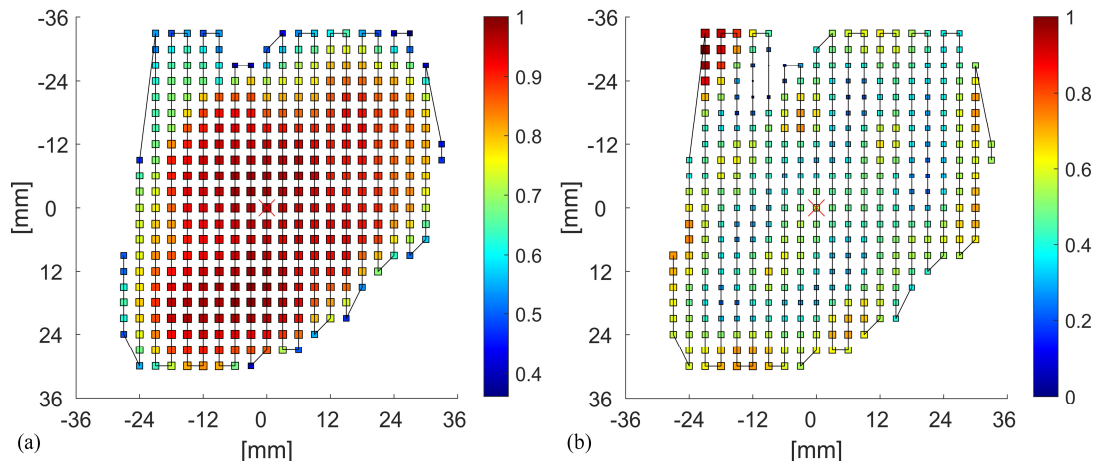


Figure 14. Number of particles in each scan spot before (a) and after the optimization (b) expressed as a scaling factor. Additionally, the scan path is plotted with a solid line and the isocenter is denoted with a red cross mark. Figure taken from (Simeonov *et al* 2022) – Figure 3.

Finally, the modulator was manufactured on the Stratasys Objet30 Pro printer using RIGUR RGD450 photopolymer with a density of  $1.2 \text{ g}\cdot\text{cm}^{-3}$  (Figure 13d). While this polymer modulator is the main scope of this work, an additional aluminum RM was also manufactured on a different machine (TRUMPF TruPrint 3000) by selective laser melting (Trevisan *et al* 2017) to demonstrate the potential of this alternative material and manufacturing technique (Figure 15). Aluminum is expected to increase both the scattering and cost of manufacturing, but results in more favourable pin aspect ratio, improved mechanical stability and robustness, therefore enabling the printing of 3D RMs for much larger targets.



Figure 15. The aluminum 3D RM with a side wall and positioning bars. Figure taken from (Simeonov *et al* 2022) – Figure 5.

In order to validate the simulation results, the dose distribution from both the polymer and aluminum modulators was measured at the Marburg Ion Beam Therapy Center. The WERNER system, synchronized to the dose delivery system of the accelerator was used in a combination with the 2D Ionization Chamber Array Octavius 1000P (Schuy *et al* 2020, Simeonov *et al* 2021).

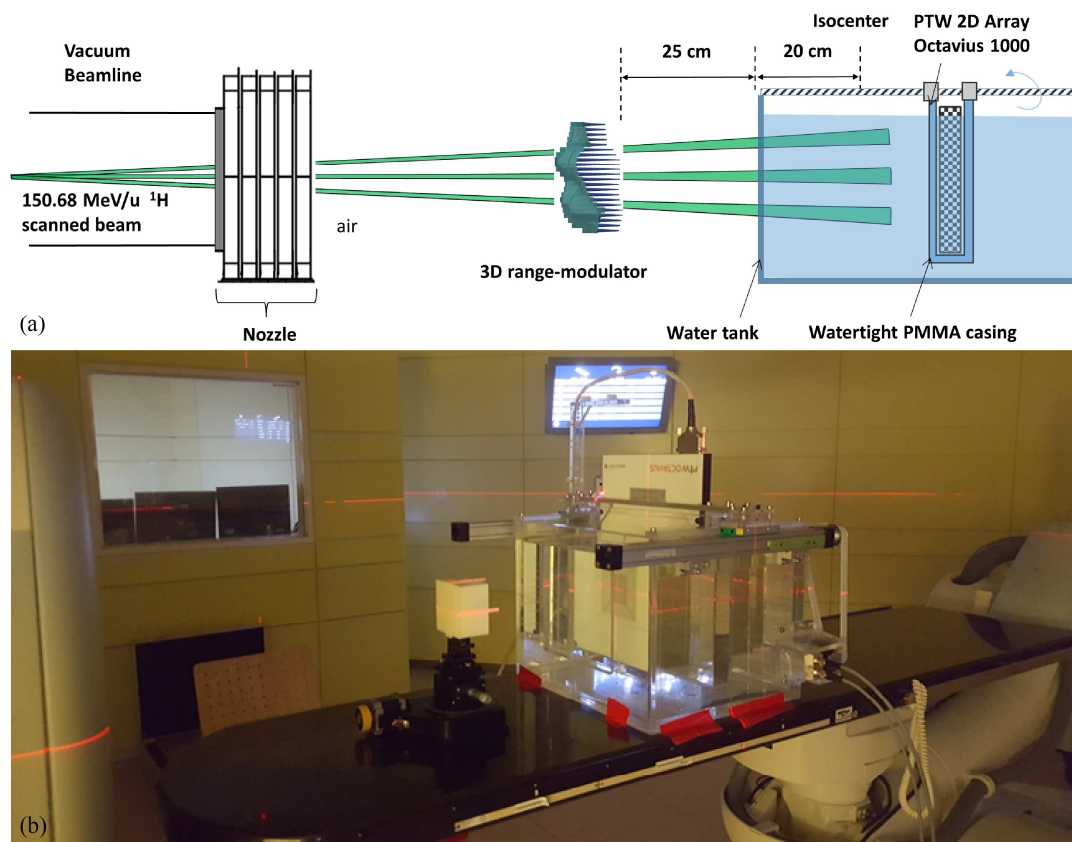


Figure 16. A schematic drawing of the dose measurement setup (a) and a picture of the measurement session (b). The 3D range-modulator was positioned 25 cm in front of the water phantom. The dose was measured with the PTW Octavius 1000P. Figure taken from (Simeonov *et al* 2022) – Figure 6.

Using a measurement setup corresponding exactly to the FLUKA simulation (Figure 16) a high-resolution, completely automated and fast dosimetric verification of the 3D range-modulators was performed. Delivering  $\sim 0.5$  Gy in the  $\sim 70$  cm<sup>3</sup> target volume took approximately 6 seconds using the maximum available intensity of  $1.9 \times 10^9$  part/s.

In the end, the measured dose profiles were validated against the FLUKA simulations.

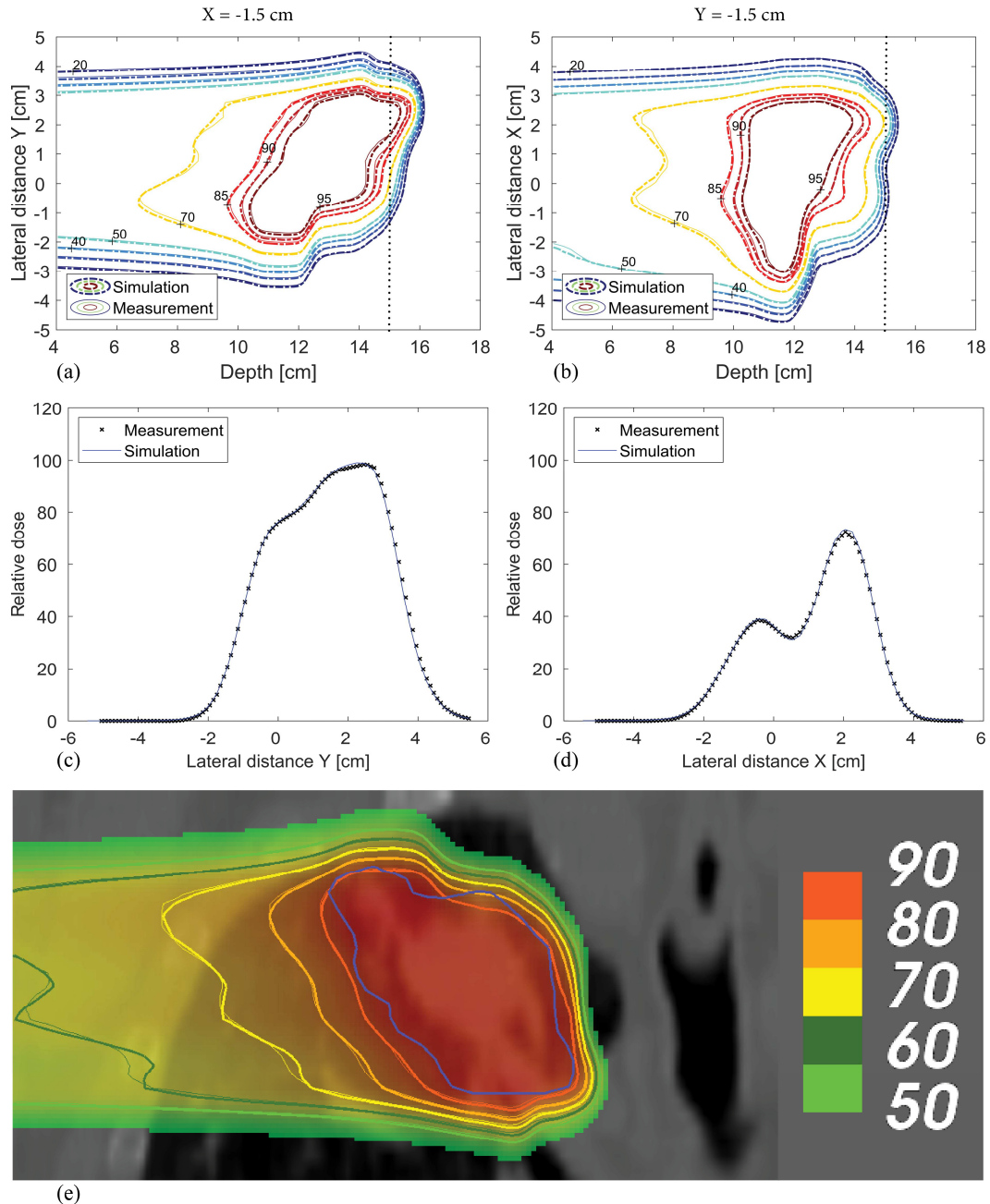


Figure 17. Isodose lines of the measured (solid line) and simulated (dashed line) dose distribution (a)-(b). The corresponding 1D profiles in panel (c) and (d) were plotted at 15 cm depth, denoted as a vertical dotted line in the panel above. Additionally, the measured (thick lines) and simulated (thin lines) dose is overlaid on top of the raw CT data (e). The blue line denotes the PTV contour. **Note:** The modulator was developed on the basis of the homogeneous “water” CT, not the heterogeneous one shown here. Figure taken from (Simeonov *et al* 2022) – Figure 7.

Figure 17 shows the dose comparison in the form of isodose lines (a)-(b) and the corresponding 1D profiles extracted at a depth of 15cm (c)-(d). While the dose was simulated in a modified homogeneous CT overwritten with water, an additional dose overlay on the original heterogeneous CT is depicted in Panel (e), just for the purpose of better visualization of the original tumour tissue and tumour delineation.

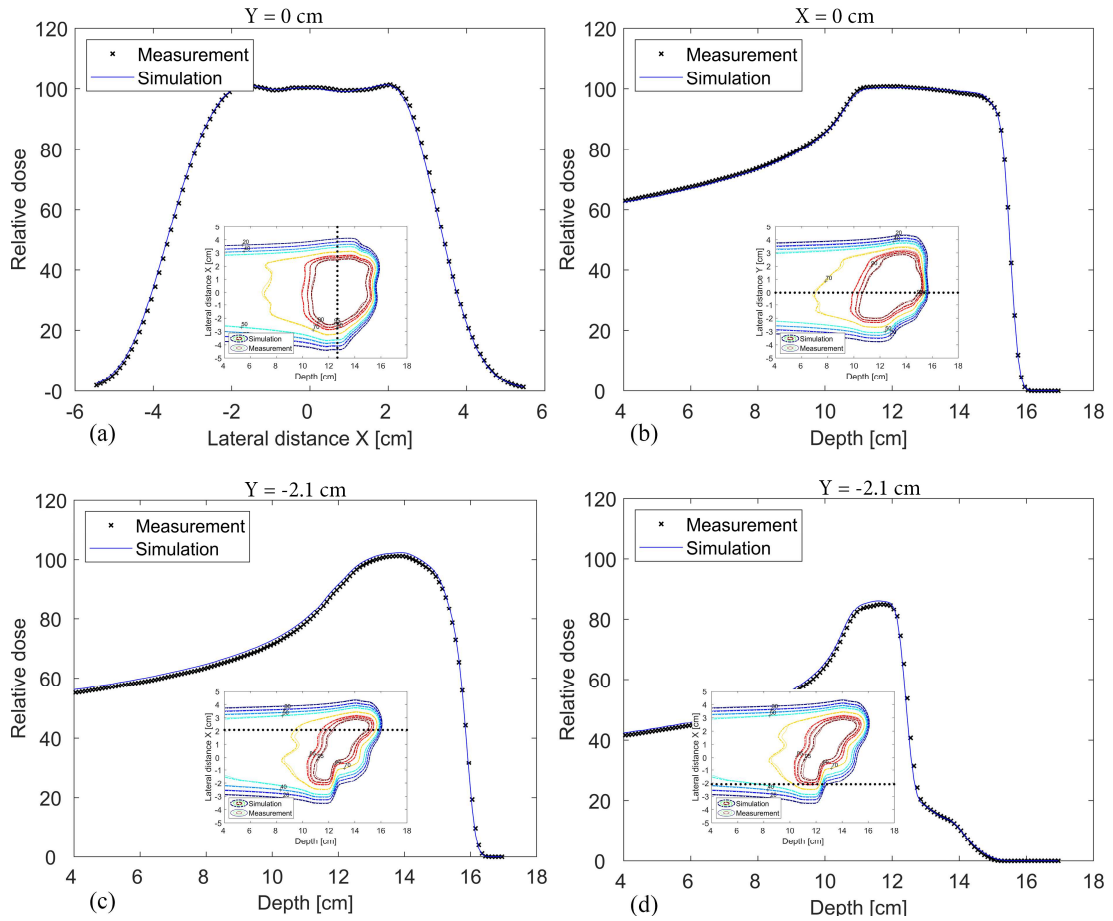


Figure 18. A lateral X profile (a) and three depth dose distributions (b)-(d). Additionally, 2D isodose line figures are included to denote the exact position, at which the 1D profiles were plotted. Figure taken from (Simeonov *et al* 2022) – Figure 8.

Figure 18 shows additional lateral (a) and SOBP depth dose profiles (b)-(d) from different positions and slices. Overall, there is a very good agreement between the measured and simulated dose values, which is also confirmed by the 2D GI analysis in Figure 19. A 2%/2 mm local acceptance criteria, applied to dose values larger than 15 % of the maximum dose, was used to quantify the dose deviations for two different slices. Both the 2D GI and the additional full 3D GI have a very high passing rate of ~99 %.

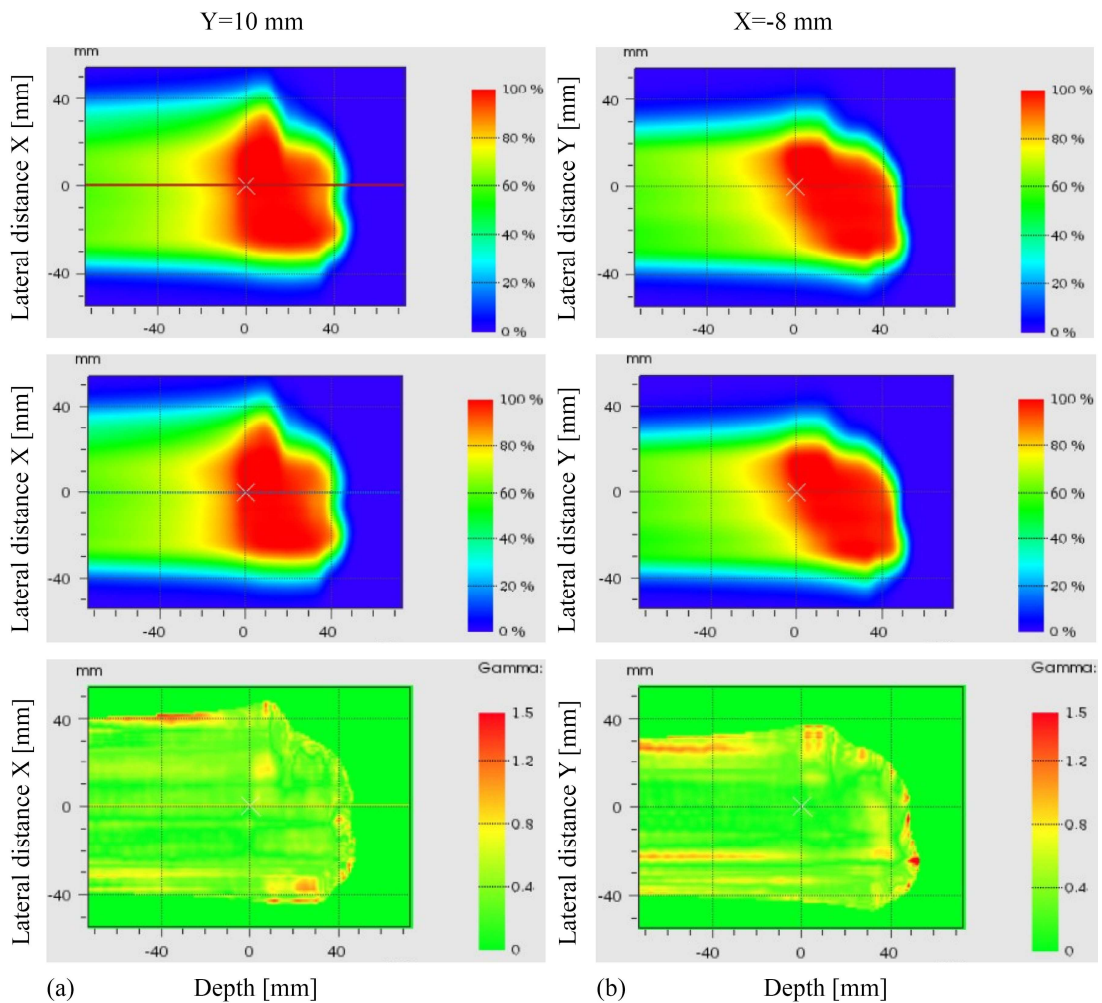


Figure 19. The dose distributions (simulated dose in the upper panel, measured dose in the middle panel) and the resulting GI (lower panel) for one transversal (a) and one sagittal (b) slice. 99 % of the evaluated voxels were found to pass the dose and distance agreement criteria. Figure taken from (Simeonov *et al* 2022) – Figure 9.

A cumulative Dose-Volume Histogram (DVH) was calculated from all dose voxels inside the PTV contour and plotted in Figure 20. A mean dose close to 100 % and approximately 105 % maximum dose were calculated with the applied dose normalization.



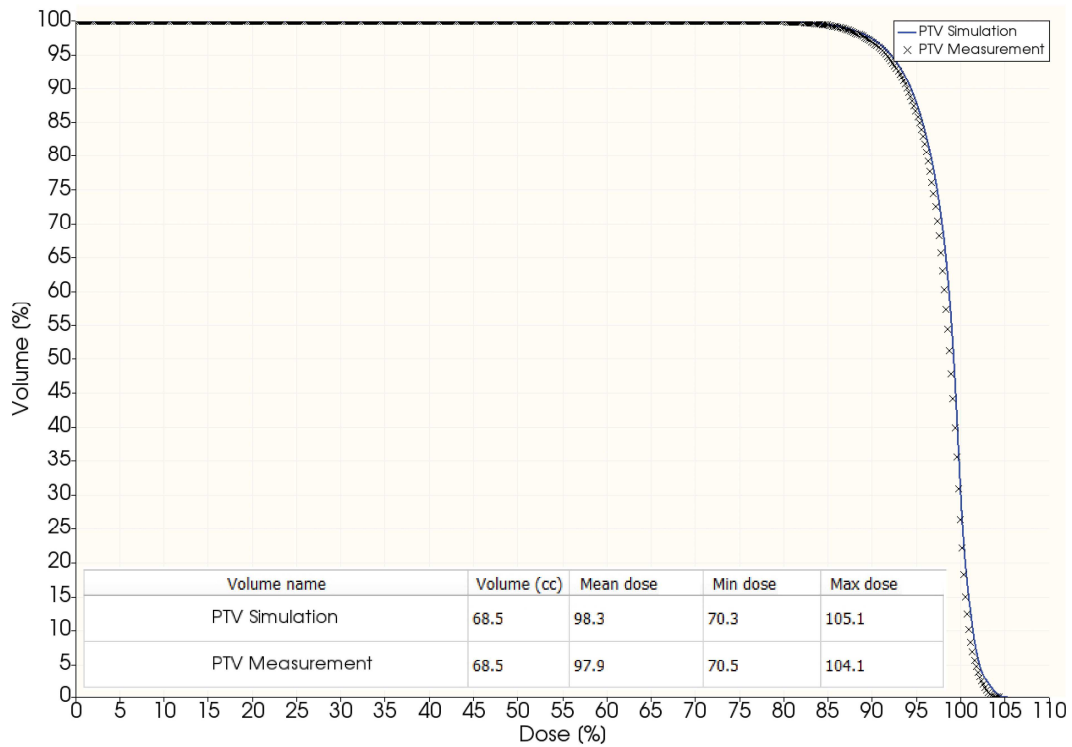


Figure 20. DVH calculated inside the PTV target for both the measured and simulated dose and the resulting statistical information. Figure taken from (Simeonov *et al* 2022) – Figure 10.

A center line depth dose profile and an isodose comparison from the aluminum modulator is shown in Figure 21 again showing a very good agreement with 99 % GI passing rate for the 2D slice and 98 % for the 3D GI.

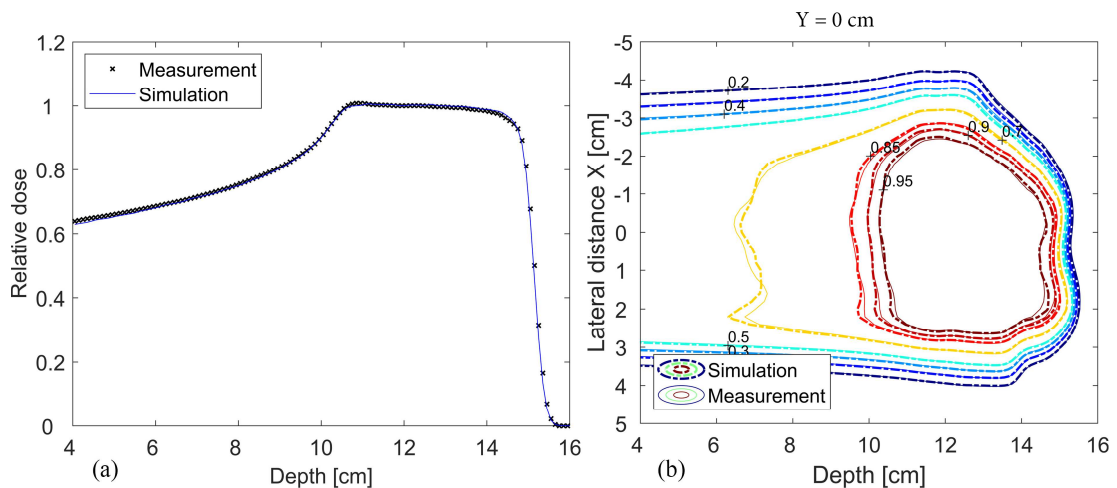


Figure 21. A center line depth dose distribution (a); Comparison between the isodose lines of the measured (solid line) and simulated (dashed line) dose distribution (b). Results are from the **aluminum** modulator. Figure taken from (Simeonov *et al* 2022) – Figure 11.

Publication 2 extended the concept of the generic 2D modulator to a target-specific 3D RM. We have demonstrated an end-to-end process chain, including the development of the 3D RM, its manufacturing using two different printing techniques and materials and the subsequent dose verification. Simulations and measurements are in excellent agreement confirming the initial expectations of a dose distribution conformed both to the proximal and distal edge. Delivering a highly homogeneous and conformal dose distribution, comparable and competitive to standard IMPT, the 3D modulator is a promising and feasible method for achieving extremely short treatment times, thus paving the way for a potential clinical application with moving targets and/or FLASH irradiation.

### 3.2.2. Contribution

Y. Simeonov wrote the manuscript and executed most of the study. He developed, optimized the modulators and printed the polymer one. Y. Simeonov conducted all Monte Carlo simulations and developed the necessary user routines. He took part in the dose measurements and analysed the final results.

U. Weber came up with the original idea of 2D/3D modulators manufactured by rapid prototyping and their advantage in the scope of very fast moving target irradiation and potential FLASH treatment. He supported the project and contributed with his expertise to all steps of the workflow process chain.

C. Schuy developed the water phantom system WERNER. U. Weber and C. Schuy took part in the dose measurements and were responsible for the post processing of the raw measured data.

P. Penchev contributed with very helpful technical ideas and programmatic skills, among other things developing routines in the Matlab environment and for the CPU cluster used for the simulations.

R. Engenhardt-Cabillic supervised the work and supported the clinical assessment with her expertise.

K. Zink took part in the dose measurements, supervised the work and helped with the physical assessment.

Veronika Flatten provided the CT data with target contouring and contributed with DICOM standard, TPS and clinical expertise.

All authors revised this manuscript, substantively.

### 3.3. Publication 3

#### **2D range modulator for high-precision water calorimetry in scanned carbon-ion beams**

##### 3.3.1. Summary of publication 3

Publication 3 (Holm *et al* 2020) describes a practical, real-world application of a 2D RM in a scanned carbon-ion beam. The modulator itself presented an important contribution from our working group to another, completely separate project about high-precision water calorimetry, conducted at the Physikalisch-Technische Bundesanstalt (PTB) and Deutsches Krebsforschungszentrum (DKFZ).

The final goal of this project was to determine experimentally the beam quality correction factor  $k_Q$  for two Farmer-type ICs at the SOBP depth in a scanned carbon-ion beam by means of water calorimetry. Necessary conditions for the reliable calorimetric measurement of the absorbed dose to water are applied dose values typically larger than 1Gy to induce a detectable temperature rise with a high signal-to-noise ratio and a large, homogeneous field, irradiated in a short time to reduce the heat conduction effects. However, the larger the dose and field size, the longer the irradiation time, which poses certain limitations on the calorimetric dose determination in a scanned particle beam. Preliminary studies had shown that irradiating a homogeneous volume of  $6 \times 6 \times 6 \text{ cm}^3$  with 1.5 Gy and full 3D active scanning, i.e., with multiple iso-energy layers, would take about 8 minutes, which is prohibitively long for the time-critical calorimetric method. Therefore, a decision was taken to try producing the necessary homogeneous SOBP in a passive way using a static 3D printed 2D modulator. The final criteria that must be satisfied were field homogeneity with standard deviation below 2 % for all values less than 2cm away from the SOBP center, reproducibility of repeated measurements expressed as standard deviation below 0.5 % and a total irradiation time less than 100s, which represented a set of highly challenging requirements.

Before proceeding with the final  $k_Q$  measurements, it is important to first optimize and then completely characterize the 3D dose distribution, resulting from the impinging scanned field on the 2D modulator, in terms of homogeneity, reproducibility, robustness and sensitivity to modulator positioning misalignments, etc., which was the main scope of this work.

In a first step, a  $10 \times 10 \text{ cm}^2$  2D RM was developed and optimized for a homogeneous, 60 mm wide SOBP using a 278 MeV/u monoenergetic carbon ion beam. The pin base

(period) of this first modulator was  $2 \times 2 \text{ mm}^2$ . Two additional RMs, with  $3 \times 3 \text{ mm}^2$  and  $4 \times 4 \text{ mm}^2$  were also designed in order to investigate the interplay effect of the base period with potential manufacturing artefacts on the dose distribution (Figure 22). After confirming the SOBP homogeneity by preliminary FLUKA simulations, all RMs were printed with RIGUR RGD45 material on the Stratasys Objet30 Pro 3D-printer.

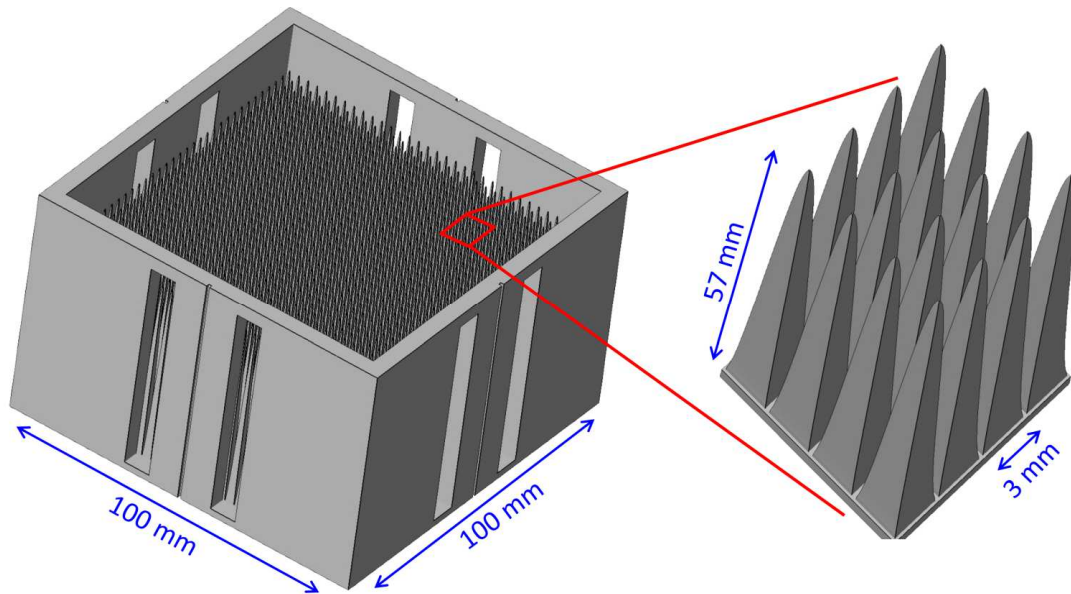


Figure 22. Oblique view of the 2D RM with  $3 \times 3 \text{ mm}^2$  pin base area and detailed view of  $4 \times 4$  pins. Figure taken from (Holm *et al* 2020) – Figure 1.

Dose measurements took place at the Heidelberg Ion Beam Therapy Center (HIT). A small positioning table, which allows defined translation, tilting and rotation of the modulator was used to precisely align the RM to the room lasers. In order to improve the homogeneity, the coordinates of the original scan spots in the raster plan ( $6 \times 6 \text{ cm}^2$  field with scan spots in 2 mm steps) were modified so that three additional raster plans were created. In the first plan the X coordinate was shifted with 1 mm, in the second plan the Y coordinate was shifted with 1 mm and the scan spots in the third plan were shifted in both X and Y. The original plan and the three modified plans were irradiated in sequence for each measurement. This scan pattern resulted in total irradiation time of 90s for a total dose of 1.5Gy.

The dose was measured by both the PTW Peakfinder and the Octavius 1000P placed in a water phantom, similar to WERNER and based on the same procedure developed by (Schuy *et al* 2020). Additionally, high-resolution film measurements were carried out to verify against the 2D Octavius results and ensure that no hot or cold dose spots are present. These Gafchromic EBT3 films were placed at three different depths inside a

phantom to also investigate the blurring of the typical pin scattering pattern behind the modulator as a function of depth.

Figure 23 shows the measured depth dose distribution from the PTW Peakfinder for all three modulators using a 278 MeV/u carbon ion beam. All SOBPs exhibit a similar, approximately 60 mm wide SOBP, apart from the difference in the dose peaks at the proximal and especially at the distal edge.

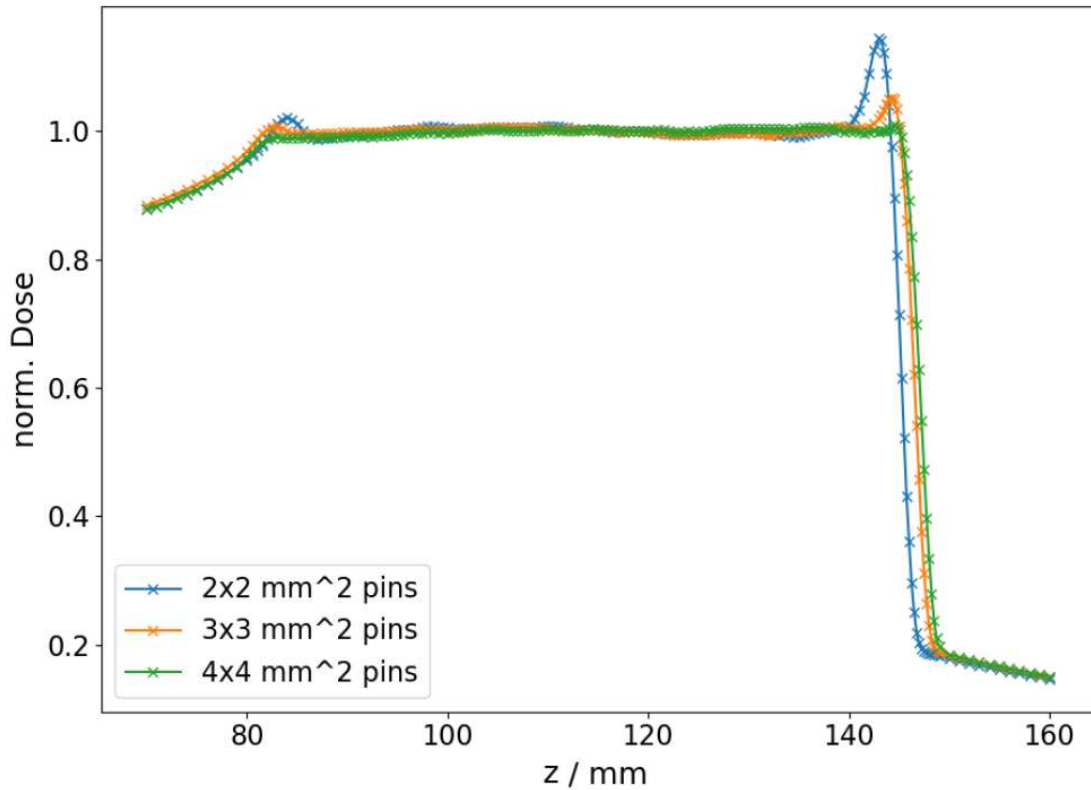


Figure 23. Comparison of the depth dose distributions of 2D RMs with different pin base areas. Measured with the Peakfinder. Figure taken from (Holm *et al* 2020) – Figure 5.

The maximum and relative standard deviations in Table 1, calculated in the plateau region excluding the dose peaks, confirm a very high degree of homogeneity. In the case of 4x4 mm<sup>2</sup> RM the SOBP is completely flat even at the proximal and distal edges.

2DRM	Rel. std. dev. / %	Max. dev. / %
2 × 2 mm <sup>2</sup> pins	0.53	2.08
3 × 3 mm <sup>2</sup> pins	0.44	1.54
4 × 4 mm <sup>2</sup> pins	0.31	1.34

Table 1. Relative standard deviation and maximum relative deviation of doses measured within the plateau region of the SOBP (excluding the dose peaks at the proximal and distal edge) for each 2DRM. Table taken from (Holm *et al* 2020) – Table 1.

This high degree of homogeneity, however, is valid for a perfectly aligned modulator, orthogonal to the impinging field. A potential tilt of the 2D RM is known to introduce dose discrepancies. In order to investigate and quantify the sensitivity of a homogeneous SOBP on the RM alignment, all three modulators were placed on the positioning table and the depth dose distribution was measured for four scenarios: accurate alignment as a reference and then tilt of the RM around the y-axis by  $0.5^\circ$ ,  $1^\circ$  and  $2^\circ$ .

The results are shown in Figure 24. A conclusion can be made that the larger the tilting angle and the smaller the pin base side, the more sensitive and less homogenous the depth dose distribution.

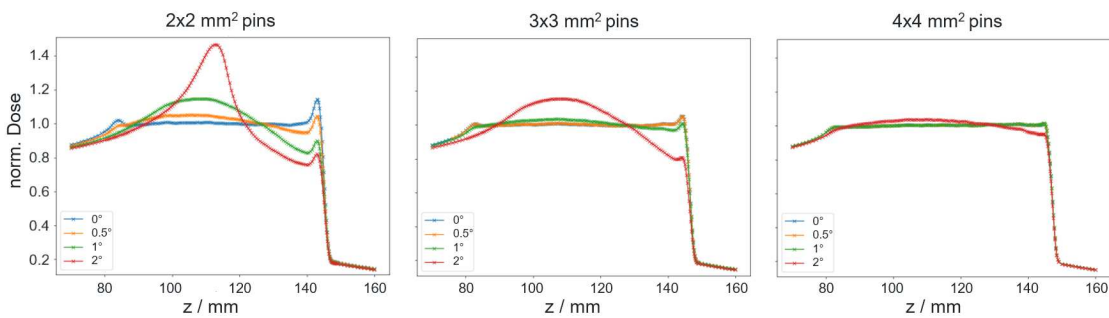


Figure 24. SOBP sensitivity on the tilting ( $0.5^\circ$ ,  $1^\circ$  and  $2^\circ$ ) of the 2D RM as a function of its pin base ( $2 \times 2 \text{ mm}^2$ ,  $3 \times 3 \text{ mm}^2$ ,  $4 \times 4 \text{ mm}^2$ ). Figure taken from (Holm *et al* 2020) – Figure 6.

The lateral homogeneity was also investigated for two modulators ( $3 \times 3 \text{ mm}^2$  and  $4 \times 4 \text{ mm}^2$  pin base) using EBT3 films. Figure 25 shows 2D lateral profiles at three different film positions: in front of the calorimeter (65.5 cm film to RM distance) and at a 5 cm and 10 cm depth in water inside the calorimeter. A scattering pattern, induced by the fine pin structures of the modulator, can be clearly observed for both RMs, especially at the first film position. These inhomogeneities blur out and eventually completely disappear with increasing distance to the RM due to scattering. The larger the pin base, the larger the distance needed to obtain a homogenous lateral profile. At 10cm depth, which corresponds to the middle of the SOBP and the calorimetric measurement position, the  $3 \times 3 \text{ mm}^2$  modulator exhibit a homogeneous profile, whereas the  $4 \times 4 \text{ mm}^2$  has still slightly visible scattering pattern. The slightly better homogeneity of the smaller pin base at this depth is also confirmed by the relative standard deviation, calculated inside the red marked square: 1.32 % for the  $3 \times 3 \text{ mm}^2$  case versus 1.51 % for the  $4 \times 4 \text{ mm}^2$ .

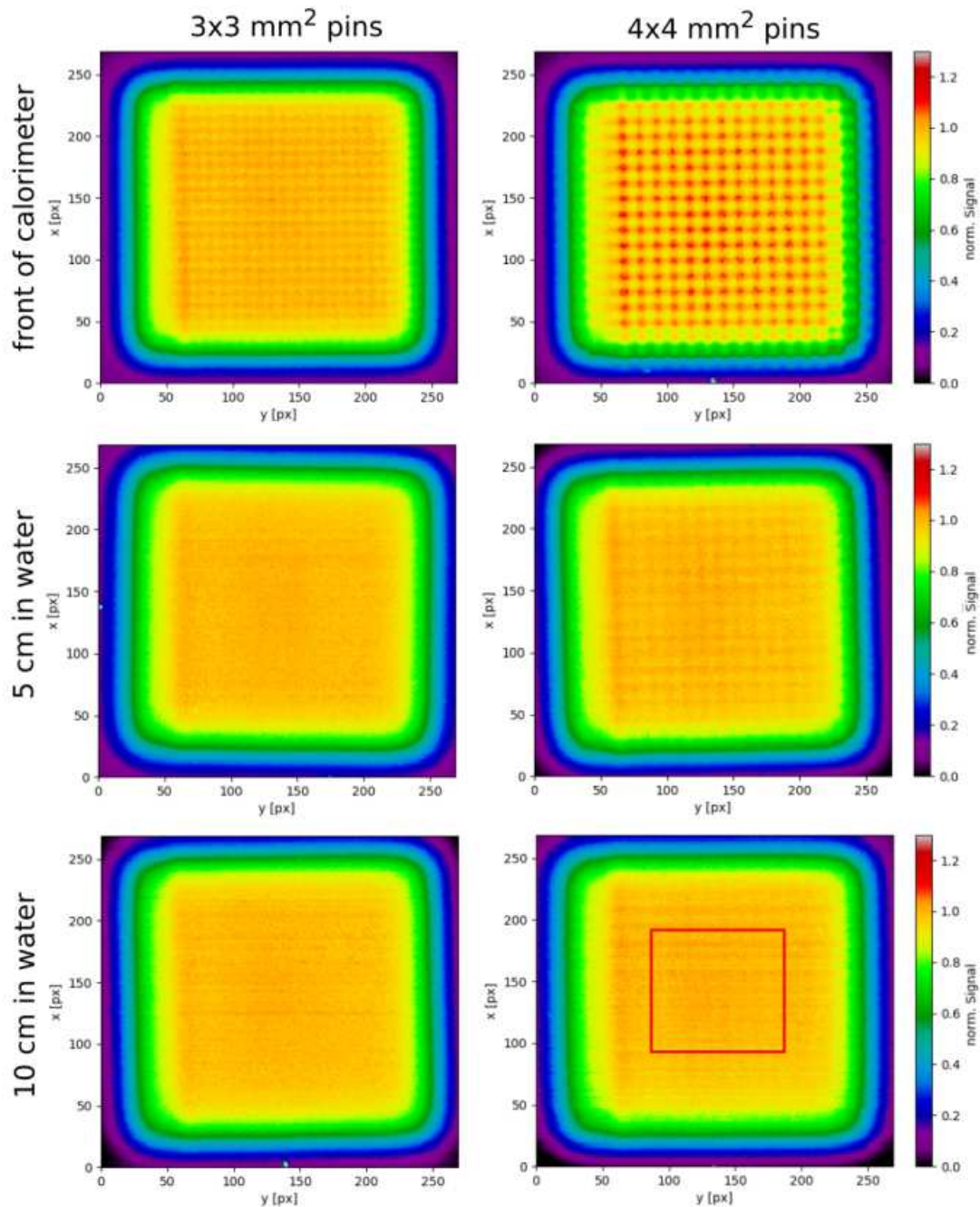


Figure 25. EBT3 film measurements of the lateral dose distributions in front of the calorimeter (top), at a 5 cm depth in water inside the calorimeter (middle) and at a 10 cm depth in water (bottom), which corresponds to the middle of the SOBP and the calorimetric measurement position. Measurements were performed with the 3x3 mm<sup>2</sup> (left) and the 4x4 mm<sup>2</sup> (right) pin base area 2DRM in the beam path. Standard deviations were calculated inside the inner red square, indicated in the lower right picture. Figure taken from (Holm *et al* 2020) – Figure 7.

Based on the presented measurements, a decision was taken to discard the 2x2 mm<sup>2</sup> RM (due to the large distal dose peak and sensitivity to tilt) and the 4x4 mm<sup>2</sup> (due to the slightly worse homogeneity at the calorimetric measurement depth) and conduct the 3D water phantom measurements and later on the final calorimetric measurements with the

3x3 mm<sup>2</sup> RM. In addition, a second identical 3x3 mm<sup>2</sup> RM was manufactured as a backup and for investigating the printer reproducibility.

In a next step, the Octavius Array was placed in the water phantom and moved in 2.5mm steps to measure and reconstruct the 3D dose distribution resulting from both 3x3 mm<sup>2</sup> modulators (original and the backup RM). The dose was measured on seven separate measurement sessions to investigate the robustness and reproducibility of the workflow, positioning, measurement setup, etc.

Figure 26 shows the results from the original RM. The SOBP comparison between the PTW Peakfinder (blue line) and Octavius on the left side reveals a very good agreement. Lateral profiles at different depths along both x and y axis are plotted in the middle and on the right side.

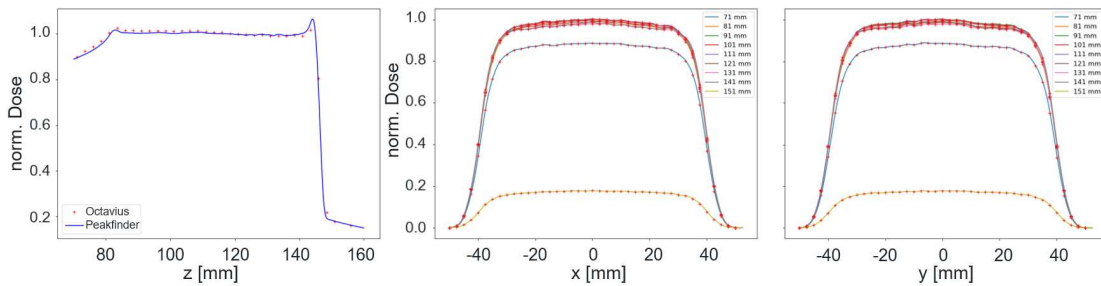


Figure 26. Results of the field characterization measurements using the Octavius water phantom setup: Comparison of the depth dose distribution measured with the Octavius and the Peakfinder (left). Lateral dose distributions for different depths across the x- (middle) and the y-axes (right). The results shown are for measurements performed with the original 3x3 mm<sup>2</sup> pin base area 2D RM. Figure taken from (Holm *et al* 2020) – Figure 8.

The relative standard deviation, calculated inside a 20 mm sphere around the SOBP center, was used to quantify the homogeneity. The results are presented in Table 2 and show very flat 3D dose field around the calorimetric measurement position with all values from both RMs being less than 1.05 %.

The relative standard deviation between the separate measurement sessions was calculated for each dose point inside the 20 mm sphere. An average value of 0.26 % for both modulators reveal a very stable and reproducible field.

This paper presented the application of a 3D printed 2D RM to address the challenge of fast calorimetric measurements in the presence of a scanned carbon ion beam. The 2D RM can create a quasi-static SOBP and its resulting 3D dose distribution was characterized in detail with repeated measurements.



Measurement	Modulator vers.	Rel. std. dev. / %
05-19-19	1	0.78
05-21-19	1	0.97
05-21-19	1	0.83
05-23-19	1	1.03
05-31-19	1	1.05
06-25-19	1	0.78
07-31-19	1	0.91
05-19-19	2	0.71
05-21-19	2	0.92
05-23-19	2	1.00
05-23-19	2	0.98
05-31-19	2	1.02
06-25-19	2	0.86
07-31-19	2	0.85

Table 2. Relative standard deviations of doses measured within a sphere with a 20 mm radius around the calorimetric measurement position for each field characterization measurement. The label “Modulator vers.” in the second column denotes merely the first manufactured prototype and the second backup prototype. Table taken from (Holm *et al* 2020) – Table 3.

The 2D RM fulfilled the strict necessary criteria in terms of time constraints, dose homogeneity and reproducibility. All in all, the modulator managed to solve an important problem and thus contribute to the successful outcome of the final project, namely the experimental determination of  $k_Q$  factors for two ICs by means of water calorimetry.

The final  $k_Q$  measurements were conducted later and published in a separate article which is not the scope of this dissertation.

### 3.3.2. Contribution

K. Holm conducted the measurements, executed the study, analysed the final results and wrote the manuscript. A. Krauss, O. Jäkel and S. Greilich supported and supervised the whole study.

Y. Simeonov and U. Weber designed and optimized the 2D modulators. Y. Simeonov conducted the initial MC simulations of all modulators to validate the correct modulating properties and sufficient SOBP homogeneity before manufacturing.

Y. Simeonov manufactured all modulators. U. Weber and Y. Simeonov contributed to the planning and development of the Octavius water phantom measurement concept.

All authors revised this manuscript, substantively.

#### 4. DISCUSSION

The 2D and 3D RMs developed and presented in this work managed to achieve the desired homogeneous SOBPs and conformal 3D dose distributions, which was initially confirmed by MC simulations. Important progress was made in the process chain by modifying and improving the filigree structures of the modulators, so that we eventually succeeded in translating the theoretical modulation function and CAD design into high-quality prototypes using advanced manufacturing techniques.

The modulating properties, resulting dose distribution and SOBP homogeneity of these beam modulating prototypes depend strongly on the absolute manufacturing accuracy of the 3D printer and particularly on the preservation of the correct height-dependent partial pin areas in the manufactured prototype. As the modulators consist of many adjacent pins, the small space between the pins (groove area) has proved to be pretty susceptible to manufacturing artefacts. Some printers might fill this groove with unnecessary material, either due to the lack of sufficient resolution and a large spot size of the laser curing the photopolymer or due to the lack of support material between the pins. Minor deviations in this area lead to dose discrepancies and/or sharp dose peaks at the distal SOBP edge, which is consistent with our observations from the prototypes manufactured on different machines over the past years.

The SOBP, resulting from the polymer RM in (Simeonov *et al* 2021), Figure 10, clearly exhibits a high degree of homogeneity. Systematic artefacts, previously observed with this same machine (extra material in the groove area, shorter pins, etc.) are not visible anymore, as the revised pin design has a more favourable profile, less prone to manufacturing issues. The measured SOBP has accordingly an excellent agreement with the FLUKA simulations with 1.4 % maximum deviation and a relative standard deviation of 0.59 % in the flat SOBP region, homogeneity considered sufficient enough for radiobiological experiments as well as potential pre-clinical experiments.

While we have managed to achieve excellent SOBP flatness with the polymer RM, it is noteworthy, however, that this was a general pin form improvement. Each manufacturing technique (Stereolithography, PolyJet, SLM) and printer have their intrinsic weaknesses and strengths and tend to introduce their specific issues and artefacts. Therefore, additional printer-specific corrections will often be necessary to produce pin shapes with partial areas corresponding exactly to the original CAD models.

For example, the SOBP of the SLM manufactured steel RM in Figure 11 has a slight dose tilt particularly towards the distal edge, which compromises the overall homogeneity. Quantifying the dose tilt reveals a 4 % maximum deviation and a relative standard deviation of 0.86 %. A printer specific correction can be applied either to the machine itself or to the pin profile to further improve the SOBP homogeneity after a thorough examination of the fundamental root cause.

In contrast to the polymer 2D modulator in Figure 10 (Simeonov *et al* 2021), which was optimized for a proton beam, (Holm *et al* 2020) used polymer modulators optimized for a carbon ion beam. Carbon modulators are generally more prone to manufacturing artefacts and SOBP inhomogeneities than the proton ones. The reason for this is twofold: Firstly, the intrinsic modulation weights distribution of a carbon RM results in adjacent pins with very little space (groove) between each other, less than the grooves of a proton RM and thus more prone to manufacturing issues (Simeonov *et al* 2017). Secondly, the sharp carbon BP is more unforgiving to small manufacturing artefacts along the pin profile than the corresponding depth-equivalent proton BP. These are some of the reasons (together with the slight groove profile improvement in Figure 7) why the proton polymer RM in Figure 10 delivered a “perfect” SOBP without a distal dose peak, whereas the carbon polymer RM in Figure 23 with the same pin base side of 3x3 mm<sup>2</sup> exhibits a distal peak. The filling of the pin grooves with ~ 2.5 mm extra material in the case of the 2x2 mm<sup>2</sup> and ~1 mm for the 3x3 mm<sup>2</sup> RM was identified to be the root cause of the distal peak, a fact also confirmed by the different relative depth shifts of the distal SOBP edges (blue and yellow curves shifted relative to the green one). Enlarging the pin base area to 4x4 mm<sup>2</sup> created enough space between the pins so that the distal peak completely disappeared. An additional advantage of the larger pin base side is the more favourable pin aspect ratio leading to less dose sensitivity when tilting the modulator (Figure 24). However, the potential of increasing the pin base side is limited as it comes at the cost of a more pronounced pin scattering pattern behind the RM (Figure 25) and more importantly less precise sampling and reproduction of the 3D proximal and distal target edges in the case of a patient-specific 3D RM.

Apart from the small distal dose peak, which was considered negligible for the calorimetric dose measurement in the SOBP middle, the 3x3 mm<sup>2</sup> pin base RM chosen for the final measurements was successful in delivering the homogeneous carbon SOBP needed. Furthermore, the multiple measurement sessions over a period of 10 weeks demonstrated the excellent long term mechanical stability and integrity of the RM, as

proven by the low relative standard deviation (0.26 %) calculated from the separate measurements. Therefore, the manufacturing and application of 2D RMs customized for solving specific problems is viable. They have a number of intrinsic advantages, i.e., relatively low cost, fast (in-house) manufacturing, SOBP easily adjustable for the specific experiment, etc. (Horst *et al* 2023). As a matter of fact, we have manufactured and provided multiple 2D RMs to our collaboration partners from several different research institutions, as the interest in the particle therapy community has been constantly growing. Among them are the Trento proton therapy centre utilizing a 2D RM for radiobiology research and cell survival experiments (Tommasino *et al* 2019), the GSI Biophysics department investigating the biological effect in ion beam therapy, the Heavy Ion Medical Accelerator at Chiba (HIMAC) testing PET imaging in the SOBP of radioactive  $^{11}\text{C}$  beam, the HollandPTC in Delft and Heidelberg Ion Beam Therapy Center (HIT) for pre-clinical biological research.

The advantages of these modulators, most importantly the quasi-instantaneous SOBP, can be applied to conform the dose to a complex target to reduce the irradiation time substantially, as demonstrated in (Simeonov *et al* 2022) with a proton beam and a right lung target. Due to the outstanding reproducibility of high-quality 3D printers, the excellent SOBP flatness observed in the case of the 2D polymer RM was completely preserved going to a much more complex 3D modulator shape. Figure 17 - Figure 19 reveal a very good agreement between the measured and predicted dose distribution. The impact of potential manufacturing artefacts, such as dose oscillations, dose peaks, etc., most easily identified in the depth dose distribution is not present (Figure 18). It is at this stage clear that, although challenging, obtaining the desired pre-calculated modulated dose distribution by means of 3D-printed prototypes is possible for complex fields and target shapes.

Apart from manufacturing issues, a tilt of the modulator and/or the Octavius array are additional uncertainties that can lead to deterioration of the measured dose and deviations from the MC simulation. As these uncertainties are, at least in our particular measurement setup, pretty much “user-dependent” and as such variable in nature and to a great extent preventable, it is important to highly prioritize a proper alignment of all devices in the beam path during the measurement.

A tilt of the RM has been shown to modify a flat SOBP into a Gaussian-like distribution. No such dose deviation can be observed in the widest, most sensitive SOBP

in Figure 18b. Consulting the multiparameter tilt investigation in Figure 24, the RM seems to have been aligned with accuracy much less than  $1^\circ$ .

The accurate alignment of the Octavius array inside the water phantom should not be neglected either. While a small tilt of the detector is irrelevant in a homogeneous dose region, it will manifest in a lateral dose tilt in high dose gradient regions like the SOBP distal edge. This is an effect that should be kept in mind and not mistakenly associated with dose artefacts from the modulator itself. In order to minimize the impact of the detector positioning on the measurements, we established a protocol to perform initial measurements at the sharp pristine BP distal edge, evaluate the lateral dose symmetry and fine tune the detector along the correct axis to reduce its tilt down to  $\leq 0.2^\circ$ . This procedure was adopted for all dose measurements with the Octavius, including the ones presented in this work and is one more of the small, but important details, leading to the excellent agreement between simulations and measurements.

Figure 17e shows an overlay of the dose on the original PTV contour. The 90 % isodose curve surrounds tightly the target confirming the very good distal and proximal dose conformity. This is relevant in the light of the fact that achieving a good proximal conformity is considered to be one of the advantages of the 3D RM method compared to the conventional passive scattering.

An important point to mention is the slight negative impact of the 3D RM on the lateral dose fall-off due to the additional scattering in the modulator material. While this effect cannot be prevented, it can be mitigated by bringing the nozzle holding the modulator closer to the patient. A slight broadening of the lateral penumbra will have to be accepted as a trade-off for a faster treatment and potential FLASH irradiation.

Additional method for assessing the dose distribution is by calculating the cumulative DVH as presented in Figure 20. Both the measured and simulated curves agree very well and exhibit a relatively sharp dose fall-off, indicative of the high degree of homogeneity inside the target.

The dose distribution from the aluminium RM, manufactured with selective laser melting is shown in Figure 21. As the material and pin shape of the modulator changed, additional MC simulations and a new scan spot weight optimization had to be conducted. Once again, both data sets are in very good agreement. These results are important insofar as a complete workflow process chain has been demonstrated and successfully validated with a new material, different printer and alternative manufacturing technique, thus

completing one more step towards establishing fast 3D manufacturing as a feasible option for patient-specific modulators.

The final question that must be answered is related to the total irradiation time, as a very fast dose application is the ultimate goal of the 3D modulator concept. A conventional multi-energy treatment plan for the right lung target in our experiment would take approximately 60 seconds, mostly due to the energy switching time, while the single-energy irradiation in combination with the 3D RM lasted only 6 seconds. This factor of 10 in the delivery time reduction was only limited by the synchrotron capabilities in MIT. A cyclotron, as used with most commercial proton facilities, can deliver much higher currents thus enabling treatment times in less than 1 second.

The presented results indicate the potential of the 3D RM concept. One important limitation that should be addressed is that, in contrast to our “water” CT simulations, a real patient consists of a complex tissue composition, which must be taken into account. Nevertheless, the fundamental mathematical and physics principles of the modulation concept are still the same. Unpublished results from our latest collaborations have shown that the 3D RM concept is completely valid for the more realistic case of a heterogeneous patient CT. Moreover, an inverse optimization of the pins and modulator shape, in contrast to the presented “forward” approach based on a pre-calculated pin database, is expected to further improve the dose conformity and homogeneity. For example, a commercial treatment planning system (TPS) with more sophisticated algorithms can be used to “inversely” optimize one or even more objective functions (dose, dose rate, etc.). This is especially relevant in the case of FLASH irradiation, where the minimum dose rate and dose rate distribution are additional parameters of vital importance. The final raster plan resulting from such an optimization contains iso-energy layers together with a scan spot map and the corresponding weights. By sorting the iso-energy layers per scan spot, the set of weights can be converted into a set of pin profiles to design a 3D modulator. Additional parameter constraints should be implemented in this case to generate more “printer-friendly” pin shapes and limit the minimum pin tip and groove area size to realistic values that can be manufactured artefact-free.

In a clinical routine, it would be optimal to find and in the best case quantify potential manufacturing issues immediately after producing the modulator and not during the later stage of dose verification. Potential QA methods could include tactile measurements, microscopic or  $\mu$ CT imaging of the modulator. These methods, however, prove to be either prohibitively complex and time consuming in practice or deliver unsatisfactory

results, mostly due to the extremely fine pin structures comprising the modulator. Therefore, the most reliable method seems to be the complete, high-resolution measurement of the resulting 3D dose distribution. While we have demonstrated a fast measurement procedure, a clinical workflow setup will differ somewhat. For example, positioning the RM on the treatment table in front of the patient is not a practical solution and anyway impossible in facilities where different gantry angles are used. Moreover, in the case of FLASH irradiation, where the maximum available beam energy will most probably be used to achieve the maximum current, an additional thick PMMA absorber is needed to shift the BP inside the patient. Given the additional scattering from the PMMA block, an aperture might be included too. All of these beam modifying and shaping devices will have to find place in the nozzle of the gantry and more importantly, be aligned accurately to each other and the beam axis. It is important to ensure that the rotation of the gantry and the additional combined weight of RM, PMMA and aperture do not introduce additional alignment and reproducibility issues. Given all other range and positioning uncertainties, etc., not related to the modulator, the RM must be aligned with accuracy way below  $1^\circ$  in order to preserve a clinically acceptable total uncertainty budget.

## 5. CONCLUSION AND OUTLOOK

This work introduced the concept of static range-modulating devices manufactured by rapid prototyping for the very fast dose application with only one fixed energy and a scanned particle beam. The development of 2D modulators was presented (Simeonov *et al* 2021) and their application was validated in a research project for high-precision water calorimetry (Holm *et al* 2020). Finally, the concept was extended to a 3D modulator customized to a patient-specific target shape (Simeonov *et al* 2022).

All modulators were manufactured with high-quality 3D printers. Different materials and printing techniques were utilized. The resulting modulated dose distribution was first validated by MC simulations. Then a sophisticated water phantom system (WERNER) was deployed to obtain fast, completely automated and high resolution dose measurements.

Overall, an end-to-end process chain has been demonstrated, from the RM development to the final dose evaluation. Highly homogeneous dose distributions were achieved with a very good agreement between the predicted and measured data. In the case of the 3D RM, the delivered dose was additionally conformed to both the proximal and distal edge of the target.

Last but not least, the modulators managed to deliver the prescribed dose in a fraction of the time required for conventional scanned particle therapy.

For a potential clinical application, the development workflow of a 3D modulator must be first implemented into a commercial treatment planning system. This will enable the utilization of the full spectrum of the most advanced optimization algorithms and objective functions. Reaching the maximum available machine current for millisecond FLASH irradiation of large targets will probably require scan spot reduction methods to increase the number of monitor units (MU) in each scan spot. The implementation and geometry generation of the 3D RM in a TPS must be carefully benchmarked whether the modulator can reproduce the energy spectrum of the original conventional raster plan. This will be particularly important in the case of scan spot reduced plans where the missing pin geometry must be interpolated between the sparse irregular scan spots in such a way that the dose homogeneity and conformity of the original plan is preserved. The integration and thorough validation of the 3D RM concept workflow in a commercial TPS is considered to be a fundamental requirement for the clinical adoption.



Regarding the impact of 3D-printed modulators in the particle therapy community, it can be stated that the initial research interest that started with the 2D modulators has also translated to 3D modulators. While several years ago our working group was one of the few if any worldwide developing 3D-printed range-modulators, many others have been formed in the meantime to investigate the potential of this method. Especially the recent surge in FLASH radiobiology experiments has generated a lot of interest towards 3D modulators not only among research institutions, but also among renowned commercial companies. The reason for this is simple as, apart from transmission therapy, the 3D RM seems to be the only clinically viable option for FLASH (Jolly *et al* 2020).

The growing interest has also manifested in a rapidly increasing number of contributions on this topic at international conferences. Our working group was recently contacted by Varian (Siemens Healthineers company), one of the major players in the particle therapy community. We have been collaborating with Varian in the framework of a research project to address remaining challenges and further advance the technical development towards a potential FLASH application.

It is noteworthy that, as a result of the recent developments, several companies have not only filed, but have also been granted patents in USA, Europa and China for a potential modulator development in FLASH therapy. More importantly, our initial fundamental work (Simeonov *et al* 2017) has contributed to the advancement of this method and has been accordingly referenced and cited in all of these patents. “*Ridge filter and method for designing same in a PBS treatment system*” from IBA and “*Static device for use in radiotherapy treatment and design method for such a device*” from RAYSEARCH LAB AB are a few to mention.

IBA has registered the trade name “ConformalFLASH®” for the application of 3D RMs for FLASH irradiation and is pushing forward to establish this method. It has recently announced different collaboration agreements, amongst others one with the University of Kansas Medical Center (KUMC) to advance preclinical research using their Proteus®ONE machine. Positive outcome from these trials will be undoubtedly beneficial for a potential adoption.

The presented work demonstrates the feasibility of using 3D-printed range-modulators in particle therapy. The 3D RM concept combines extremely short irradiation times with a high degree of dose conformity and homogeneity, promising clinically applicable dose distributions for lung and/or FLASH treatment, potentially comparable and competitive to those from conventional irradiation techniques. While bringing a final, approved

medical class product to the market and establishing a new treatment procedure, based and backed by (pre)-clinical studies is a complex long-term process, given the aforementioned development in this field and the multiple ongoing projects, the author of this work is hopeful and cautiously optimistic for the transition of the range-modulator concept from a purely research topic into a clinically feasible option.

## 6. REFERENCES

- Adrian G, Konradsson E, Lempart M, Bäck S, Ceberg C and Petersson K 2019 The FLASH effect depends on oxygen concentration *Br. J. Radiol.* **93** 20190702
- Akagi T, Higashi A, Tsugami H, Sakamoto H, Masuda Y and Hishikawa Y 2003 Ridge filter design for proton therapy at Hyogo Ion Beam Medical Center *Phys. Med. Biol.* **48** N301
- Andreo P, Burns D and Nahum A 2017 *Fundamentals of Ionizing Radiation Dosimetry von Pedro/Burns Andreo (gebundenes Buch)* (John Wiley & Sons)
- Baskar R, Lee K A, Yeo R and Yeoh K-W 2012 Cancer and Radiation Therapy: Current Advances and Future Directions *Int. J. Med. Sci.* **9** 193–9
- Battistoni G, Bauer J, Boehlen T T, Cerutti F, Chin M P W, Dos Santos Augusto R, Ferrari A, Ortega P G, Kozłowska W, Magro G, Mairani A, Parodi K, Sala P R, Schoofs P, Tessonier T and Vlachoudis V 2016 The FLUKA Code: An Accurate Simulation Tool for Particle Therapy *Front. Oncol.* **6** Online: <http://www.ncbi.nlm.nih.gov/pmc/articles/PMC4863153/>
- Battistoni G, Boehlen T, Cerutti F, Chin P W, Esposito L S, Fassò A, Ferrari A, Lechner A, Empl A, Mairani A, Mereghetti A, Ortega P G, Ranft J, Roesler S, Sala P R, Vlachoudis V and Smirnov G 2015 Overview of the FLUKA code *Ann. Nucl. Energy* **82** 10–8
- Battistoni G, Cerutti F, Engel R, Fasso A, Gadioli E, Garzelli M V, Ranft J, Roesler S and Sala P R 2006 Recent Developments in the FLUKA nuclear reaction models *Proc 11th Int Conf Nucl. React. Mech.* 13
- Baumann K-S, Derksen L, Witt M, Burg J M, Engenhardt-Cabillic R and Zink K 2021 Monte Carlo calculation of beam quality correction factors in proton beams using FLUKA *Phys. Med. Biol.* **66** 17NT01
- Bert C, Grözinger S O and Rietzel E 2008 Quantification of interplay effects of scanned particle beams and moving targets *Phys. Med. Biol.* **53** 2253
- Blattmann H, Coray A, Pedroni E and Greiner R 1990 Spot scanning for 250 MeV protons *Strahlenther. Onkol. Organ Dtsch. Rontgengesellschaft Al* **166** 45–8
- Böhlen T T, Cerutti F, Chin M P W, Fassò A, Ferrari A, Ortega P G, Mairani A, Sala P R, Smirnov G and Vlachoudis V 2014 The FLUKA Code: Developments and Challenges for High Energy and Medical Applications *Nucl. Data Sheets* **120** 211–4
- Chu W T, Ludewigt B A and Renner T R 1993 Instrumentation for treatment of cancer using proton and light-ion beams *Rev. Sci. Instrum.* **64** 2055–122
- Diffenderfer E S, Sørensen B S, Mazal A and Carlson D J 2022 The current status of preclinical proton FLASH radiation and future directions *Med. Phys.* **49** 2039–54

- Diffenderfer E S, Verginadis I I, Kim M M, Shoniyozov K, Velalopoulou A, Goia D, Putt M, Hagan S, Avery S, Teo K, Zou W, Lin A, Swisher-McClure S, Koch C, Kennedy A R, Minn A, Maity A, Busch T M, Dong L, Koumenis C, Metz J and Cengel K A 2020 Design, Implementation, and in Vivo Validation of a Novel Proton FLASH Radiation Therapy System *Int. J. Radiat. Oncol. • Biol. • Phys.* **106** 440–8
- Durante M, Bräuer-Krisch E and Hill M 2018 Faster and safer? FLASH ultra-high dose rate in radiotherapy *Br. J. Radiol.* **91** Online: <https://www.ncbi.nlm.nih.gov/pmc/articles/PMC5965780/>
- Durante M, Orecchia R and Loeffler J S 2017 Charged-particle therapy in cancer: clinical uses and future perspectives *Nat. Rev. Clin. Oncol.* **14** 483–95
- Favaudon V, Caplier L, Monceau V, Pouzoulet F, Sayarath M, Fouillade C, Poupon M-F, Brito I, Hupé P, Bourhis J, Hall J, Fontaine J-J and Vozenin M-C 2014 Ultrahigh dose-rate FLASH irradiation increases the differential response between normal and tumor tissue in mice *Sci. Transl. Med.* **6** 245ra93-245ra93
- Ferrari A, Sala P R, Fassò A and Ranft J 2005 *FLUKA: A multi-particle transport code (program version 2005)* (CERN)
- Ferrari A, Sala P R, Guaraldi R and Padoani F 1992 An improved multiple scattering model for charged particle transport *Nucl. Instrum. Methods Phys. Res. Sect. B Beam Interact. Mater. At.* **71** 412–26
- Folkerts M M, Abel E, Busold S, Perez J R, Krishnamurthi V and Ling C C 2020 A framework for defining FLASH dose rate for pencil beam scanning *Med. Phys.* **47** 6396–404
- Furukawa T, Inaniwa T, Sato S, Shirai T, Takei Y, Takeshita E, Mizushima K, Iwata Y, Himukai T, Mori S, Fukuda S, Minohara S, Takada E, Murakami T and Noda K 2010 Performance of the NIRS fast scanning system for heavy-ion radiotherapy *Med. Phys.* **37** 5672–82
- Gardey K-U, Oelfke U and Lam G K Y 1999 Range modulation in proton therapy - an optimization technique for clinical and experimental applications *Phys. Med. Biol.* **44** N81
- Gottschalk B, Koehler A M, Schneider R J, Sisterson J M and Wagner M S 1993 Multiple Coulomb scattering of 160 MeV protons *Nucl. Instrum. Methods Phys. Res. Sect. B Beam Interact. Mater. At.* **74** 467–90
- Haberer Th, Becher W, Schardt D and Kraft G 1993 Magnetic scanning system for heavy ion therapy *Nucl. Instrum. Methods Phys. Res. Sect. Accel. Spectrometers Detect. Assoc. Equip.* **330** 296–305
- Highland V L 1975 Some practical remarks on multiple scattering *Nucl. Instrum. Methods* **129** 497–9
- Holm K M, Weber U, Simeonov Y, Krauss A, Jäkel O and Greilich S 2020 2D range modulator for high-precision water calorimetry in scanned carbon-ion beams *Phys. Med. Biol.* **65** 215003

- Horst F, Beyreuther E, Bodenstern E, Gantz S, Misseroni D, Pugno N M, Schuy C, Tommasino F, Weber U and Pawelke J 2023 Passive SOBP generation from a static proton pencil beam using 3D-printed range modulators for FLASH experiments *Front. Phys.* **11** Online: <https://www.frontiersin.org/articles/10.3389/fphy.2023.1213779>
- Hughes J R and Parsons J L 2020 FLASH Radiotherapy: Current Knowledge and Future Insights Using Proton-Beam Therapy *Int. J. Mol. Sci.* **21** 6492
- Ishikawa H, Tsuji H, Murayama S, Sugimoto M, Shinohara N, Maruyama S, Murakami M, Shirato H and Sakurai H 2019 Particle therapy for prostate cancer: The past, present and future *Int. J. Urol.* **26** 971–9
- Ishizaki A, Ishii K, Kanematsu N, Kanai T, Yonai S, Kase Y, Takei Y and Komori M 2009 Development of an irradiation method with lateral modulation of SOBP width using a cone-type filter for carbon ion beams *Med. Phys.* **36** 2222–7
- Jolly S, Owen H, Schippers M and Welsch C 2020 Technical challenges for FLASH proton therapy *Phys. Med.* **78** 71–82
- Ju S G, Kim M K, Hong C-S, Kim J S, Han Y, Choi D H, Shin D and Lee S B 2014 New Technique for Developing a Proton Range Compensator With Use of a 3-Dimensional Printer *Int. J. Radiat. Oncol.* **88** 453–8
- Koehler A M, Schneider R J and Sisterson J M 1975 Range modulators for protons and heavy ions *Nucl. Instrum. Methods* **131** 437–40
- Konda Gokuldoss P, Kolla S and Eckert J 2017 Additive Manufacturing Processes: Selective Laser Melting, Electron Beam Melting and Binder Jetting—Selection Guidelines *Materials* **10** Online: <https://www.ncbi.nlm.nih.gov/pmc/articles/PMC5554053/>
- Kraft G 2000 Tumor therapy with heavy charged particles *Prog. Part. Nucl. Phys.* **45** S473–544
- Krieger M, van de Water S, Folkerts M M, Mazal A, Fabiano S, Bizzocchi N, Weber D C, Safai S and Lomax A J 2022 A quantitative FLASH effectiveness model to reveal potentials and pitfalls of high dose rate proton therapy *Med. Phys.* **49** 2026–38
- Kruth J, Mercelis P, Van Vaerenbergh J, Froyen L and Rombouts M 2005 Binding mechanisms in selective laser sintering and selective laser melting *Rapid Prototyp. J.* **11** 26–36
- Lambert J, Suchowerska N, McKenzie D R and Jackson M 2005 Intrafractional motion during proton beam scanning *Phys. Med. Biol.* **50** 4853
- Lindsay C, Kumlin J, Jirasek A, Lee R, Martinez D M, Schaffer P and Hoehr C 2015 3D printed plastics for beam modulation in proton therapy *Phys. Med. Biol.* **60** N231

- Lindsay C, Kumlin J, Martinez D M, Jirasek A and Hoehr C 2016 Design and application of 3D-printed stepless beam modulators in proton therapy *Phys. Med. Biol.* **61** N276
- Linz U 2012 *Ion Beam Therapy: Fundamentals, Technology, Clinical Applications* vol 320 (Berlin, Heidelberg: Springer) Online: <https://link.springer.com/10.1007/978-3-642-21414-1>
- Low D A, Harms W B, Mutic S and Purdy J A 1998 A technique for the quantitative evaluation of dose distributions *Med. Phys.* **25** 656–61
- van Marlen P, Dahele M, Folkerts M, Abel E, Slotman B J and Verbakel W 2021 Ultra-High Dose Rate Transmission Beam Proton Therapy for Conventionally Fractionated Head and Neck Cancer: Treatment Planning and Dose Rate Distributions *Cancers* **13** Online: <https://www.ncbi.nlm.nih.gov/pmc/articles/PMC8070061/>
- Moliere G 1948 Theorie der Streuung schneller geladener Teilchen II Mehrfach-und Vielfachstreuung *Z. Für Naturforschung A* **3** 78–97
- Möller T and Trumbore B 2005 Fast, Minimum Storage Ray/Triangle Intersection *ACM SIGGRAPH 2005 Courses SIGGRAPH '05* (New York, NY, USA: ACM) Online: <http://doi.acm.org/10.1145/1198555.1198746>
- Paganetti H 2016 *Proton Beam Therapy* (IOP Publishing) Online: <http://iopscience.iop.org/book/978-0-7503-1370-4>
- Paganetti H 2012 *Proton therapy physics* (Boca Raton, FL: CRC Press/Taylor & Francis) Online: <http://www.crcnetbase.com/isbn/9781439836453>
- Parodi K, Ferrari A, Sommerer F and Paganetti H 2007 Clinical CT-based calculations of dose and positron emitter distributions in proton therapy using the FLUKA Monte Carlo code *Phys. Med. Biol.* **52** 3369
- Parodi K, Mairani A, Brons S, Hasch B G, Sommerer F, Naumann J, Jäkel O, Haberer T and Debus J 2012 Monte Carlo simulations to support start-up and treatment planning of scanned proton and carbon ion therapy at a synchrotron-based facility *Phys. Med. Biol.* **57** 3759
- Podgorsak E B 2016 *Radiation Physics for Medical Physicists* (Cham: Springer International Publishing) Online: <http://link.springer.com/10.1007/978-3-319-25382-4>
- Rietzel E and Bert C 2010 Respiratory motion management in particle therapy *Med. Phys.* **37** 449–60
- Ringbæk T P, Weber U, Petersen J B, Thomsen B and Bassler N 2014 Monte Carlo simulations of new 2D ripple filters for particle therapy facilities *Acta Oncol.* **53** 40–9
- Romano F, Bailat C, Jorge P G, Lerch M L F and Darafsheh A 2022 Ultra-high dose rate dosimetry: Challenges and opportunities for FLASH radiation therapy *Med. Phys.* **49** 4912–32

- Rothwell B, Lowe M, Traneus E, Krieger M and Schuemann J 2022 Treatment planning considerations for the development of FLASH proton therapy *Radiother. Oncol.* **175** 222–30
- Safai S, Bula C, Meer D and Pedroni E 2012 Improving the precision and performance of proton pencil beam scanning *Transl. Cancer Res.* **1** 196–206
- Sakae T, Nohtomi A, Maruhashi A, Sato M, Hosono K, Terunuma T, Kohno R, Akine Y and Hayakawa Y 2001 Three-dimensional conformal irradiation with a multilayer energy filter for proton therapy *Rev. Sci. Instrum.* **72** 234–6
- Sakae T, Nohtomi A, Maruhashi A, Sato M, Terunuma T, Kohno R, Akine Y, Hayakawa Y and Koike Y 2000 Multi-layer energy filter for realizing conformal irradiation in charged particle therapy *Med. Phys.* **27** 368–73
- Sakae T, Nohtomi A, Tsunashima Y, Terunuma T, Sato M, Hayakawa Y and Maruhashi A 2003 Conformal irradiation by proton beam scanning and multilayer energy filter *Rev. Sci. Instrum.* **74** 1292–5
- Schaffner B, Kanai T, Futami Y, Shimbo M and Urakabe E 2000 Ridge filter design and optimization for the broad-beam three-dimensional irradiation system for heavy-ion radiotherapy *Med. Phys.* **27** 716–24
- Schlegel W, Karger C P and Jäkel O 2018 *Medizinische Physik: Grundlagen – Bildgebung – Therapie – Technik* (Berlin, Heidelberg: Springer) Online: <http://link.springer.com/10.1007/978-3-662-54801-1>
- Schuy C, Simeonov Y, Durante M, Zink K and Weber U 2020 Technical note: Vendor-agnostic water phantom for 3D dosimetry of complex fields in particle therapy *J. Appl. Clin. Med. Phys.*
- Schwarz M, Traneus E, Safai S, Kolano A and van de Water S 2022 Treatment planning for Flash radiotherapy: General aspects and applications to proton beams *Med. Phys.* **49** 2861–74
- Simeonov Y, Weber U, Penchev P, Ringbæk T P, Schuy C, Brons S, Engenhardt-Cabillic R, Bliedtner J and Zink K 2017 3D range-modulator for scanned particle therapy: development, Monte Carlo simulations and experimental evaluation *Phys. Med. Biol.* **62** 7075–96
- Simeonov Y, Weber U, Schuy C, Engenhardt-Cabillic R, Penchev P, Durante M and Zink K 2021 Monte Carlo simulations and dose measurements of 2D range-modulators for scanned particle therapy *Z. Für Med. Phys.* **31** 203–14
- Simeonov Y, Weber U, Schuy C, Engenhardt-Cabillic R, Penchev P, Flatten V and Zink K 2022 Development, Monte Carlo simulations and experimental evaluation of a 3D range-modulator for a complex target in scanned proton therapy *Biomed. Phys. Eng. Express* **8** 035006
- Sommerer F, Parodi K, Ferrari A, Poljanc K, Enghardt W and Aiginger H 2006 Investigating the accuracy of the FLUKA code for transport of therapeutic ion beams in matter *Phys. Med. Biol.* **51** 4385

- Strijckmans K 2001 The isochronous cyclotron: principles and recent developments *Comput. Med. Imaging Graph.* **25** 69–78
- Sung H, Ferlay J, Siegel R L, Laversanne M, Soerjomataram I, Jemal A and Bray F 2021 Global Cancer Statistics 2020: GLOBOCAN Estimates of Incidence and Mortality Worldwide for 36 Cancers in 185 Countries *CA. Cancer J. Clin.* **71** 209–49
- Tommasino F, Rovituso M, Bortoli E, La Tessa C, Petringa G, Lorentini S, Verroi E, Simeonov Y, Weber U, Cirrone P, Schwarz M, Durante M and Scifoni E 2019 A new facility for proton radiobiology at the Trento proton therapy centre: Design and implementation *Phys. Med.* **58** 99–106
- Trevisan F, Calignano F, Lorusso M, Pakkanen J, Aversa A, Ambrosio E P, Lombardi M, Fino P and Manfredi D 2017 On the Selective Laser Melting (SLM) of the AlSi10Mg Alloy: Process, Microstructure, and Mechanical Properties *Materials* **10** Online: <https://www.ncbi.nlm.nih.gov/pmc/articles/PMC5344617/>
- Tsai Y-S 1974 Pair production and bremsstrahlung of charged leptons *Rev. Mod. Phys.* **46** 815–51
- Vozenin M-C, Fornel P D, Petersson K, Favaudon V, Jaccard M, Germond J-F, Petit B, Burki M, Ferrand G, Patin D, Bouchaab H, Ozsahin M, Bochud F, Bailat C, Devauchelle P and Bourhis J 2019 The Advantage of FLASH Radiotherapy Confirmed in Mini-pig and Cat-cancer Patients *Clin. Cancer Res.* **25** 35–42
- Water S van de, Safai S, Schippers J M, Weber D C and Lomax A J 2019 Towards FLASH proton therapy: the impact of treatment planning and machine characteristics on achievable dose rates *Acta Oncol.* **58** 1463–9
- Weber U A, Scifoni E and Durante M 2022 FLASH radiotherapy with carbon ion beams *Med. Phys.* **49** 1974–92
- Weber U and Kraft G 2009 Comparison of Carbon Ions Versus Protons: *Cancer J.* **15** 325–32
- Weber U and Kraft G 1999 Design and construction of a ripple filter for a smoothed depth dose distribution in conformal particle therapy *Phys. Med. Biol.* **44** 2765
- Wieser H-P, Cisternas E, Wahl N, Ulrich S, Stadler A, Mescher H, Müller L-R, Klinge T, Gabrys H, Burigo L, Mairani A, Ecker S, Ackermann B, Ellerbrock M, Parodi K, Jäkel O and Bangert M 2017 Development of the open-source dose calculation and optimization toolkit matRad *Med. Phys.* **44** 2556–68



## 7. PUBLISHED ARTICLES

In the following, the original articles are presented:

[1] Monte Carlo simulations and dose measurements of 2D range-modulators for scanned particle therapy

[2] Development, Monte Carlo simulations and experimental evaluation of a 3D range-modulator for a complex target in scanned proton therapy

[3] 2D range modulator for high-precision water calorimetry in scanned carbon-ion beams

# Monte Carlo simulations and dose measurements of 2D range-modulators for scanned particle therapy

Yuri Simeonov<sup>a,c,\*</sup>, Uli Weber<sup>b</sup>, Christoph Schuy<sup>b</sup>, Rita Engenhardt-Cabillic<sup>d</sup>, Petar Penchev<sup>a</sup>, Marco Durante<sup>b,f</sup>, Klemens Zink<sup>a,d,e</sup>

<sup>a</sup> Institut für Medizinische Physik und Strahlenschutz (IMPS), University of Applied Sciences, Giessen, Germany

<sup>b</sup> Biophysics Division, GSI Helmholtzzentrum für Schwerionenforschung GmbH, Darmstadt, Germany

<sup>c</sup> Philipps-University, Marburg, Germany

<sup>d</sup> Department of Radiotherapy and Radiooncology, University Medical Center Giessen-Marburg, Marburg, Germany

<sup>e</sup> Marburg Ion Beam Therapy Center (MIT), Marburg, Germany

<sup>f</sup> Technical University of Darmstadt, Institute for Condensed Matter Physics, Germany

Received 28 February 2020; accepted 22 June 2020

## Abstract

**Abstract:** *This paper introduces the concept of a 2D range-modulator as a static device for generating spread-out Bragg peaks at very small distances to the target. The 2D range-modulator has some distinct advantages that can be highly useful for different research projects in particle therapy facilities. Most importantly, it creates an instantaneous, quasi-static irradiation field with only one energy, thus decreasing irradiation time tremendously. In addition, it can be manufactured fast and cost efficiently and its SOBP width and shape can be adjusted easily for the specific purpose/experiment. As the modulator is a static element, there is no need for rotation (e.g. like in a modulation wheel) or lateral oscillation and due to the small base structure period it can be positioned close to the target.*

*Two different rapid prototyping manufacturing techniques were utilized. The modulation properties of one polymer and one steel modulator were investigated with both simulations and measurements. For this purpose, a sophisticated water phantom system (WERNER), that can perform fast, completely automated and high resolution dose measurements, was developed. Using WERNER, the dose distribution of a modulator can be verified quickly and reliably, both during experiments, as well as in a time constrained clinical environment.*

*The maximum deviation between the Monte Carlo simulations and dose measurements in the spread-out Bragg peak region was 1.4% and 4% for the polymer and steel modulator respectively. They were able to create spread-out Bragg peaks with a high degree of dose homogeneity, thus validating the whole process chain, from the mathematical optimization and modulator development, to manufacturing, MC simulations and dose measurements.*

*Combining the convenience, flexibility and cost-effectiveness of rapid prototyping with the advantages of highly customizable modulators, that can be adapted for different experiments, the 2D range-modulator is considered a very useful tool for a variety of research objectives. Moreover, we have successfully shown that the manufacturing of 2D modulators with high quality and high degree of homogeneity is possible, paving the way for the further development of the more complex 3D range-modulators, which are considered a viable option for the very fast treatment of moving targets and/or FLASH irradiation.*

**Keywords:** Particle therapy, Proton therapy, 3D range-modulator, 2D range-modulator, FLUKA, Monte Carlo simulation, SLM

\* Corresponding author. Yuri Simeonov, Institut für Medizinische Physik und Strahlenschutz (IMPS), University of Applied Sciences, Giessen, Germany.  
E-mail: [juri.simeonov@lse.thm.de](mailto:juri.simeonov@lse.thm.de) (Y. Simeonov).

## 1 Introduction

Previous studies have shown that the so-called patient-specific 3D range-modulator (3D RM) could be a feasible technique for the very fast treatment of tumors in scanned particle therapy [1]. The modulator consists of a ground plate similar to a conventional range-compensator combined with many pyramid-shaped fine structures (pins), whose shape and height are optimised and adjusted to the form of an individual patient's tumour. The modulator is manufactured with high-quality 3D rapid prototyping techniques. By irradiating the 3D RM with only one fixed energy, highly homogeneous dose distributions can be achieved with a significant reduction in the treatment time. Moreover, the delivered dose is conformed not only to the distal edge of the target, but also to the proximal edge. Irradiation time is in the order of several seconds, depending on the applied dose and the accelerator intensity capabilities. Especially moving targets (e.g., lung cancer or liver cancer), where “interplay effects” between the tumour motion and the scanned ion beam lead to a deterioration in the dose distribution [2,3], can benefit greatly from the newly proposed method. The tremendous decrease in irradiation time can make the delivery of a homogeneous dose to moving targets more reliable and enable the vast majority of the patients to hold their breath during treatment, avoiding all motion-induced interplay effects.

Furthermore, there has been increased interest in the so-called “FLASH” particle therapy in the recent years. Even though the FLASH effect is controversial and research still in its early stages, a number of studies suggest that a very fast irradiation (in the order of ms) with dose rates over 40 Gy/s may reduce side effects in healthy tissue and increase the therapeutic window [4–7]. As of now, the major manufacturers of particle therapy facilities are trying to increase their accelerators' intensity and improve the dose delivery and monitoring systems to enable FLASH therapy. When comparing the different commercially available dose delivery techniques, a multi iso-energy irradiation seems to be too slow due to the relatively long time needed to actively change the primary beam energy, ranging from 80 to 500 ms [8,9] up to several seconds. The conventional passive scattering method, on the other hand, has very low efficiency, resulting in loss of particles and reduced intensity.

Taking into consideration the aforementioned issues, the 3D RM in combination with only one energy and a laterally scanned beam could be a viable option for the extremely fast FLASH delivery of high dose in less than a second.

However, further research is needed in order to improve the different aspects of the 3D RM dose delivery technique. Special emphasis should be placed on the manufacturing accuracy and reproducibility, as manufacturing artefacts are known to have a negative impact on the homogeneity of the dose distribution. In addition, a fast, reliable and reproducible dose quality assurance procedure would be very beneficial and

necessary for the successful implementation of the 3D RM in the clinical routine.

In this paper we present a very useful variant of the 3D RM, which is called a 2D range-modulator (2D RM). In contrast to the 3D RM, the pins of the 2D RM have the same shape and height, not optimised for a specific tumour form. Similar to the conventional Ridge Filters [10–12], the 2D RM is developed to deliver a spread-out Bragg peak (SOBP) of a specific width. The simpler modulator with a well-defined geometry of identical pins results in a simpler dose distribution (in comparison to the 3D RM), because it should provide a laterally constant depth-dose distribution in the inner part of the target volume. This makes it much easier to identify dose deviations coming explicitly from manufacturing artefacts and trace them back. Thus it is possible to quickly iterate between different pin shapes to find an optimum solution and improve the accuracy and precision of the manufacturing process.

Just as important, however, is the increasing interest in the particle therapy community and among our collaboration partners for the practical usage of our 2D modulators in different applications with particle beams, as they have a number of intrinsic advantages, compared to the conventional Ridge Filters:

- cheaper (if printed in plastic) and faster manufacturing
- the SOBP width and shape can be adjusted easily for the specific purpose/experiment
- they can be used as a static element, no need of rotation or lateral oscillation
- due to the small periodicity of the pins (3 mm) they can be positioned relatively close to the target and have relatively low scattering, when manufactured from photopolymer. This enables an easy and compact setup. The structures of the pins are blurred out at a distance between 30 and 60 cm in air [1].

We are currently collaborating and have provided 2D RMs to several different research/clinical intuitions for a number of different joint research projects:

- The Trento proton therapy centre utilizes a 2D RM for radiobiology research and cell survival experiments [13].
- The Physikalisch-Technische Bundesanstalt (PTB) is using the 2D RM for a fast SOBP delivery for the direct determination of the  $k_Q$  factor for a Farmer-type ionization chamber with high-precision calorimetry [14].
- The GSI Biophysics department performs a large variety of radiobiological experiments in order to improve the understanding (e.g. the RBE dependencies) of the biological effect in ion beam therapy. Since 2019 the biophysics department has been using a 2D RM for SOBP irradiations (Fig. 1), which is 5–10 times faster than the standard multilayer scanning and significantly shortens the time the samples remain outside the incubator, reducing the stress for the cells.

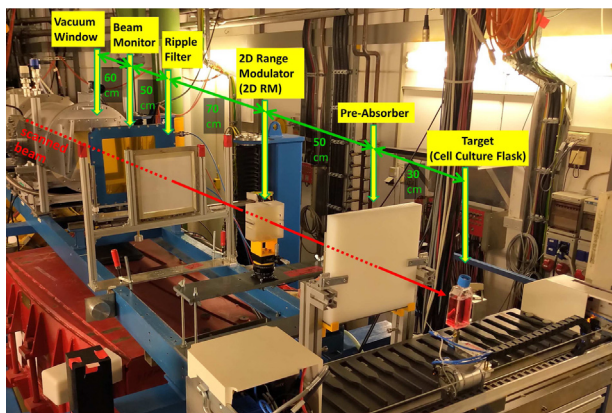


Figure 1. Application example for a 2D RM in a setup for irradiation of biological samples in the experimental room Cave-A of GSI: The scanned beam of 240 MeV/u  $^{12}\text{C}$  ions passes the vacuum window, a parallel plate ionization chamber for beam monitoring, a 3 mm Ripple Filter for additional smoothing of the depth dose profile, the 2D RM for a 40 mm SOBP with a max. lateral area of  $10 \times 10 \text{ cm}^2$ , a pre-absorber of ca. 90 mm thickness ( $\text{H}_2\text{O}$  equ.), before it hits the target. In this way the biological sample is irradiated in the middle of the SOBP region created by the 2D RM.

- At the Heidelberg Ion Beam Therapy Centre (HIT) research groups from GSI and the German Cancer Research Centre (DKFZ) are performing experiments at HIT with biological samples with a 2D RM for a 6 cm SOBP in order to assess the biological effects under FLASH conditions in comparison to conventional irradiations.
- The Heavy Ion Medical Accelerator at Chiba (HIMAC) provides ion beams of  $^{11}\text{C}$  and  $^{15}\text{O}$ . A 2D RM for a 2.5 cm SOBP was designed, manufactured and tested in order to enable PET imaging experiments in the Bragg peak region of these radioactive beams [15].

As 3D prototyping techniques are advancing rapidly, we consider the 2D RM not only a necessary intermediate step towards a much improved 3D RM, but also a very useful tool that can be adjusted to the specific needs of a variety of different experiments and can be developed and manufactured in-house in a fast and cost-efficient manner.

This work presents Monte Carlo (MC) simulations and the corresponding dose measurements of two 2D range-modulators. Several specific improvements in the pin design have been implemented in order to increase the manufacturing accuracy and to achieve clinically acceptable dose distribution. Besides the modulators that we manufacture in the established 3D polymer printing technique, a fast evolving manufacturing technique, selective laser melting (SLM) is also proposed. The two models shown here represent our latest development status in the long series of modulator designs and printing techniques for various applications (see also the list above) during the last 4 years.

In addition, a brief description of the successfully implemented concept for fully automated, fast and high resolution dosimetric verification of the modulators is included.

## 2 Materials and methods

### 2.1 2D range-modulators: development

Monoenergetic particles, passing through a modulator, produce Bragg peaks (BP) with different ranges, whose weighted superposition should result in a homogeneous SOBP. Consequently, the first step in developing the 2D RM was to optimize the BP weights and convert them to a high-resolution step-less pyramid-shaped pin profile (Fig. 2) as already described in Simeonov et al. [1]. The pin form was optimized for a 5 cm SOBP and a 150.68 MeV/u monoenergetic proton beam simulated with the FLUKA MC transport code.

Some slight, but important changes were implemented in the pin design, e.g. the pin base was increased from  $1.5 \text{ mm} \times 1.5 \text{ mm}$  to  $3 \text{ mm} \times 3 \text{ mm}$  base area, resulting in a more favourable pin aspect ratio and better mechanical long-term stability. Additionally, the groove between adjacent pins and the pin tip area were optimised to be slightly wider (Fig. 2), as they have proven to be especially susceptible to deviations from the optimal design during the 3D printing process. It is important to note that while the difference between the original and improved pin design might seem very small to the eye, this is not the case, considering the  $\mu\text{m}$  resolution of the 3D printer. The subsequently fabricated test prototypes confirmed that the aforementioned modifications lead to a substantial improvement in manufacturing accuracy.

It is noteworthy, that the original pin profile exhibits some small “ripples”, observed at approximately 5–15 mm height. These ripples are of no significant importance and resulted from oscillations in the modulation function in the inverse SOBP optimization. Nevertheless, as the optimization algorithm evolved slightly in time, the new pin has a somewhat smoother profile.

A 2D RM consisting of  $27 \times 27$  periodically positioned adjacent pins was developed (Fig. 3). This modulator was intended to be manufactured with PMMA-like photopolymer (resin). Even though we use a propriety printing material (RIGUR RGD450), its properties are very similar to the well-established PMMA. For the sake of simplicity, we will refer to this modulator throughout the paper as the “polymer RM”.

A steel 2D RM, consisting of the same periodically positioned adjacent pins ( $19 \times 19$  pins), was also developed (Fig. 3). This modulator was intended to be manufactured with stainless steel (316L alloy) and will be referred to further on as the “steel RM”.

Both modulators have a 1 mm thick base plate to hold the pins together and increase the mechanical stability. 3 mm thick side walls were implemented for pin protection during transport and measurements. Additionally, so-called “positioning bars” were added. They were used later on during the dose

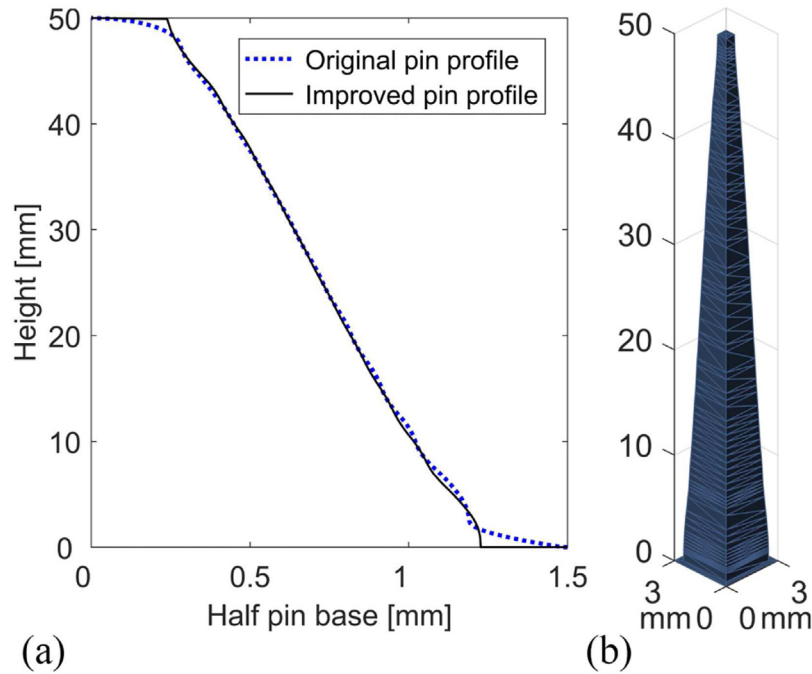


Figure 2. Comparison between the original and improved pin profile. The main difference is in the pin base (groove) and the pin tip (a). A single pyramid-shaped pin optimized for a 5 cm SOBP in water for 150.68 MeV/u monoenergetic proton beam (b).

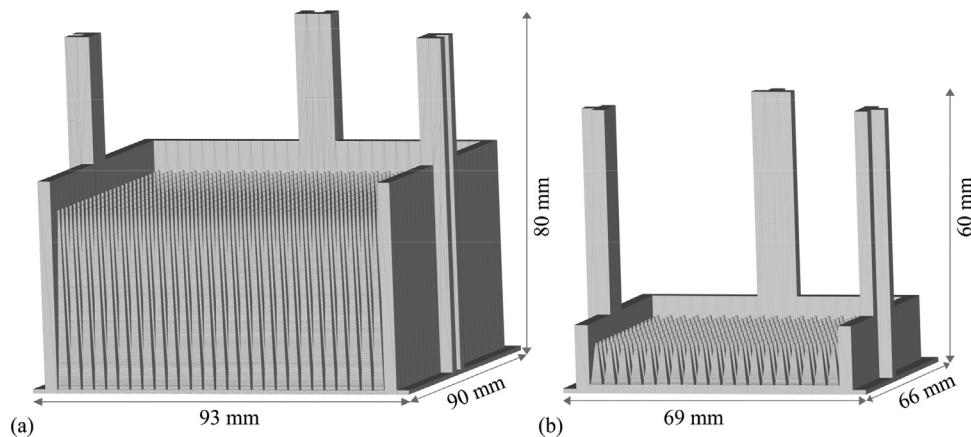


Figure 3. A 2D RM computer model with  $27 \times 27$  pins intended to be manufactured with photopolymer (a). A 2D RM computer model with  $19 \times 19$  pins intended to be manufactured with stainless steel 316L alloy (b).

measurements to accurately align the modulators to the room lasers.

In order to preserve the correct resulting SOBP width in water, the pin heights of both modulators have to be scaled with the corresponding water equivalent relative stopping power of the fabricating material. For RIGUR RGD450, the scaling factor was calculated by measuring two BPs in water, a pristine one and one with a  $5 \text{ cm}^3$  cube in the beam path. Dividing the water shift between both BPs by the 5 cm material thickness resulted in a factor of 1.18. As the exact stoichiometric composition of RIGUR was not disclosed, but needed for

the MC simulations, a carbon, hydrogen and nitrogen (CHN) analyser, thermogravimetric analysis and X-ray fluorescence spectroscopy were carried out at the chemistry department of the University of Applied Sciences Gießen. The resulting atomic composition was implemented in FLUKA using the official manufacturer density specifications of  $1.2 \text{ g cm}^{-3}$ . We carried out subsequent MC simulations, which confirmed the factor of 1.18.

In contrast to RIGUR, the stoichiometric composition of the 316L stainless steel material was known and directly implemented in FLUKA. Subsequent simulations showed a water

equivalent relative stopping power of 5.60, which was used to scale the pin height of the steel RM.

## 2.2 2D range-modulators: manufacturing

Rapid prototyping is a quickly evolving group of techniques, used to create three-dimensional models mostly by means of 3D printing. Recent research in this field showed the feasibility of using 3D printing in proton therapy with physical accuracy and dosimetric characteristics similar to or better than conventional compensators [16–18].

The polymer RM was manufactured using the Stratasys Objet30 Pro PolyJet 3D-printer (Fig. 4). PolyJet works by jetting thousands of photopolymer droplets on a build platform and curing them with UV light. It's among the fastest and most accurate 3D printing technologies available. An advanced simulated polypropylene (RIGUR RGD450), which exhibits a high degree of toughness and elasticity, was used as a material. No support material was used, as it would have been impossible to remove it without damaging the pins.

While photopolymers have previously demonstrated good manufacturing accuracy [1], utilising a metal alloy, on the other hand, will further improve the mechanical stability, the aspect ratio of the base structures and the overall robustness. Therefore, in addition to the PolyJet technique, we tried a different approach for the second modulator, the so-called selective laser melting.

In the SLM process, a layer of metal powder is spread over the build area and a laser source is directed onto the powder bed to selectively melt and fuse the material [19,20]. In this way very well-bonded and high density structures can be created [21]. The build platform is repeatedly lowered by one layer of thickness and a new layer of powder is applied and melted until the complete part is built. The SLM technology has undergone vast improvements in the achievable resolution and accuracy in recent years.

In order to investigate the feasibility of this technique, the second 2D RM was manufactured using a TRUMPF TruPrint 1000 SLM machine with stainless steel 316L alloy of  $7.95 \text{ g cm}^{-3}$  density. The size of the steel modulator was smaller ( $19 \times 19$  pins vs  $27 \times 27$  for the polymer) due to the limitations in the maximum effective build area (Fig. 4).

The 316L alloy is definitely not the material of choice, due to its high average  $Z$  and thus increased scattering. Due to a variety of reasons, not relevant to the scope of this paper, it was the only material available at the time. Another metal powder, which is very widely used, is the aluminum alloy AlSi10Mg. It is expected to cause less scattering than 316L steel, when placed in the beam path and will most probably be the scope of future research.

The manufacturing duration depends among other things strongly on the manufacturing technique, the height and volume of the modulators. In our case it took 15 h for the polymer RM ( $90 \times 93 \times 80 \text{ mm}^3$ ) and around 7 h for the steel RM ( $66 \times 69 \times 60 \text{ mm}^3$ ). The new pin design with 3 mm basis was

found to be quite robust. The experience in our working group and the feedback coming from our research partners show that given dry storage and a proper handling (e.g. no drops on the floor and/or deliberate impact on the pin structures) the modulators can be reused for years.

## 2.3 Monte Carlo simulations

### 2.3.1 FLUKA transport code

FLUKA is a general purpose Monte Carlo transport code capable of calculating particle transport and interactions with matter [22,23]. It is used in a wide range of applications, such as activation, radiation protection and dosimetry, and has been repeatedly shown to reproduce measured dose profiles in water, produced by particles, sufficiently well [24–26]. There are a number of different user-routine templates included in the FLUKA distribution package, which can be customized and linked with the original code, thus extending its capabilities to some more special cases. The FLUKA MC code version 2011.2x.6 was used for this work.

### 2.3.2 Physics settings

For an optimum set of parameters, the “HADROTHERapy” defaults were activated in all simulations. This ensures the detailed transport of all primary and secondary particles. Low-energy neutrons were transported down to thermal energies. Electron/positron transport cutoff (Ecut) and photon transport cutoff (Pcut) were left to the default values of 100 keV and 33.3 keV respectively. The “flukadpm3” executable linked to the relevant libraries (rqmd, dpmjet, etc) was used. The average excitation energy of water was set to  $I = 78 \text{ eV}$ .

## 2.4 Simulation setup

The standard FLUKA Combinatorial Geometry is not capable to exactly describe the form of complex 2D and 3D modulators, consisting of numerous very fine pyramid-shaped structures (that also have different heights in the case of a 3D RM). Therefore, extending the proposal of Bassler et al. [27], a special FLUKA user routine, already developed and described in [1], was used to model the shape of the modulators. In this routine the following concept is applied: a homogeneous plate with thickness, corresponding to the maximum thickness of the modulator, is used as a substitute. The triangulated modulator in STL (Standard Tessellation Language) file format is loaded during simulation initialization and saved in the memory. Using the intersection points between the projected path of each particle and the range modulator, the total material thickness  $D$  the particle would travel through the modulator is calculated. Finally, the particle is shifted along its original 3D directional vector in the plate substitute in such a way, that the material thickness, which remains in front of the particle, equals the calculated total material thickness  $D$  through

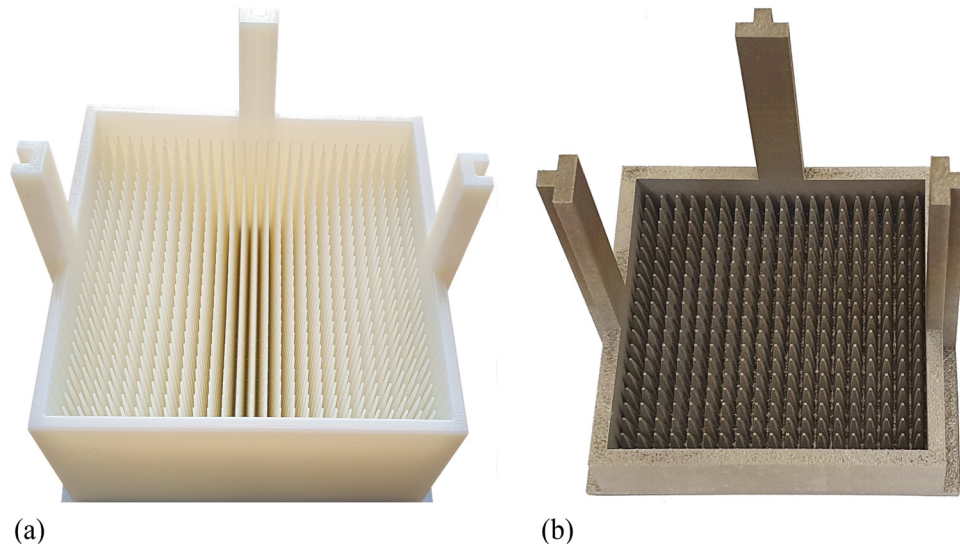


Figure 4. The manufactured **polymer RM** (a) and the **steel RM** (b) with a protection wall around and positioning bars.

the modulator. At this point the standard FLUKA executable takes back control and the particle is simulated as usual in the rest of the plate.

This user routine was previously benchmarked against the well-established FLUKA voxel geometry in a preliminary study. It was shown that it could successfully reproduce the accurate modulation properties of a complex geometrical contour.

To directly compare MC simulations with measurements from particle therapy facilities with pencil beam scanning (PBS), an intensity modulated raster scanning was implemented in the “Source.f” user routine. A so-called “raster” file, containing all the necessary information, i.e., the beam energy, beam spot size,  $x/y$  coordinates of the scan spots and the corresponding number of particles in each of them, can be loaded and simulated. The exact energy value was taken from the Marburg Ion-Beam Therapy Centre (MIT) accelerator database.

Fig. 5 shows a schematic drawing of the simulation setup. The virtual “isocenter” in FLUKA (equivalent to the room isocenter in MIT) is defined at  $Z=0$  cm, where the positive  $z$ -axis is the beam direction.

The “Source.f” routine is called to load the raster file and generate primary  $^1\text{H}$  particles with 150.68 MeV/u kinetic energy and energy spread typical for the MIT synchrotron ( $\sigma = 1.0\%$ ). The protons start in vacuum at  $Z = -775$  cm, which corresponds to the middle position between the vertical and horizontal scanning magnets in MIT. The primary particles in each scan spot are sampled from a Gaussian distribution, whose FWHM width has been adjusted, so that the resulting beam width at the isocenter is the same as the isocenter beam width in MIT.

A 2.5 mm homogeneous water slab is placed at the vacuum region exit, serving as a water equivalent nozzle substitute.

The surrounding material is set to air. The 30 cm thick water phantom is positioned in such a way, that the isocenter is in 20 cm water depth. The modulator material composition, density and its distance to the water phantom can be changed variably according to the requirements and the current modulator being simulated (polymer or steel RM). Dose deposition (GeV/g per unit primary weight) is scored in the water phantom using the USRBIN card.

As the SOBP from the polymer RM was measured with a water column (Peakfinder, PTW Freiburg, Germany), we used an R-Phi-Z scoring region correspondingly, integrating over the radius  $R$  and the angle  $\Phi$ .  $R$  was set to 41 mm in accordance with the circular sensitive area of the Peakfinder measuring detector. The voxel size in depth was set to 1 mm. This simulation was run with  $2 \times 10^6$  total number of primary particles.

A full 3D dose distribution was measured in the case of the steel modulator; therefore, a Cartesian X-Y-Z voxel mesh was chosen for the simulation. The voxel size was set to 2.5 mm in the XY direction (corresponding to the 2.5 mm resolution of the PTW Octavius 1000P) and 1 mm in Z. A total number of  $2 \times 10^8$  particles was simulated. The statistical uncertainty for all simulations in this work is below 0.3% in the homogeneous SOBP region.

## 2.5 Dose measurements

### 2.5.1 Polymer RM

In order to verify the simulation results, the polymer 2D range-modulator was irradiated at MIT. A 150.68 MeV/u undeflected ( $X, Y=0$ ) proton beam with FWHM of 11.1 mm at the isocenter was used. Fig. 7 shows a schematic drawing of the dose measurement setup. The modulator was precisely

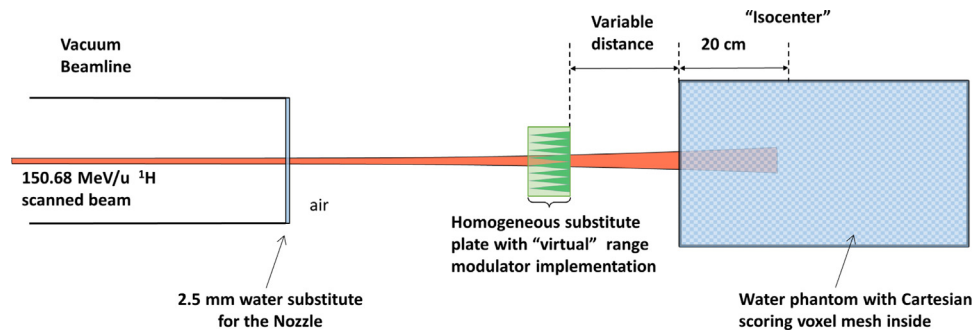


Figure 5. Schematic drawing of the FLUKA simulation setup. The modulator is implemented via a homogeneous substitute plate. Dose distribution is scored in a water phantom.

positioned and aligned with the lasers 72 cm behind the nozzle. The dose was measured with the PTW Peakfinder, which is a variable depth water column with two plane-parallel ionization chambers, a fixed reference and a movable measuring one. The circular measuring detector has a 41 mm radius and can be moved with a resolution of 0.01 mm.

### 2.5.2 Fast, completely automated, high-resolution 3D dose measurements

The PTW Peakfinder measures a laterally integrated depth dose curve. However, high-resolution, 3D dosimetry is an absolute necessity not only for conventional quality assurance, but also for benchmarking and optimization of different beam application modalities, such as 2D and 3D RMs.

For this purpose, a universal, vendor-agnostic water phantom was developed at the GSI, (WATER column for 2D ionization chamber array detectors (WERNER)). It consists of a PMMA water tank and a stepper-driven watertight detector holder for a standard medical 2D ionization chamber array (Fig. 6). The system is synchronized to the dose delivery system of the medical accelerator using the available digital signals. For a fully automated measurement the user has to provide the desired measurement positions in depth to the controller of the water phantom and a treatment plan, which consists of many repeating energy layers, to the accelerator. During irradiation, a digital signal is generated at the end of each energy layer, which triggers the phantom to move the detector to the next measurement position. All acquired external signals and the position (water depth) of the motor are logged.

The system was successfully validated at MIT using proton and carbon beams and two different detectors (PTW Octavius 1500XDR and 1000P). By using the newly developed method, high resolution 3D dosimetry of complex radiation fields can be performed in a fast and completely automated manner.

### 2.5.3 Steel RM

In the case of the steel RM, the aforementioned WERNER system was used to carry out high resolution, 3D dose

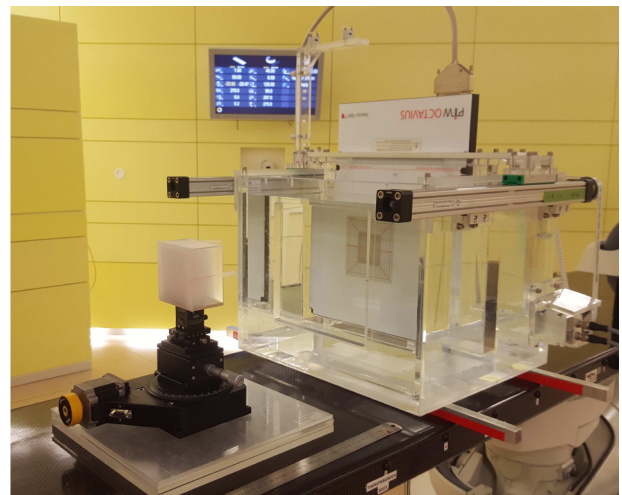


Figure 6. The WERNER water phantom with the PTW Octavius 1000P inserted in the detector holder. An exemplary modulator is placed in front of the water phantom on a multi-axis positioning system.

measurements. The modulator was precisely positioned and aligned with the lasers 82 cm behind the nozzle (Fig. 7). The water phantom was placed 10 cm behind the modulator. The lateral dose distribution at each depth was measured with the prototype 2D ionization chamber array PTW Octavius 1000P, which consists of 977 air-filled ICs with  $11 \times 11 \text{ cm}^2$  max. field size. The centre area ( $5.5 \times 5.5 \text{ cm}^2$ ) has a very fine spatial resolution of 2.5 mm. A monoenergetic treatment plan with 150.68 MeV/u and  $3.2 \times 3.2 \text{ cm}^2$  field size was used. The field size was limited by the size of the modulator and the need not to irradiate the thicker side walls. The number of particles at the field edges was deliberately increased (“edge boost”) to account for the strong scattering in steel.

A beta version of the PTW BeamAdjust Software (V2.1 T182) was used, as it offers a continuous measuring mode with a timestamped detector readout. The fast, automated dose measurement proceeds as follows: Firstly, the raster file with repetitive energy layers and a file with the predefined measurement depth positions are loaded. The PTW Octavius detector



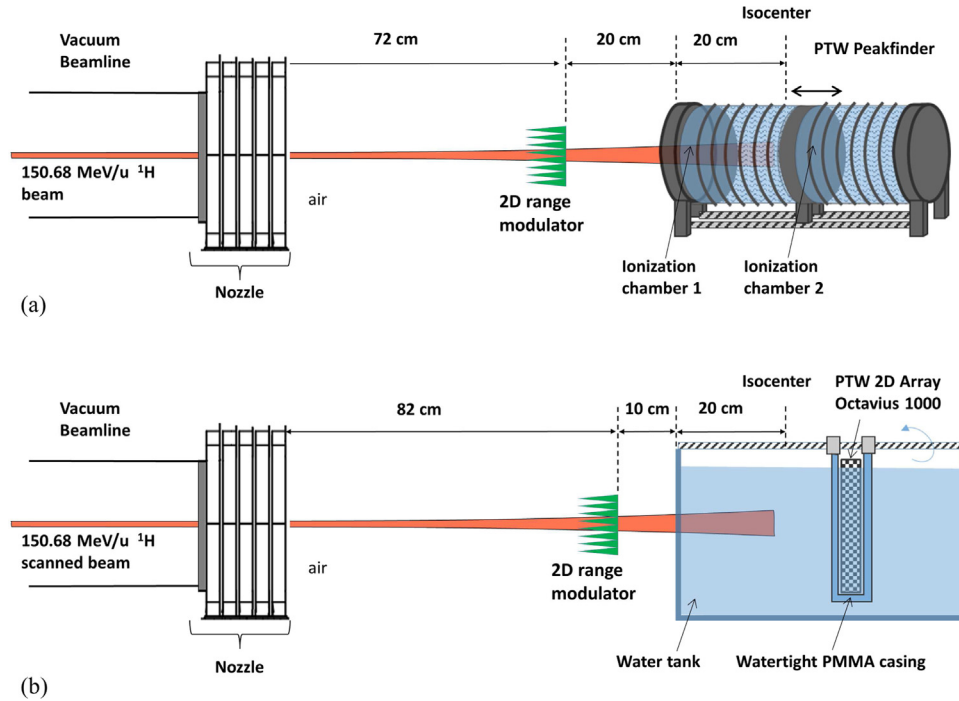


Figure 7. Schematic drawing of the dose measurement setup. Panel (a) shows the 2D polymer RM, which was positioned 40 cm in front of the isocenter and irradiated with an undeflected beam. The dose was measured with the PTW Peakfinder. Panel (b) shows the 2D steel RM, which was positioned 30 cm in front of the isocenter and irradiated with a scanned  $3.2 \text{ cm}^2$  rectangular field. The dose was measured with the newly developed WERNER system using the PTW Octavius 1000P. All measurements were conducted with a  $150.68 \text{ MeV/u}$  proton beam.

starts a continuous integrated (in time, not among single ICs) timestamped dose measurement (200 ms). At the end of each energy layer the detector moves automatically to the next position. The whole process repeats until all predefined depths are measured.

An in-house developed MATLAB (R2016b) script was used to combine and process the timestamped information, contained in the dose file itself and the log files from WERNER and obtain the separate dose contribution from each single measured depth. In this way a high resolution 3D dose distribution is reconstructed from the integrated 2D measurements. This enables very fine dose verification of complex fields generated by different 2D RMs and 3D RMs.

The depth dose distribution in the SOBP region was scored in 1 mm steps, whereas the steps outside the SOBP region varied between 2 and 10 mm. The measured dose profiles were subsequently compared to the FLUKA simulations.

### 3 Results

#### 3.1 Polymer RM with Peakfinder

Fig. 8 shows a comparison between measured and simulated depth dose distributions from the polymer 2D RM, both of which were normalized to one in the middle of the SOBP.

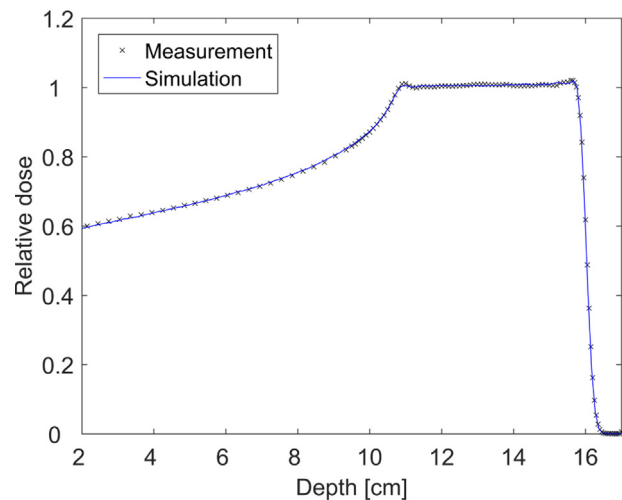


Figure 8. A comparison between the measured and simulated SOBP. Both depth dose distributions are normalized to one in the middle of the SOBP.

There is a very good agreement between both data sets with a maximum dose deviation in the SOBP region of 1.4%. The standard deviation of the measured data points calculated for the 5 cm homogeneous SOBP region (10.7 cm to 15.7 cm) is 0.59%.

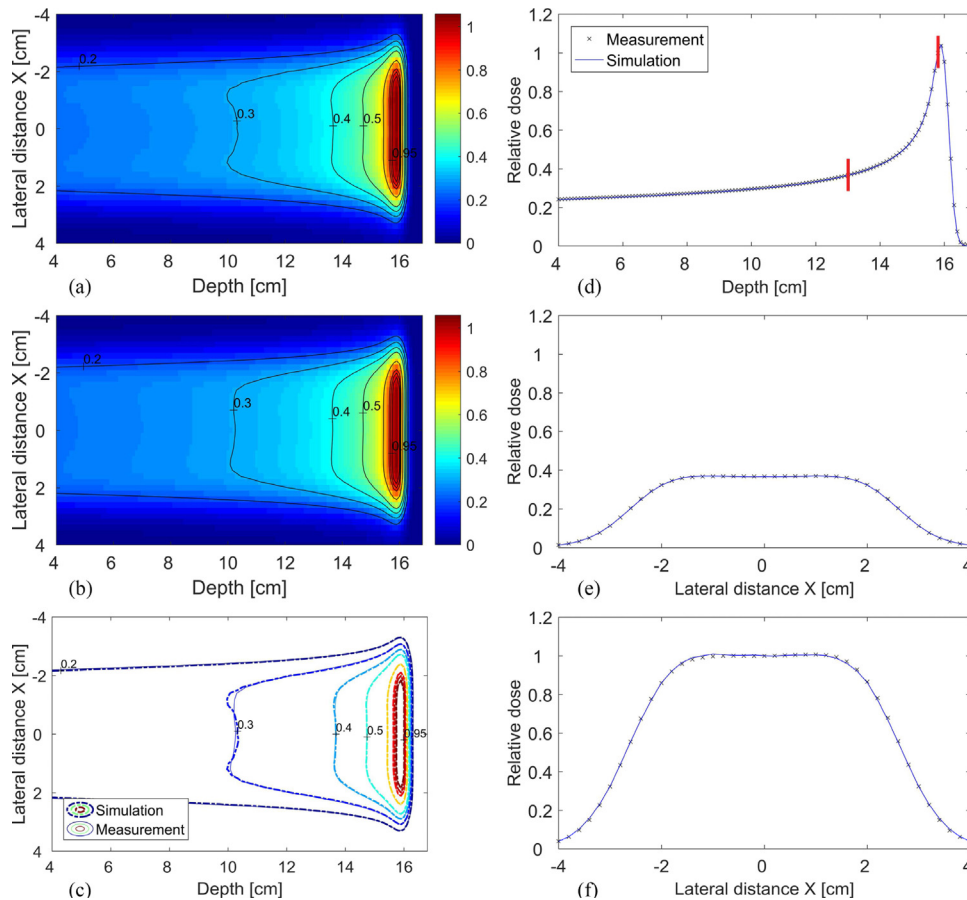


Figure 9. Simulated (a) and measured (b)  $X$ - $Z$  midplane profile. Comparison between the isodose lines is shown in (c) with solid lines for the measurement and dotted lines for the simulation. Centre line BP (d) and two 1D  $X$  profiles (e)–(f). The vertical red lines in (d) denote the depths, at which the  $X$  profiles were plotted. Both dose distributions were normalized to one in the centre line BP at 15.8 cm, also denoted by the second vertical red line at 15.8 cm in Panel (d).

### 3.2 Base data with WERNER

Fig. 9 shows measured and simulated “base data”, i.e., a 3D dose distribution without a modulator in the beam path. This base data was obtained immediately preceding the modulator measurements and used to validate the simulation model and exclude potential dose deviations, coming from sources other than the modulator itself. The 3D dose distributions were normalized to one in the centre line Bragg Peak, also denoted by the second vertical red line at 15.8 cm in Panel (d).

A simulated  $X$ - $Z$  midplane profile (a), a measured one (b) and a comparison between the isodose lines (c) are plotted in the left panel of Fig. 9. The contour profiles are in good agreement with each other. The corresponding local 2D gamma index [28] with strict 2%/2 mm acceptance criteria has a 100% passing rate (not shown in the figure). The 3D gamma index with the same criteria results in 99.8% passing rate.

The right panel of Fig. 9 compares 1D data extracted from the 2D dose distribution on the left side, a centre line depth

dose distribution (d) and lateral profiles (e)–(f), taken at two different depths.

### 3.3 Steel RM with WERNER

Fig. 10 shows the results obtained with the steel 2D RM in the beam path. Using the automated WERNER system, a total set of over 60 000 measured dose values (63 depths  $\times$  977 ICs) were obtained in 8 min, thus enabling a high resolution validation of the modulator.

The 3D dose distributions were normalized to one in the homogeneous centre line SOBP region (Panel (a), 11 cm). Panel (a) shows a centre line SOBP comparison. There is a very good agreement in the proximal region with dose deviations well below 1%. The increasing discrepancies, which are observed towards the distal edge, have a maximum deviation of 4% and result from slight manufacturing artefacts of the SLM produced modulator.

Fig. 10(b) and (c) shows the isodose lines of a  $X$ - $Z$  midplane profile and the corresponding gamma index. The dose

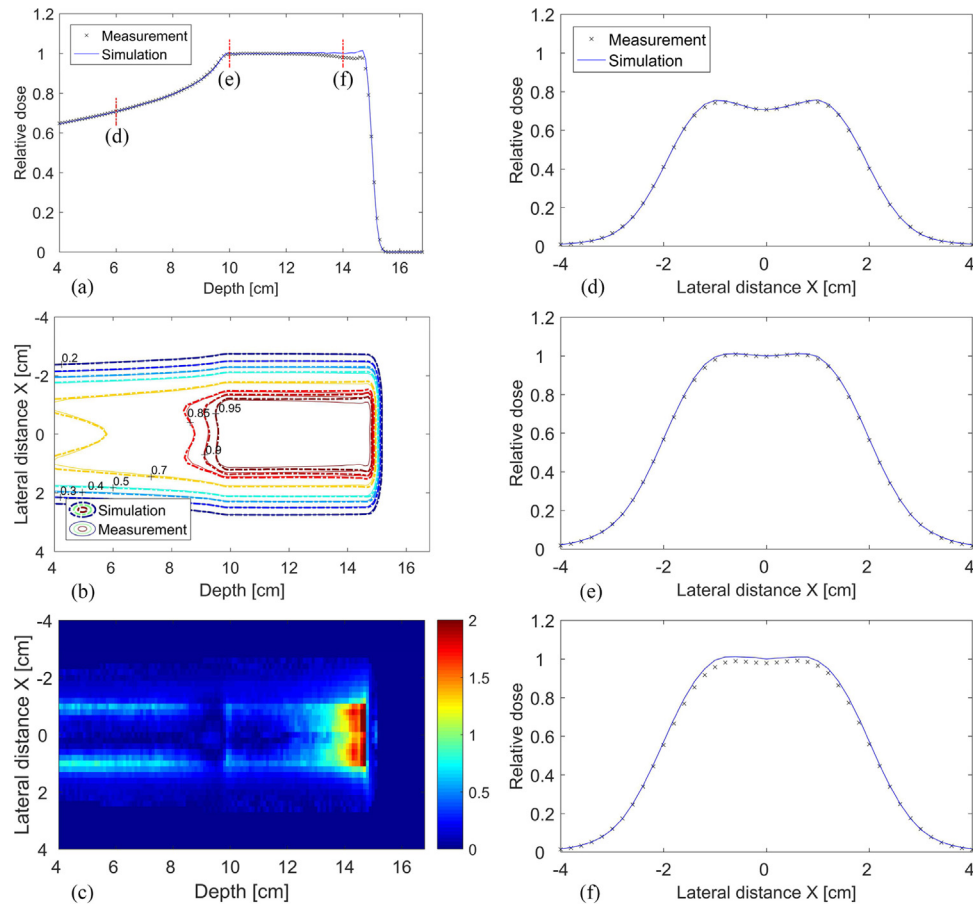


Figure 10. Centre line SOBP (a), isodose lines comparison of a X–Z midplane profile (b) and the corresponding local gamma index for 2%/2 mm acceptance criteria (c). Three lateral X profiles (d)–(f), plotted at 6 cm, 10 cm and 14 cm respectively. The vertical red lines in (a) denote the depths, at which the X profiles were plotted.

deviations in the distal region can be clearly seen in both plots. 96.2% of the voxels in the 2D plot pass the local gamma index acceptance criteria and 97.4% of all voxels pass the 3D gamma index.

Fig. 10(d)–(f) compares three lateral profiles taken at 6 cm, 10 cm and 14 cm. The slight “edge boost” implemented in the treatment plan can be seen as a small increase in the dose at the edges of the irradiation field in panel (d), but disappears almost completely with increasing depth due to scattering.

## 4 Discussion

The SOBP homogeneity strongly depends on the manufacturing accuracy of the modulator. A perfect prototype will deliver a SOBP with a very high degree of homogeneity, consistent and limited only by the homogeneity and quality of the mathematical SOBP optimisation used as a basis for the pin geometry.

Generally, the groove area between successive pins is more susceptible to manufacturing artefacts and even minor deviations from the optimal pin form can have a visible impact

on the dose distribution, as the weights of the corresponding BPs are here the highest. The experience the authors have gained in the last years from numerous manufactured prototypes and measurements has shown that dose deviations tend to be observed (if at all) most often in the distal SOBP edge.

In the case of the polymer 2D RM manufactured with the Stratasys Objet30 Pro, we have clearly achieved to create a highly homogeneous SOBP. The revised pin design resulted in an improved manufacturing accuracy and better prototypes. While each manufacturing technique (PolyJet, Stereolithography, SLM) has its intrinsic strengths and weaknesses and each 3D printer in its subclass will exhibit different and specific properties, the proposed pin design is expected to improve the overall prototype quality among all classes. With the polymer RM, the systematic artefacts from previous measurements, i.e. too short pins, extra material in the grooves, etc. [1], which led to measurable dose deviations in the depth dose distribution, are not observed any more in the latest models. Accordingly, the measured SOBP exhibits a very good agreement with the MC simulations with a max deviation of 1.4%. The standard deviation of 0.59% is certainly small enough to justify not only

a high quality application in radiobiological experiments, but also potentially in a clinical environment.

In the case of the steel RM, the homogeneity of the SOBP is compromised by dose deviations in the distal region. Accordingly, we have a slightly higher, but still satisfactory value for the standard deviation of 0.86%. However, a local maximum deviation of up to 4% is certainly not acceptable for many experiments (or for a future clinical application with a 3D RM) and should be reduced further by investigating the fundamental cause and applying corrections either to the pin profile or manufacturing machine.

An in-house developed tool, capable of introducing virtual manufacturing artefacts in the pin form and “simulating” their impact on the dose distribution, was used to investigate the obtained results from the steel RM. This tool is based on a pure mathematical implementation. It adds a user input offset (positive or negative, i.e., additional or missing material) to the original pin geometry, converts the new pin geometry into a modulation function and performs a convolution with the pristine BP to calculate the new SOBP. This tool was used to obtain an approximation of the deviations. The slight dose tilt and dose decrease towards the distal SOBP edge for the steel RM could be reproduced by adding additional material to the pin profile. However, the exact offset values and their distribution on the 3D pin geometry can only be confirmed by a precise and thorough investigation in a  $\mu$ CT scan.

A constant and reproducible material offset deviation would obviously be the best case scenario, as it could potentially be compensated by changing the printer’s internal parameters. It is noteworthy, however, that there are many other parameters that affect the manufacturing quality of a SLM machine, e.g. different laser focus size, powder particle size, numerous internal offsets that can be fine-tuned, etc.

Overall, the authors are very satisfied with the measured dose distribution and consider the SLM technique a promising alternative method for manufacturing high quality 2D and 3D modulators. Further research in this field is expected to improve the results and lead to similar SOBP homogeneity and modulator quality as with the polymer RM.

## 5 Conclusion

The concept of a 2D range-modulator was introduced in this paper. A revised and improved pin design was validated and the successful utilisation of two different rapid prototyping techniques to manufacture modulators with a high degree of SOBP homogeneity was demonstrated. The modulation properties of one polymer and one steel modulator were successfully verified with both simulations and measurements. For this purpose, a sophisticated water phantom system (WERNER) was developed. Using a fully automated measurement setup, fast and high resolution dose measurements can be performed, enabling a reliable modulator verification not only

during experiments, but potentially in the future, in a busy, time-constrained clinical routine. Overall, a complete workflow process chain, from the mathematical optimization and modulator development, to manufacturing, MC simulations and dose measurements, has been demonstrated.

The 2D range-modulator has some distinct advantages, that proved to be especially useful in a variety of ongoing research projects in pencil beam scanning particle therapy facilities, especially for radiobiological and small animal experiments. Most importantly, it creates an instantaneous, quasi-static irradiation field with only one energy, thus decreasing tremendously irradiation time. In addition, in-house manufacturing combines convenience, flexibility and cost-effectiveness on one side with the advantages of highly customizable modulators that can be adapted for many different specific purposes and experiments.

Last, but not least, we have shown that the manufacturing of 2D RMs with high quality and with a high degree of homogeneity is feasible, thus paving the way for further development of the more complex 3D range-modulators. Combining high dose conformity, very good homogeneity and extremely short irradiation times, the 3D range-modulators could potentially open new possibilities for the very fast treatment of moving targets and/or FLASH irradiation.

## 6 Conflict of interests

The authors declare that they have no known competing financial interests or personal relationships that could have appeared to influence the work reported in this paper.

## Acknowledgements

The project was supported by the Federal Ministry of Education and Research within the scope of the grant “Physikalische Modellierung für die individualisierte Partikel-Strahlentherapie und Magnetresonanztomographie”, (MiPS, grant number 13FH726IX6). The experiments in MIT were supported by the Hessian state government.

The manufacturing of modulator prototypes was supported by the grant “Wissens-und Technologietransfer im Bereich der innovativen 3D-Fertigungstechnologien für die individualisierte Medizin” within the scope of the IWB-EFRE-Program grant number 20004997 in Hessen.

We acknowledge MIT, Matthias Witt and Yannick Senger for the technical support during measurements and the beam time provided. The authors are thankful to Prof. Dr. Klaus Behler and Daniel Thölken for the manufacturing of the steel modulator. We express our appreciation to all the colleagues from the Institute of Medical Physics and Radiation Protection (IMPS Giessen) and to Marc-André Runkel and Dr. Christina Zinecker, who provided expertise that greatly assisted our research.

## References

- [1] Simeonov Y, Weber U, Penchev P, Ringbæk TP, Schuy C, Brons S, et al. 3D range-modulator for scanned particle therapy: development Monte Carlo simulations and experimental evaluation. *Phys Med Biol* 2017;62(17):7075, <http://dx.doi.org/10.1088/1361-6560/aa81f4>.
- [2] Lambert J, Suchowerska N, McKenzie DR, Jackson M. Intrafractional motion during proton beam scanning. *Phys Med Biol* 2005;50(20):4853, <http://dx.doi.org/10.1088/0031-9155/50/20/008>.
- [3] Bert C, Grözinger SO, Rietzel E. Quantification of interplay effects of scanned particle beams and moving targets. *Phys Med Biol* 2008;53(9):2253, <http://dx.doi.org/10.1088/0031-9155/53/9/003>.
- [4] Diffenderfer ES, Verginadis II, Kim MM, Shoniyozov K, Velalopoulou A, Goia D, et al. Design, implementation, and in vivo validation of a novel proton FLASH radiation therapy system. *Int J Radiat Oncol Biol Phys* 2020;106(2):440–8, <http://dx.doi.org/10.1016/j.ijrobp.2019.10.049>.
- [5] Durante M, Bräuer-Krisch E, Hill M. Faster and safer? FLASH ultra-high dose rate in radiotherapy. *Br J Radiol* 2018;91(1082), <http://dx.doi.org/10.1259/bjr.20170628>.
- [6] Favaudon V, Caplier I, Monceau V, Pouzoulet F, Sayarath M, Fouillade C, et al. Ultrahigh dose-rate FLASH irradiation increases the differential response between normal and tumor tissue in mice. *Sci Transl Med* 2014;6(245), <http://dx.doi.org/10.1126/scitranslmed.3008973.245ra93>.
- [7] Vozenin M-C, Fornel PD, Petersson K, Favaudon V, Jaccard M, Germond J-F, et al. The advantage of FLASH radiotherapy confirmed in mini-pig and cat-cancer patients. *Clin Cancer Res* 2019;25(1):35–42, <http://dx.doi.org/10.1158/1078-0432.CCR-17-3375>.
- [8] Furukawa T, Inaniwa T, Sato S, Shirai T, Takei Y, Takeshita E, et al. Performance of the NIRS fast scanning system for heavy-ion radiotherapy. *Med Phys* 2010;37(11):5672–82, <http://dx.doi.org/10.1118/1.3501313>.
- [9] Safai S, Bula C, Meer D, Pedroni E. Improving the precision and performance of proton pencil beam scanning. *Transl Cancer Res* 2012;1(3):196–206, <http://dx.doi.org/10.21037/599>.
- [10] Koehler AM, Schneider RJ, Sisterson JM. Range modulators for protons and heavy ions. *Nucl Instrum Methods* 1975;131(3):437–40, [http://dx.doi.org/10.1016/0029-554X\(75\)90430-9](http://dx.doi.org/10.1016/0029-554X(75)90430-9).
- [11] Akagi T, Higashi A, Tsugami H, Sakamoto H, Masuda Y, Hishikawa Y. Ridge filter design for proton therapy at Hyogo Ion Beam Medical Center. *Phys Med Biol* 2003;48(22):N301, <http://dx.doi.org/10.1088/0031-9155/48/22/N01>.
- [12] Schaffner B, Kanai T, Futami Y, Shimbo M, Urakabe E. Ridge filter design and optimization for the broad-beam three-dimensional irradiation system for heavy-ion radiotherapy. *Med Phys* 2000;27(4):716–24, <http://dx.doi.org/10.1118/1.598934>.
- [13] Tommasino F, Rovituso M, Bortoli E, La Tessa C, Petringa G, Lorentini S, et al. A new facility for proton radiobiology at the Trento proton therapy centre: design and implementation. *Phys Med* 2019;58:99–106, <http://dx.doi.org/10.1016/j.ejmp.2019.02.001>.
- [14] Holm K, Weber U, Simeonov Y, Krauss A, Jäkel O, Greilich S. 2D range-modulator for high precision water calorimetry in scanned carbon-ion beams. *Phys Med Biol* 2020, <http://dx.doi.org/10.1088/1361-6560/aba6d5>.
- [15] dos Santos Augusto R. On the feasibility of using radioactive ion beams in hadrontherapy: dosimetric and imaging studies. CERN Document Server 2018. Available from: <https://cds.cern.ch/record/2637861> [accessed 11.02.20].
- [16] Lindsay C, Kumlin J, Jirasek A, Lee R, Martinez DM, Schaffer P, et al. 3D printed plastics for beam modulation in proton therapy. *Phys Med Biol* 2015;60(11):N231, <http://dx.doi.org/10.1088/0031-9155/60/11/N231>.
- [17] Ju SG, Kim MK, Hong C-S, Kim JS, Han Y, Choi DH, et al. New technique for developing a proton range compensator with use of a 3-dimensional printer. *Int J Radiat Oncol* 2014;88(2):453–8, <http://dx.doi.org/10.1016/j.ijrobp.2013.10.024>.
- [18] Lindsay C, Kumlin J, Martinez DM, Jirasek A, Hoehr C. Design and application of 3D-printed stepless beam modulators in proton therapy. *Phys Med Biol* 2016;61(11):N276, <http://dx.doi.org/10.1088/0031-9155/61/11/N276>.
- [19] Trevisan F, Calignano F, Lorusso M, Pakkanen J, Aversa A, Ambrosio EP, et al. On the selective laser melting (SLM) of the AlSi10Mg alloy: process, microstructure, and mechanical properties. *Materials* 2017;10(1), <http://dx.doi.org/10.3390/ma10010076>.
- [20] Konda Gokuldoss P, Kolla S, Eckert J. Additive manufacturing processes: selective laser melting, electron beam melting and binder jetting-selection guidelines. *Materials* 2017;10(6), <http://dx.doi.org/10.3390/ma10060672>.
- [21] Kruth J, Mercelis P, Van Vaerenbergh J, Froyen L, Rombouts M. Binding mechanisms in selective laser sintering and selective laser melting. *Rapid Prototyp J* 2005;11(1):26–36, <http://dx.doi.org/10.1108/13552540510573365>.
- [22] Böhlen TT, Cerutti F, Chin MPW, Fassó A, Ferrari A, Ortega PG, et al. The FLUKA code: developments and challenges for high energy and medical applications. *Nucl Data Sheets* 2014;120:211–4, <http://dx.doi.org/10.1016/j.nds.2014.07.049>.
- [23] Ferrari A, Sala PR, Fassó A, Ranft J. FLUKA: a multi-particle transport code (program version 2005). CERN 2005.
- [24] Parodi K, Ferrari A, Sommerer F, Paganetti H. Clinical CT-based calculations of dose and positron emitter distributions in proton therapy using the FLUKA Monte Carlo code. *Phys Med Biol* 2007;52(12):3369, <http://dx.doi.org/10.1088/0031-9155/52/12/004>.
- [25] Parodi K, Mairani A, Brons S, Hasch BG, Sommerer F, Naumann J, et al. Monte Carlo simulations to support start-up and treatment planning of scanned proton and carbon ion therapy at a synchrotron-based facility. *Phys Med Biol* 2012;57(12):3759, <http://dx.doi.org/10.1088/0031-9155/57/12/3759>.
- [26] Sommerer F, Parodi K, Ferrari A, Poljanc K, Enghardt W, Aiginger H. Investigating the accuracy of the FLUKA code for transport of therapeutic ion beams in matter. *Phys Med Biol* 2006;51(17):4385, <http://dx.doi.org/10.1088/0031-9155/51/17/017>.
- [27] Bassler N, Kantemiris I, Karaikos P, Engelke J, Holzschleiter MH, Petersen JB. Comparison of optimized single and multifield irradiation plans of antiproton, proton and carbon ion beams. *Radiother Oncol* 2010;95(1):87–93, <http://dx.doi.org/10.1016/j.radonc.2010.02.026>.
- [28] Low DA, Harms WB, Mutic S, Purdy JA. A technique for the quantitative evaluation of dose distributions. *Med Phys* 1998;25(5):656–61, <http://dx.doi.org/10.1118/1.598248>.

Available online at [www.sciencedirect.com](http://www.sciencedirect.com)

**ScienceDirect**



PAPER • OPEN ACCESS

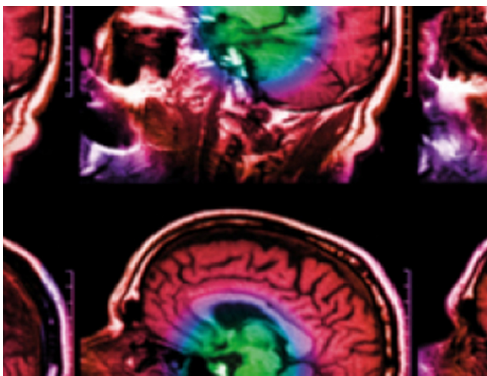
## Development, Monte Carlo simulations and experimental evaluation of a 3D range-modulator for a complex target in scanned proton therapy

To cite this article: Yuri Simeonov *et al* 2022 *Biomed. Phys. Eng. Express* **8** 035006

View the [article online](#) for updates and enhancements.

### You may also like

- [A modular method to handle multiple time-dependent quantities in Monte Carlo simulations](#)  
J Shin, J Perl, J Schümann *et al.*
- [Theoretical Modeling of Catalyst Layers for Polymer Electrolyte Fuel Cells with Different Fabrication Processes and Analysis of the Morphologies](#)  
Hiroshi Ishikawa, Yasushi Sugawara and Makoto Uchida
- [3D range-modulator for scanned particle therapy: development, Monte Carlo simulations and experimental evaluation](#)  
Yuri Simeonov, Uli Weber, Petar Penchev *et al.*



**IPEM | IOP**

Series in Physics and Engineering in Medicine and Biology

Your publishing choice in medical physics,  
biomedical engineering and related subjects.

Start exploring the collection—download the  
first chapter of every title for free.

# Biomedical Physics & Engineering Express



## PAPER

# Development, Monte Carlo simulations and experimental evaluation of a 3D range-modulator for a complex target in scanned proton therapy

### OPEN ACCESS

RECEIVED  
3 January 2022

REVISED  
22 February 2022

ACCEPTED FOR PUBLICATION  
28 February 2022

PUBLISHED  
11 March 2022

Original content from this work may be used under the terms of the [Creative Commons Attribution 4.0 licence](#).

Any further distribution of this work must maintain attribution to the author(s) and the title of the work, journal citation and DOI.



Yuri Simeonov<sup>1,2,\*</sup> , Uli Weber<sup>3</sup>, Christoph Schuy<sup>3</sup>, Rita Engenhart-Cabillic<sup>4,5</sup>, Petar Penchev<sup>1,2</sup>, Veronika Flatten<sup>1,2,4,5</sup> and Klemens Zink<sup>1,4,5</sup>

<sup>1</sup> University of Applied Sciences, Institute of Medical Physics and Radiation Protection (IMPS), Giessen, Germany

<sup>2</sup> Philipps-University, Marburg, Germany

<sup>3</sup> GSI Helmholtzzentrum für Schwerionenforschung GmbH, Biophysics division, Darmstadt, Germany

<sup>4</sup> University Medical Center Giessen-Marburg, Department of Radiotherapy and Radiooncology, Marburg, Germany

<sup>5</sup> Marburg Ion Beam Therapy Center (MIT), Marburg, Germany

\* Author to whom any correspondence should be addressed.

E-mail: [juri.simeonov@lse.thm.de](mailto:juri.simeonov@lse.thm.de)

**Keywords:** particle therapy, proton therapy, 3D range-modulator, 3D printing, FLUKA, monte carlo simulation

## Abstract

The purpose of this work was to develop and manufacture a 3D range-modulator (3D RM) for a complex target contour for scanned proton therapy. The 3D RM is considered to be a viable technique for the very fast dose application in patient-specific tumors with only one fixed energy. The RM was developed based on a tumor from a patient CT and manufactured with high-quality 3D printing techniques with both polymer resin and aluminum. Monte Carlo simulations were utilized to investigate its modulating properties and the resulting dose distribution. Additionally, the simulation results were validated with measurements at the Marburg Ion-Beam Therapy Centre. For this purpose, a previously developed water phantom was used to conduct fast, automated high-resolution dose measurements. The results show a very good agreement between simulations and measurements and indicate that highly homogeneous dose distributions are possible. The delivered dose is conformed to the distal as well as to the proximal edge of the target. The 3D range-modulator concept combines a high degree of dose homogeneity and conformity, comparable to standard IMPT with very short irradiation times, promising clinically applicable dose distributions for lung and/or FLASH treatment, comparable and competitive to those from conventional irradiation techniques.

## 1. Introduction

3D-printed range-modulators (RM) optimized for a single energy have been shown to enable a very fast dose delivery in scanned particle therapy and have proven to be very useful for a wide variety of different experiments (Tommasino *et al* 2019, Holm *et al* 2020, Simeonov *et al* 2021). Their application suffers neither from the intrinsic ‘dead time’ between successive energy layers in the state-of-the-art pencil beam scanning, nor from the beam losses typically observed with conventional passive scattering application method.

Especially the so-called 3D range-modulator (3D RM) is considered to be a potential technique for the very fast dose application in patient-specific tumors

(Simeonov *et al* 2017). These 3D RMs are a one-piece integration of a range-compensator part, responsible for ‘shifting’ and shaping the dose at the distal target edge and a modulating part, realized by using many pyramid-shaped fine structures (pins). As the pins’ shape and height is optimized and adjusted to the form of an individual patient’s tumor, highly homogeneous dose distributions are possible with the delivered dose conformed to the distal as well as to the proximal edge of the target.

By using only one fixed beam energy to create a laterally modulated homogenous spread-out Bragg peak (SOBP), a large decrease in the treatment time can be achieved with irradiation times in the order of several seconds or even less than a second in the case of an accelerator with high intensity. This opens up

new possibilities, for example in the case of moving targets (e.g., lung cancer or liver cancer), where the dose is deteriorated due to ‘interplay effects’ between the scanned ion beam and the tumor motion (Lambert *et al* 2005, Bert *et al* 2008). These modalities are expected to benefit from the 3D RM as a breath-hold technique can be utilized to make use of the decreased treatment time to avoid motion induced interplay effects.

Another very interesting application of the 3D RM could be in combination with very high dose rates for the ‘FLASH’ particle therapy. Studies conducted recently indicate that the very fast dose application (in the order of ms) with dose rates over  $40 \text{ Gy s}^{-1}$  might be beneficial and less harmful to the healthy tissue, while simultaneously maintaining tumor control, thus increasing the therapeutic window (Favaudon *et al* 2014, Durante *et al* 2018, Adrian *et al* 2019, Vozenin *et al* 2019a, 2019b, Diffenderfer *et al* 2020). There has been a steadily increasing number of publications and research interest on this topic recently. However, numerous technical challenges remain, one of which is the dose delivery in the time-frame of milliseconds. While further investigation is needed to evaluate the clinical applicability and explore the limits of the 3D RM approach, it seems to be promising and viable option for the extremely fast conformal FLASH irradiation. The 3D RM concept was referenced in different publications stating that it presents the most likely route to clinical delivery for FLASH irradiation with protons and carbon ions (Jolly *et al* 2020, Weber *et al* 2021).

As a consequent continuation of our extensive research in the field of 3D-printed modulating devices, in this work we present the development of a patient-specific 3D range-modulator for scanned proton therapy. The RM was developed using real anonymized patient CT data, utilizing a ray tracing algorithm to calculate the necessary information. It should be noted that in order to reduce the complexity and validate the complete workflow one step at a time, the whole CT including the target were overwritten with water. Multiple Monte Carlo (MC) simulations were conducted to further optimize the RM and the dose distribution. The final modulator was manufactured on a high-quality 3D printer and irradiated at the synchrotron-based Marburg Ion-Beam Therapy Centre (MIT, Germany) in order to validate the simulation results as well as the manufacturing accuracy.

## 2. Materials and methods

### 2.1. 3D range-modulator development

The optimization of the base structures (pins) has been already extensively described (Simeonov *et al* 2017, 2021). One important point worth mentioning is the pin base size, i.e. the pin period. Starting with 1.5 mm in the initial RM prototypes, the pin base was

gradually increased to 3 mm, as this value is not expected to compromise the dose distribution conformity, while offering many advantages like more favorable pin aspect ratio, increased overall robustness and improved mechanical long term stability of the pins, especially the pin tips. Most importantly, the 3 mm pins exhibit a strongly diminished sensitivity to rotation and tilting displacement during positioning compared to the 2 mm ones (Holm *et al* 2020). This is of particular importance, because the risk of over- or underdosage due to a potential misplacement of the RM is significantly reduced.

The development of this particular 3D RM was based on a ‘forward’ approach, i.e., using a pre-calculated database of pins with different heights, each of which is optimized to deliver a homogeneous SOBPs of a specified width on its own. In a first step, an anonymized patient CT was chosen with a target (will be referred to as PTV) in the middle of the therapeutic energy range. We opted for a  $68 \text{ cm}^3$  tumor in the right lung with a non-circular complex 3D contour, irregular distal and proximal edges.

The original PTV was then extended with 4 mm (figure 1, will be referred to as PTV\_4 mm). The idea behind this was to use PTV\_4 mm to create a modulator slightly larger than the tumor, in order to account for the pencil beam width (see below) and the resulting penumbra of the fluence distribution of the scanned field and, additionally, the lateral scattering at the modulator and in the patient and the resulting typical dose decrease.

Using an in-house developed MATLAB-based software environment a single coplanar beam from the right patient side was chosen. The isocenter was placed at the center of volume of PTV\_4 mm. The MatRad implementation of a ray tracing algorithm (‘matRad\_siddonRayTracer’, according to Siddon 1985 Medical Physics, (Wieser *et al* 2017)) was used to iterate stepwise through the voxels and calculate the necessary information, such as the pin length and the length/form of the integrated ‘compensator’. During ray tracing all voxels of the CT including the target were set to water. The lateral raster step size of the ray-tracer was set to 3 mm (identical to the 3 mm pin base) and the source to isocenter distance (SID) to 775 cm, which corresponds approximately to the distance between the scanning magnets and the treatment room isocenter at MIT. Such a large distance results in quasi-parallel ‘rays’ and scanned beam during the ray tracing and the real irradiation later on.

A  $150.68 \text{ MeV u}^{-1}$  monoenergetic proton beam was used, an energy, which was already well-tuned to previous experimental measurements with and without 2D modulators. Using this energy, a database of many pins, optimized for homogeneous SOBPs with extensions from 10 mm to 60 mm in steps of 10 mm was created. Sampling from this database, the output information from the ray tracing was used to



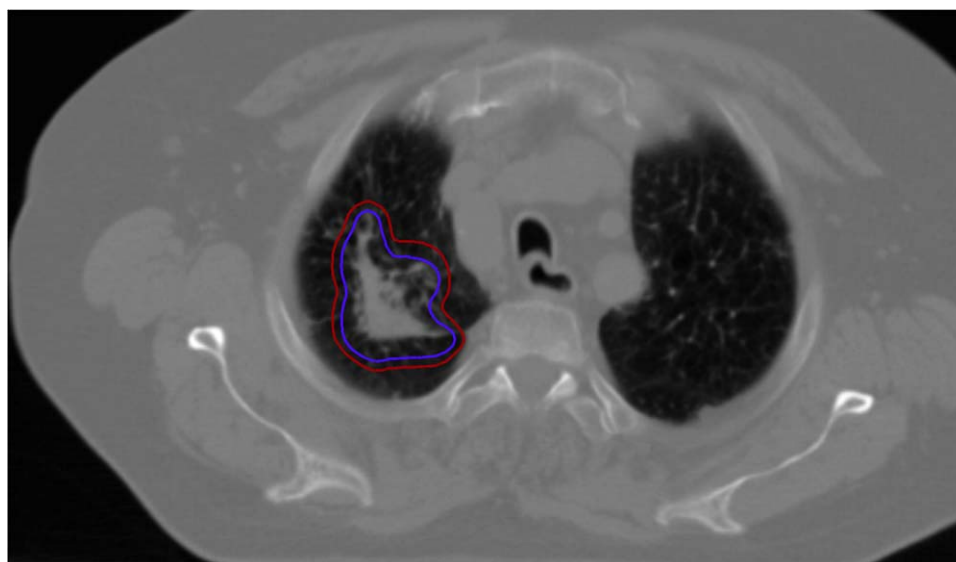


**Figure 1.** A single slice view of the used CT with the original PTV (inner blue contour) and the extended PTV\_4 mm (outer red contour).

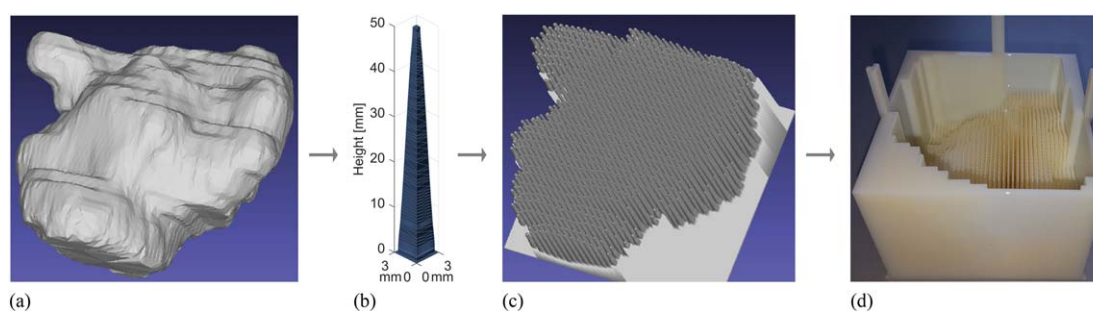


**Figure 2.** 3D view of the lung target (a), a single triangulated 50 mm pin (b), a 3D view of the optimized modulator (c) and the corresponding manufactured prototype (d). The prototype has positioning bars defining the isocenter, used for alignment with the in-room lasers and side walls for better stability and usability.

interpolate the single pins and to develop an initial version of the 3D RM.

While calculating the initial coordinates of the raster file needed to irradiate the modulator, a single scan spot (scan spot FWHM at the isocenter is approx. 11 mm) was assigned to each pin with a clinically typical value of 3 mm lateral raster step size. Many of the particles from the edge scan spots, irradiating the edge pins of the modulator, will fly unmodulated around it and cause a measurable and undesirable dose contribution at the range depth of the maximum energy. Instead of an aperture collimator, we opted for another approach to mitigate this issue. The lateral edge contour of the RM, as seen from the Beam's Eye View (BEV), was extended adding some extra pins, which length was calculated by averaging the length of the neighboring pins. These additional pins, although not directly irradiated with scan spots, but partly by the Gaussian tail of the scan spots, contribute also to some extent to the dose distribution and preserving the lateral dose homogeneity.

Finally, so-called 'positioning bars' were added to the modulator to define the reference center (figure 2).

These bars can be aligned to the room lasers so that the modulator is precisely positioned during irradiation. Additionally, side walls were added to the modulator. It should be clarified that these walls are not irradiated by scans spots and don't serve the purpose to stop or attenuate the beam, but only to improve the mechanical stability and protect the pins.

In order to complete the whole workflow from the development of the modulator, through the simulations till the measurements in the treatment room, the correct relationship had to be established between different coordinate systems (MATLAB, FLUKA, DICOM, accelerator raster file, etc). Based on this relationship, it is possible to import and position the CT in FLUKA at the same isocenter as during the ray tracing and create the corresponding raster files for the simulation and the accelerator.

## 2.2. Dose calculations

### 2.2.1. FLUKA

The FLUKA Monte Carlo (MC) package (Ferrari *et al* 2005, Böhlen *et al* 2014) was used to investigate the

modulating properties of the range-modulator and calculate the resulting dose distribution. In-house developed user routines, based on 'SOURCE.f' and 'USRMED.f' (Simeonov *et al* 2017, 2021) were additionally implemented into FLUKA to enable intensity modulated raster scanning and take into account the complex geometry contour of the modulator.

The 'HADROTHERapy' defaults were activated in all simulations (Battistoni *et al* 2016, FLUKA 2021) to ensure optimal parameters and the detailed transport of all primary and secondary particles. The PEANUT model (Battistoni *et al* 2006) is used to describe nuclear interactions for hadrons and photons. A modified version of relativistic quantum molecular dynamics (RQMD-2.4) model (Andersen *et al* 2004) is implemented for ions in the range down to 0.1 GeV  $n^{-1}$ , the Boltzman master equation (BME) handles nuclear reactions below 150 MeV  $n^{-1}$  (Cerutti *et al* 2006).

Low-energy neutrons were transported down to thermal energies. The 'flukadpm3' executable linked to the relevant libraries (rqmd, dpmjet, etc) was used. The mean excitation energy of water was set to  $I = 78$  eV. The CT data was imported and converted to the FLUKA voxel based file format (.vxl). Slices, not necessary for the simulation, were deleted in order to decrease the memory and storage requirements as several hundred simulations were conducted in parallel.

### 2.2.2. Simulation setup

The 3D range-modulator must be irradiated with an intensity modulated scanned beam in order to produce a homogenous dose distribution. The 'SOURCE.f' routine was used to sample i.e., the beam energy, spot size, x/y coordinates and the number of particles. As a single scan spot was assigned to each pin, the initial number of particles in each scan spot was calculated in such a way that it is related directly to the sum of the optimization weights (the modulating partial areas) of its corresponding pin. This initial fluence was then simulated and optimized in a subsequent step to obtain the final intensity distribution (see section 2.3.).

The isocenter, equivalent to the room isocenter at MIT (figure 6), is defined at  $Z = 0$  cm, where the positive z-axis points in beam direction. Sampling from the raster file, primary protons with 150.68 MeV  $u^{-1}$  kinetic energy are generated in vacuum at  $Z = -775$  cm, which corresponds to the middle position between the vertical and horizontal scanning magnets at MIT. A scan spot specific angle is pre-calculated (the direction cosines are determined from the lateral deflection of the scan spots and the distance between the particle sampling point and the isocenter) and assigned to the particles on a per-spot basis, accounting for the fact that the laterally deflected pencil beam from a real accelerator is not parallel to the beam direction axis. To account for the small beam divergence of the accelerator from the ion optics, an

additional angle is sampled randomly for each particle from a Gaussian angular distribution with  $\sigma = 1$  mrad and added to the scan spot specific angle. The coordinates of the primary particles in each scan spot are sampled from a Gaussian distribution, where the FWHM width has been previously adjusted to match the beam width at the isocenter at MIT.

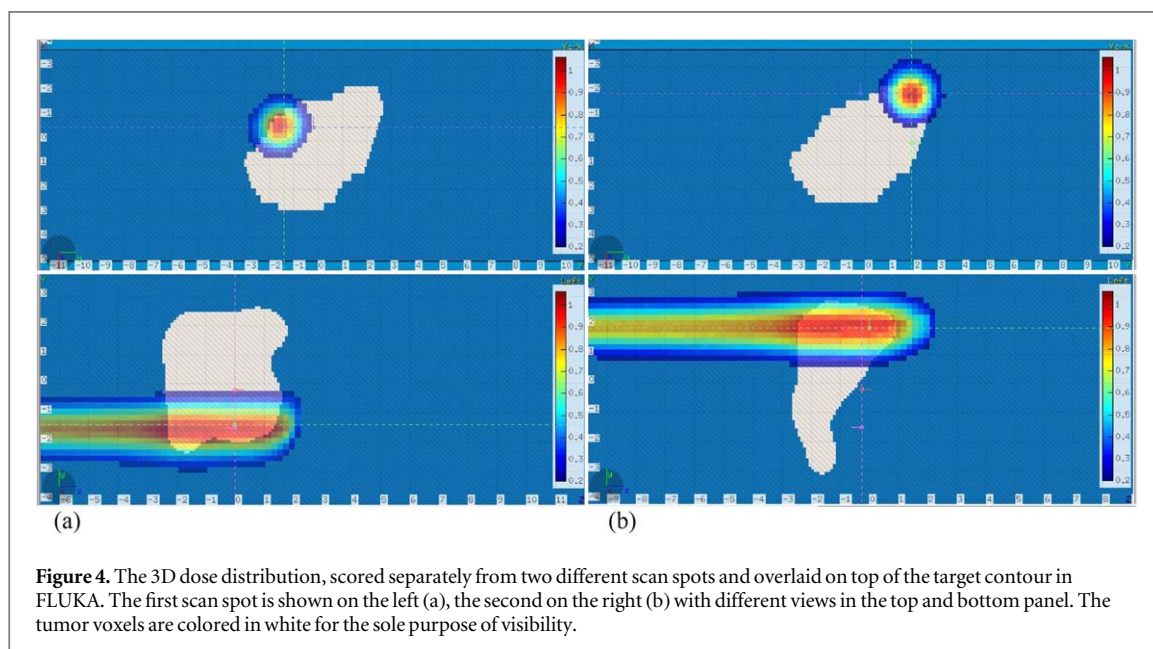
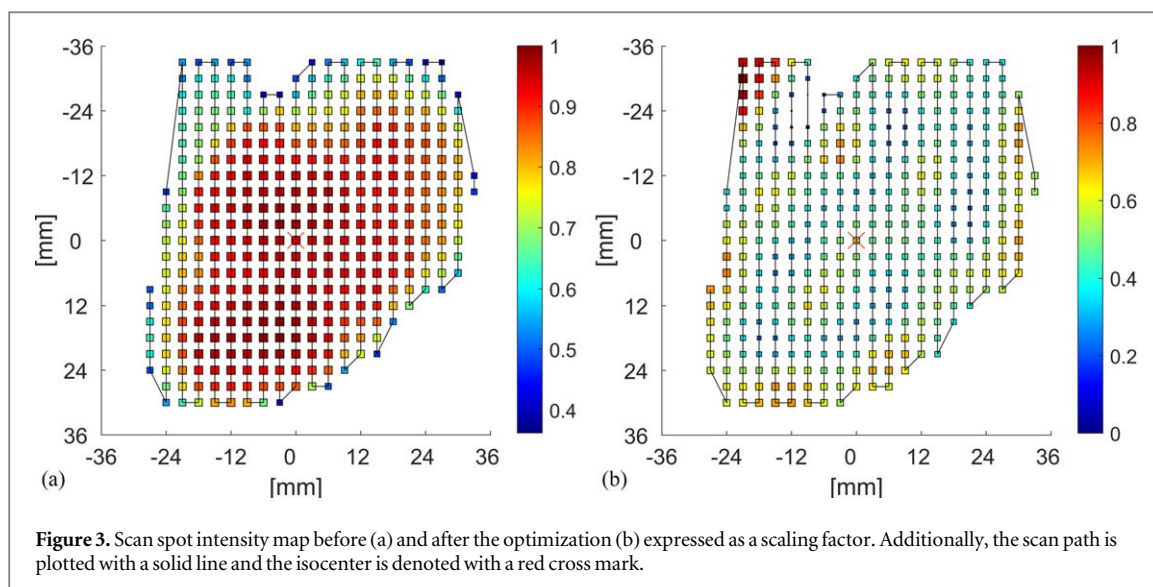
Using the established coordinate system relationship and FLUKA rotation definition, the CT voxel region was translated and rotated (using 'ROT-DEFI' cards) in such a way that the FLUKA isocenter is identical to the isocenter previously set during the ray tracing. All voxels of the imported CT were set to water. The 3D RM was positioned 25 cm in front of the CT region. At this distance the lateral fluence ripple, typically observed behind the modulator due to pin edge scattering, has already completely blurred out (Ringbæk *et al* 2015). This is in contrast to heavy carbon ions, where a much larger distance of e.g. 40 cm to 60 cm is needed (Simeonov *et al* 2017).

The 3D dose deposition (GeV/g per unit primary weight) was scored using the USRBIN card with a Cartesian X-Y-Z voxel mesh. The voxel size was set to 2.5 mm in the 'lateral' direction as seen from the BEV (this corresponds to the 2.5 mm resolution of the PTW Octavius 1000P later used for the measurements) and 1 mm in Z. A total number of  $7 \times 10^8$  particles was simulated resulting in a statistical uncertainty below 0.3% in the homogeneous target region. The statistical uncertainty is calculated by FLUKA automatically and corresponds to the square root of the variance of the mean of the estimated quantity (e.g., dose) among the different CPU runs.

### 2.3. Scan spot optimization

In order to increase the dose homogeneity in the target region and to achieve a clinically applicable dose distribution, an optimization of the initial number of particles (figure 3(a)) in each scan spot is necessary. For this purpose, the FLUKA 'SOURCE.f' routine and our CPU cluster were adjusted so that each scan spot from the initial raster file and its corresponding 3D dose distribution can be simulated and scored separately, i.e., a raster file with 367 scan spots, as in our case, will result in 367 separate 3D dose files (figure 4). The whole process is completely automated and the scan spots are distributed on a cluster of  $\sim 800$  CPUs.

At the end of the simulation all dose files were loaded in the in-house developed MATLAB environment and matched to the CT data. An initial weighting factor was assigned to each of these 3D dose distributions and the weighted dose sum inside the PTV was calculated. Optimization was implemented to calculate and minimize the difference between the weighted dose sum and a prescribed homogeneous dose distribution. The resulting optimized weighting factors were used in the raster file for the final simulation (figure 3(b)).



Note that while the original 3D RM was developed on the basis of the slightly larger PTV\_4 mm, the dose is optimized for homogeneity only inside the original PTV contour. No OAR were taken into account, the only ‘dose constraint’ was the homogeneity inside the PTV target.

## 2.4. 3D range-modulator manufacturing

### 2.4.1. Polymer modulator

The modulator was manufactured on a high-quality PolyJet 3D-printer. These printers use photopolymers to additively build detailed prototypes with high reproducibility and accuracy. Recently, there has been an increased interest in the deployment of 3D printing techniques in the field of radiation therapy (Ju *et al* 2014, Lindsay *et al* 2015, 2016).

The Stratasys Objet30 Pro was used to manufacture the 3D RM (figure 2). An advanced simulated polypropylene (RIGUR RGD450) was used as a

material with a polymerized density of  $1.2 \text{ g}^* \text{ cm}^{-3}$ . Printing time was about 12 h in the presented case. This polymer modulator is the main scope of this work.

### 2.4.2. Aluminum modulator

Apart from the photopolymer resin, which is accepted and broadly used in many different fields and applications, our research group has been investigating different materials and manufacturing techniques. Based on this experience a decision was taken to additionally consider an aluminum modulator manufactured with the selective laser melting (SLM) method. In the SLM process, a laser is used to melt and fuse metal powder to create high-density structures (Kruth *et al* 2005, Konda Gokuldoss *et al* 2017, Trevisan *et al* 2017). Using aluminum, we intend to validate the complete workflow process with a



Figure 5. The aluminum 3D RM with a side wall and positioning bars.

different material, a second completely different 3D printer and a new manufacturing technique.

Aluminum has some advantages, i.e. much better stability and robustness, much shorter pins (due to the higher density) with better pin aspect ratio, which are both easier to manufacture and would enable the design and printing of modulators for larger targets. Additionally, at the same stopping power, aluminum produces less light fragments and neutrons compared to the polymer resin. This can be shown by the Bradt-Peters formula (Bradt and Peters 1950), which indicates that the fragmentation cross section per areal density scales to  $A^{-1/3}$  (Durante and Cucinotta 2011). On the other hand, there will be increased scattering and the cost and complexity of the SLM technique are higher.

To test the limits of this technique, the 3D RM was manufactured using aluminum on a TRUMPF TruPrint 3000 SLM printer (figure 5). It is out of the scope of this publication to present extensive results from this modulator, but rather demonstrate and briefly discuss the potential of the aluminum material and SLM technique as an alternative approach.

## 2.5. Dose measurements

A fast, completely automated, high-resolution dosimetric verification of the 3D range-modulator was performed at MIT to validate the simulation results. The universal, water phantom WERNER, developed at GSI, was used (Schuy *et al* 2020, Simeonov *et al* 2021). It has a holder for a standard medical 2D ionization chamber array (e.g. PTW Octavius 1500XDR or 1000P) and can be synchronized to the dose delivery system of the accelerator.

Figure 6 shows a schematic drawing of the dose measurement setup and a picture of the measurement session. The positioning setup corresponds exactly to the FLUKA simulations setup with the isocenter placed at 20 cm depth inside WERNER. The modulator was precisely positioned and aligned with the lasers 25 cm in front of WERNER.

The raster file, previously used in the FLUKA simulations, was used to steer the beam delivery system of the accelerator. The prototype PTW 2D Ionization Chamber Array Octavius 1000P (977 air-filled detectors) with very fine 2.5 mm spatial resolution was placed inside the detector holder and used to measure the lateral dose distribution at each depth. The depth dose distribution in the SOBP region was scored in 1 mm steps. Outside of the SOBP region the steps were varied between 2 and 10 mm. Subsequently, we compared the measured dose profiles with the FLUKA simulations.

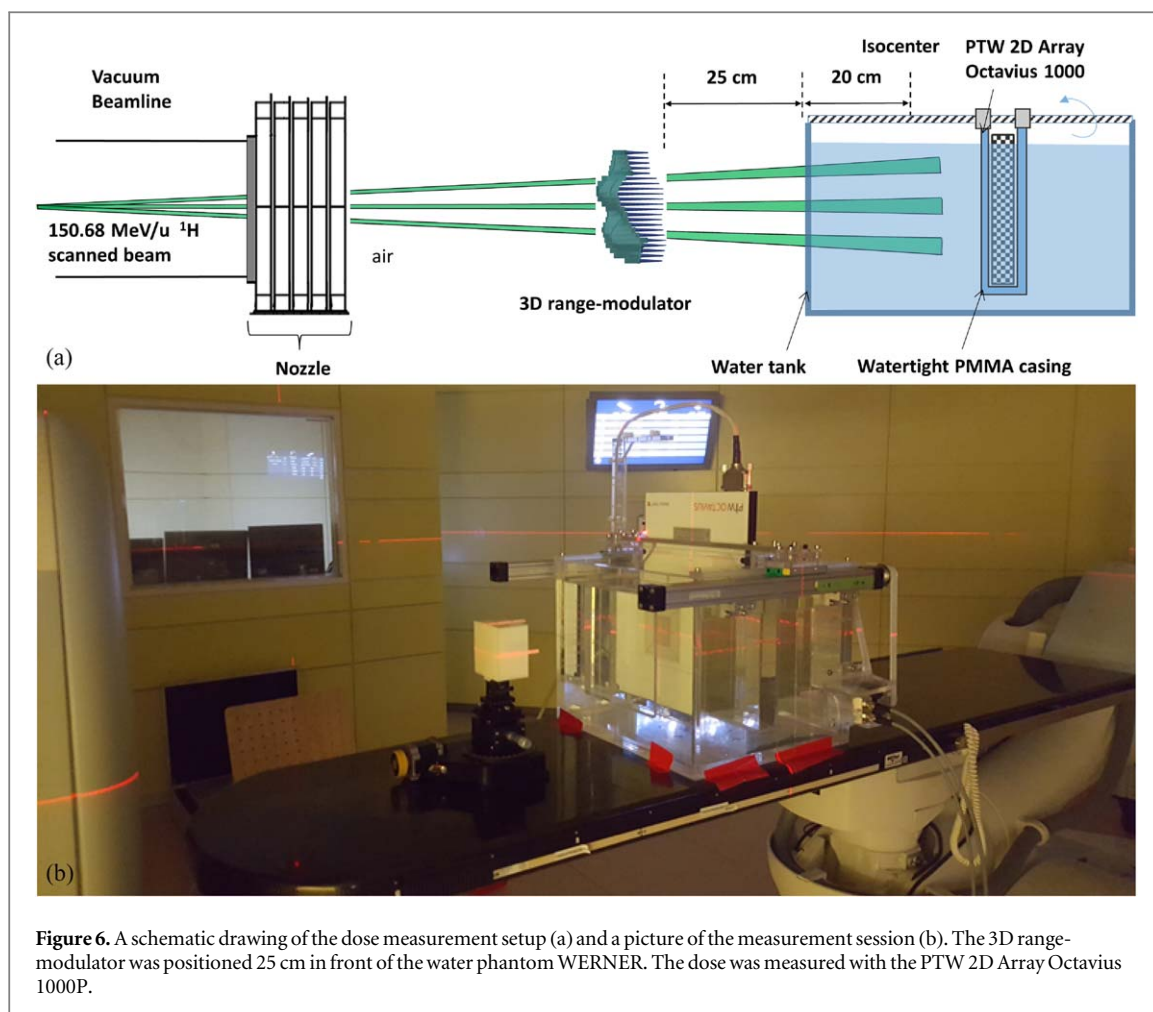
## 3. Results

### 3.1. Polymer modulator

#### 3.1.1. Dose application

The raster plan was normalized to  $\sim 1.1 \times 10^{10}$  total number of particles and irradiated with the maximum clinically available accelerator intensity of  $1.9 \times 10^9$  part/s in approx. 6 s. This resulted in  $\sim 0.5$  Gy inside the  $\sim 70$  cm<sup>3</sup> target volume.

A total set of 61,551 measured dose points (977 detectors\*63 measurements in different depths) were obtained. The raster plan was irradiated 63 times resulting in a total measurement time of 9 min. Raster plan irradiation, the synchronized depth movement of



the Octavius detector array and the dose scoring were completely automated.

### 3.1.2. Comparison of dose distributions from simulation and measurement

Both the measured and simulated 3D dose distributions were interpolated on a regular 1 mm grid. Both dose distributions were normalized to 100 in the middle of the central SOBP depth dose, then matched to the PTV in the DICOM coordinates and exported to an RT Dose file.

Figures 7(a), (b) show an isodose comparison of 2 different slices between the measured and simulated dose distribution. The corresponding 1D dose profiles, taken at 15 cm depth (denoted as a vertical dotted line in the 2D plots above) are additionally plotted in panel (c) and (d). Panel (e) shows the measured and simulated dose overlaid on top of the raw CT data. It is important to note again, that, as already stated, the CT was first overwritten with water material and the modulator was developed on the basis of this ‘water’ CT with no inhomogeneities inside. However, in order to visualize the original tumor tissue and tumor delineation, we have plotted the heterogeneous CT data in the background. The red line denotes the PTV contour, the rest are isodose lines, whereby the thick lines correspond to the measurement and the thinner lines to the

simulation. The 50% transparent color-wash dose corresponds to the simulated dose.

Figure 8 shows several more 1D profiles extracted from the 3D dose distributions. A lateral dose profile from a broad homogeneous dose region is depicted in panel (a). Panels (b)–(d) show SOBPs from different slices and positions. Smaller 2D isodose figures are additionally included, denoting the exact positions, at which the 1D profiles were plotted.

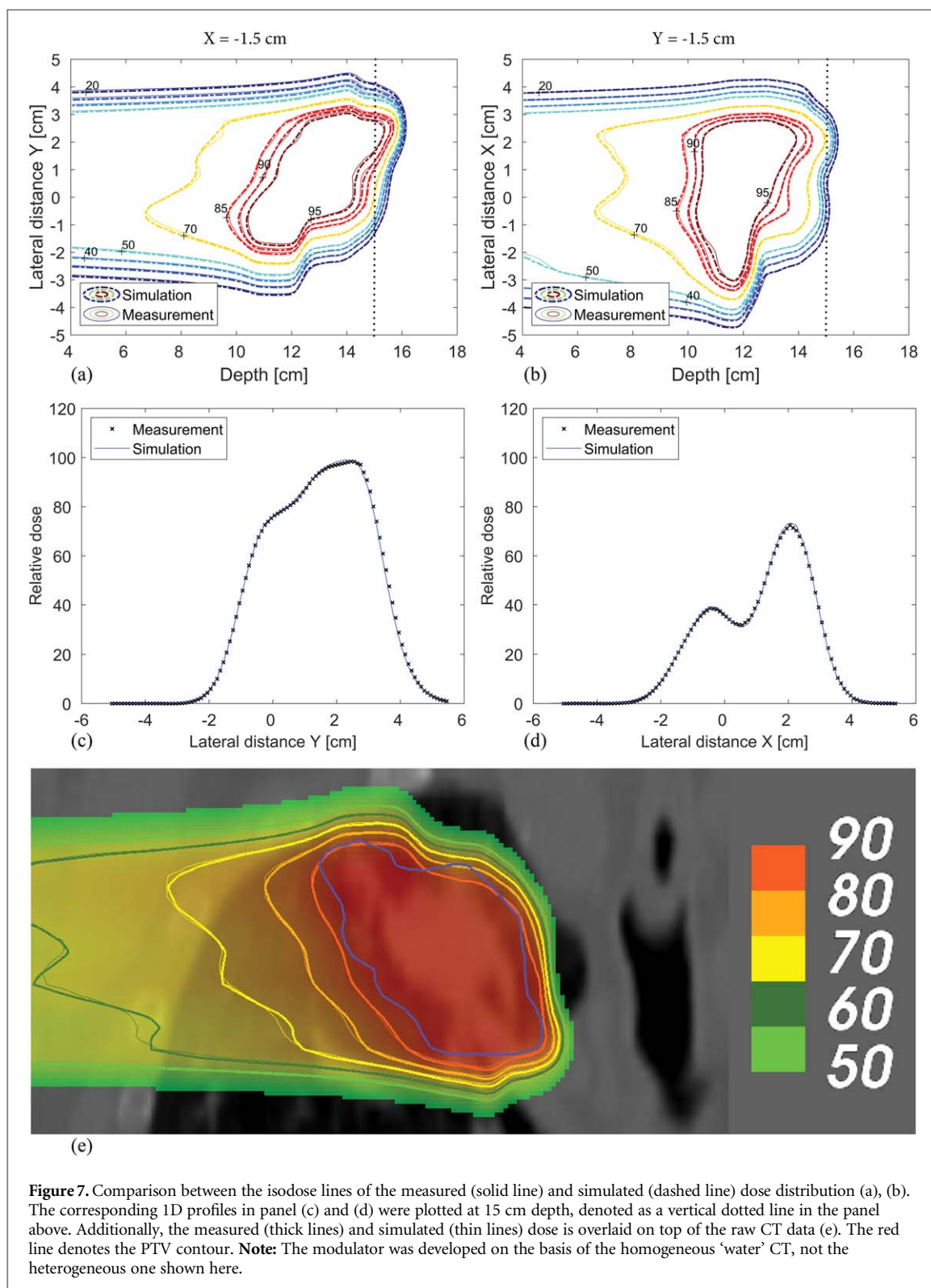
Overall, a very good agreement between measured and simulated dose distributions can be observed in all slices.

### 3.1.3. Gamma index

In order to quantify the agreement between the measured and simulated dose distributions, a 2D gamma index (GI) of two slices (figure 9) and the full 3D gamma index were calculated. For this purpose, the PTW VeriSoft software was utilized as an established and validated tool. A local GI with 2%/2 mm acceptance criteria was used, whereby dose values less than 15% of the maximum dose were not evaluated. Both 2D and 3D GI show a high passing rate of ~99%.

### 3.1.4. Dose-volume histogram

Figure 10 shows the cumulative Dose-Volume Histogram (DVH) calculated inside the PTV contour and



the resulting statistical information. The applied dose normalization results in maximum dose of approximately 105% and mean dose close to 100%.

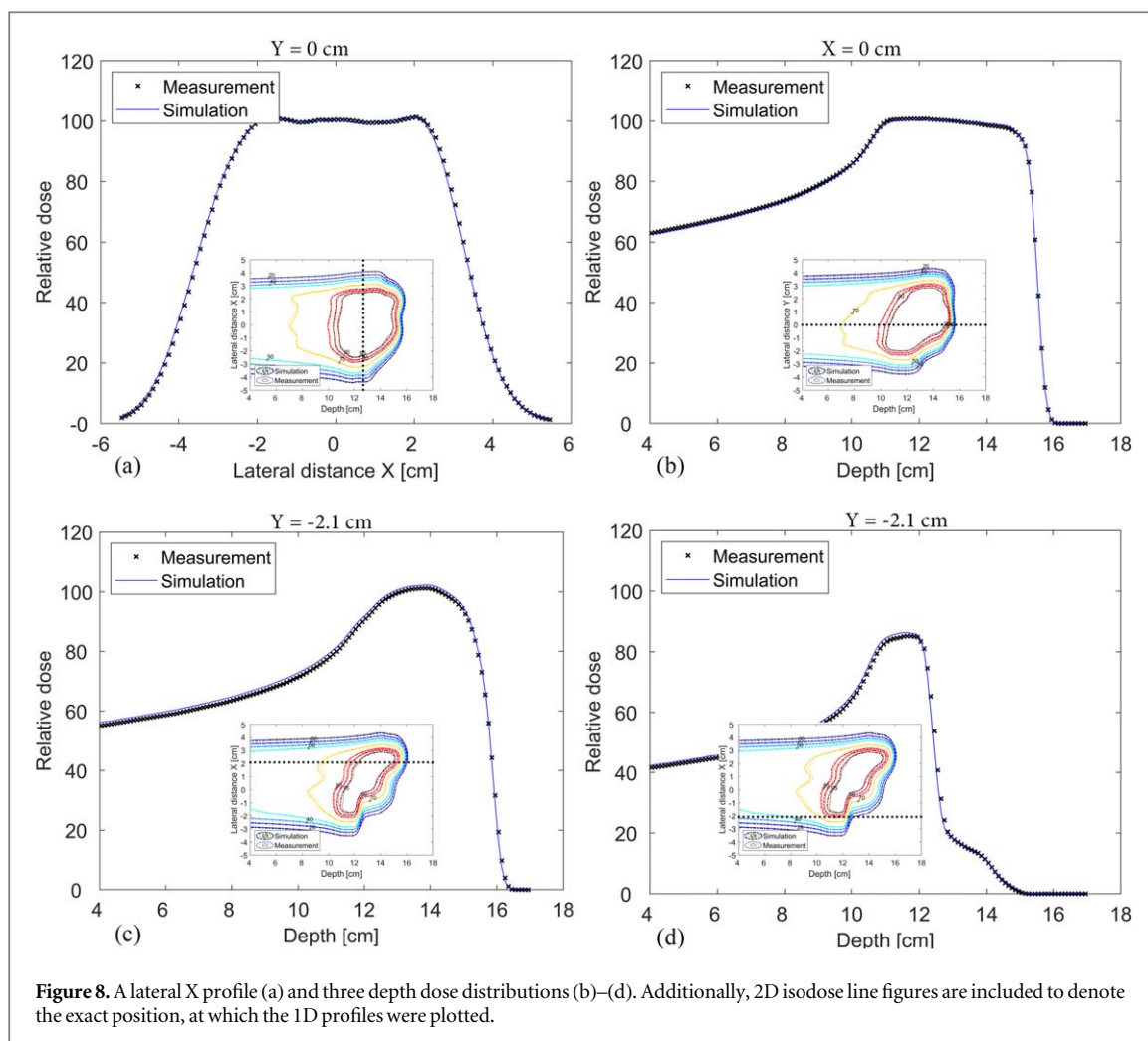
### 3.2. Aluminum modulator

Figure 11 shows a depth dose distribution and an isodose comparison of one slice between the measured and simulated dose distribution for the aluminum RM. As in the case with the polymer modulator, there

is a very good agreement between the simulations and measurements. The 2D GI of the shown dose slice is 99% and the 3D GI was found to be 98%.

### 4. Discussion

Judging by the dose comparisons in figures 7–9, owing to our previous research in this field (Simeonov *et al* 2017, 2021), we have managed to obtain a very good



**Figure 8.** A lateral X profile (a) and three depth dose distributions (b)–(d). Additionally, 2D isodose line figures are included to denote the exact position, at which the 1D profiles were plotted.

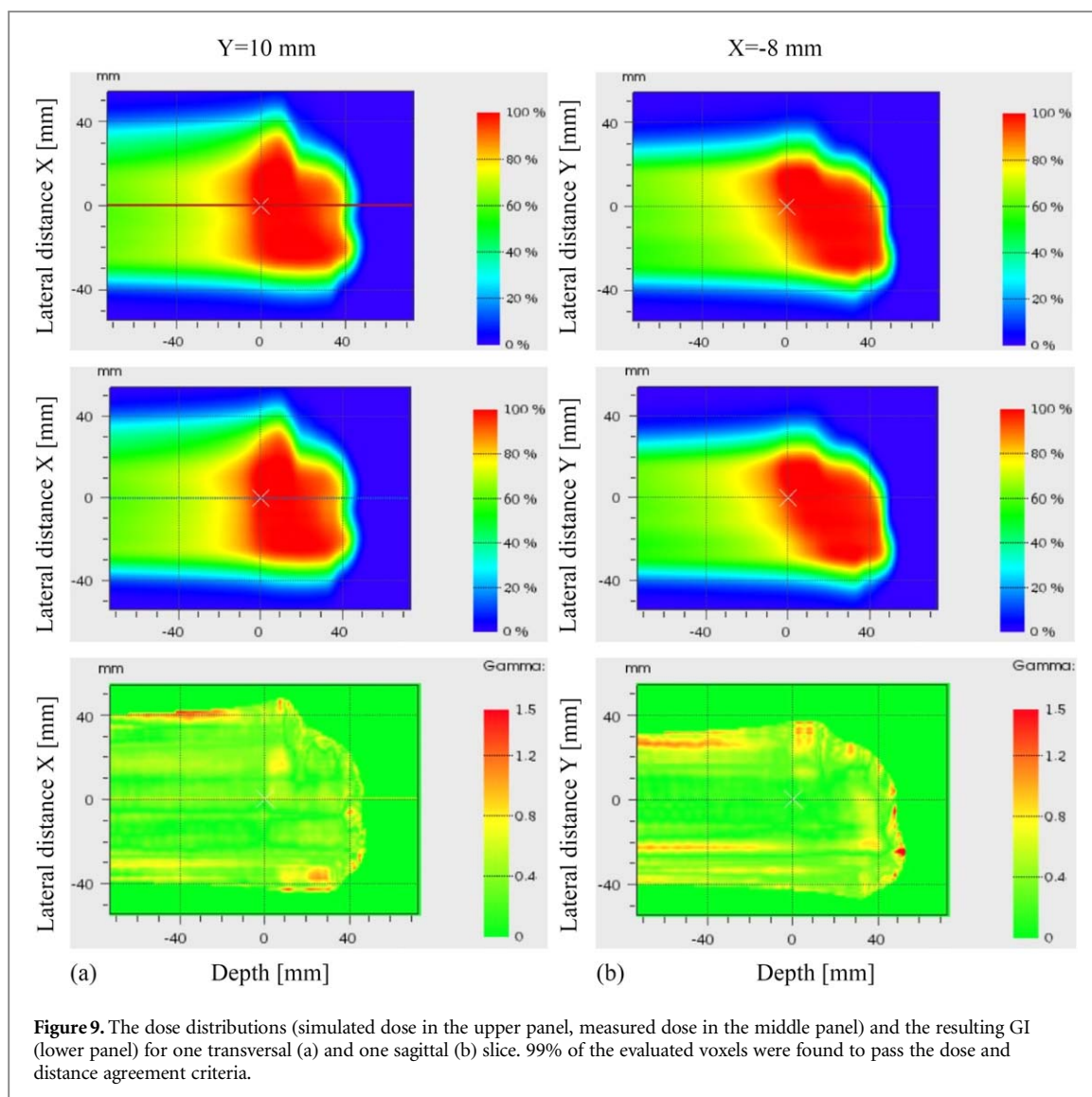
agreement between the predicted and measured dose distribution. The introduction of a 3 mm pin base (up from 1.5 mm initially) improved not only the mechanical (long-term) stability, but also the manufacturing of the sharp pin tips and greatly reduced the sensitivity of the modulator to tilt/rotation misplacement. The latter was investigated in preliminary simulations and also validated with dose measurements (Holm *et al* 2020) by placing the modulator on a positioning table and rotating it with a defined and reproducible angle around one axis.

In contrast to some of the first 3D RM prototypes, an effect of potential printing artefacts is not visible in the dose distribution of the newly developed prototype. Such dose deviations are most easily identified in the depth dose distribution. For example, figure 8(b) shows a wide SOBP extracted from the middle of the target. Common and characteristic dose deteriorations, which originate from manufacturing artefacts (e.g. too much material in the groove between successive pins as with the spherical target, (Simeonov *et al* 2017)), are not present. The results indicate that the manufacturing of 3D-printed RMs for dose modulation, while admittedly still challenging, should be feasible. Most probably, some kind of a printer specific

correction will be necessary with most printers to obtain sufficiently good results.

Overall, FLUKA delivers a very reasonable prediction of the dose distribution. As all simulations were conducted in water, the initial measurement concept using a range shifter with multiple PMMA plates (Simeonov *et al* 2017) was abandoned and the automated water phantom WERNER, already developed and utilized for previous measurements, was used, which further improved the agreement between the simulations and measurements.

The positioning of the modulator and the Octavius ionization chamber array is also relevant to reduce the deviations between the measured and simulated dose distribution. While the 3D RM can be aligned fast and precisely with the room lasers and is not very sensitive to minor deviations, the alignment of the water phantom and especially the detector inside might be more challenging and present a source of dose deviations. For example, in the case of a tilt of the water phantom only (not the detector) the lateral profiles of the measurement and the ‘perfect’ simulation diverge with increasing depth, as the detector moves on an axis not parallel to the beam axis. In the case of a tilt of the detector (not the water phantom) a dose tilt is observed along the chamber array detectors in high



dose gradient regions, e.g., the distal edge of the BP or SOBP. Both of these effects might be present to some extent and should be kept in mind so that they are not mistakenly associated with dose artefacts from the modulator itself.

In our initial measurements a dose tilt was observed in some higher dose gradient regions and especially at the distal edge, which turned out to originate from a  $0.5^\circ$  positioning tilt along the longer vertical side of the Octavius detector. Based on this experience, a measurement protocol was established to minimize these deviations and obtain the best possible measurement results. This protocol includes among other things an initial measurement performed at the distal edge of the pristine BP with a broad homogeneous field without a modulator to evaluate the dose homogeneity and fine-tune the ion chamber array positioning to reduce its tilt down to  $\leq 0.2^\circ$ . This value represents more or less a practical limit and do not have a measurable impact on the quality of the dose distribution.

After gaining some experience with the newly developed water phantom WERNER, highly

reproducible dose measurements were conducted in the course of several measurement sessions leading to the presented results.

Figure 7(e) shows the PTV contour from two CT slices with the overlaid dose distributions. The PTV is mostly surrounded by the 90% isodose curve in both the simulated and measured dose distributions. The high dose region is well conformed to the distal as well as to the proximal edge of the target, confirming the initial expectations on the modulating properties of the 3D-printed prototype.

The quantitative comparison, shown in figure 9 in the form of a 2D gamma index, supports the initial impression from the dose distributions in figure 7. Both 2D and 3D GI exhibit a high passing rate of  $\sim 99\%$  pointing to a very good agreement between the measured and simulated values.

In order to obtain a better understanding of the overall 3D dose distribution, the DVH was calculated and plotted in figure 10. Both curves are in a very good agreement and have a relatively sharp fall-off indicating a homogeneous dose distribution inside the target



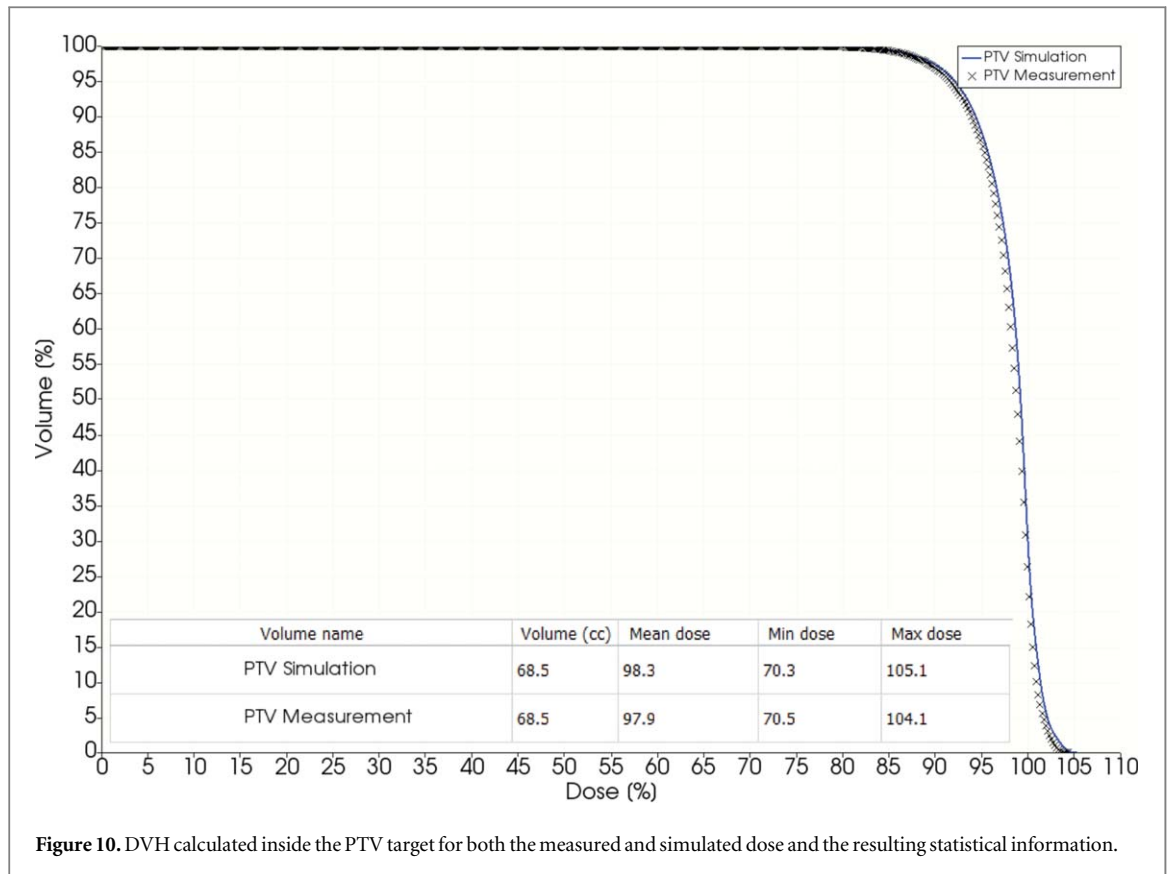


Figure 10. DVH calculated inside the PTV target for both the measured and simulated dose and the resulting statistical information.

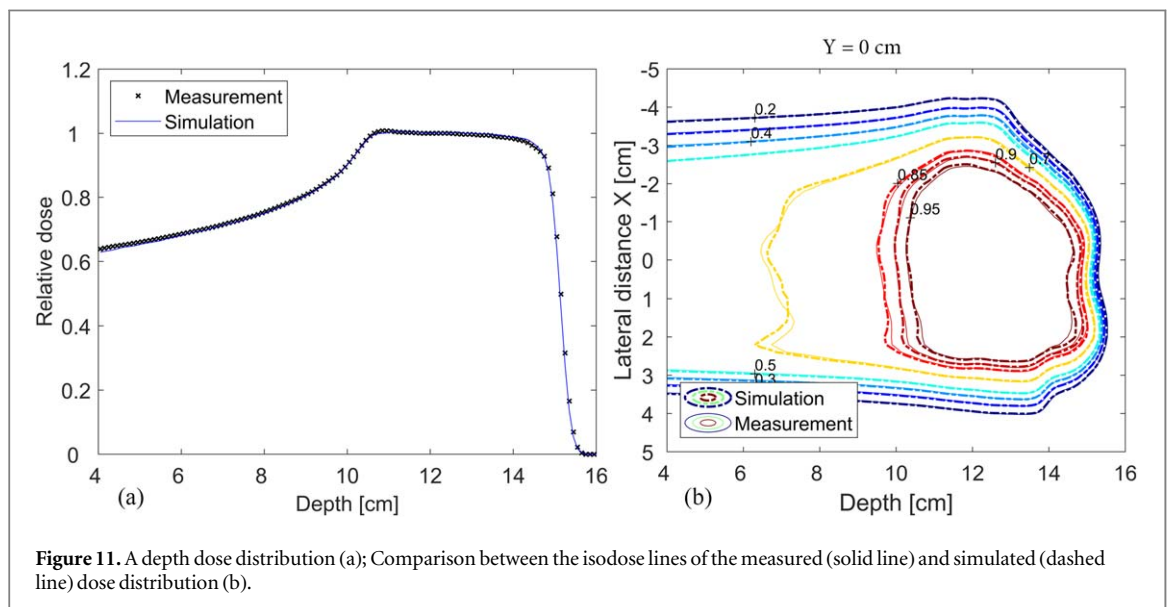


Figure 11. A depth dose distribution (a); Comparison between the isodose lines of the measured (solid line) and simulated (dashed line) dose distribution (b).

volume. There is no deterioration of the measured DVH relative to the simulated DVH, pointing to the improved 3D RM prototype quality.

In the case of the 3D aluminum modulator, a completely new material and manufacturing technique were introduced. Moreover, due to the stronger scattering of the aluminum new MC simulations had to be conducted together with new scan spot optimization. Despite these additional uncertainties there is an excellent agreement between the measured and simulated dose distributions.

By printing and measuring the aluminum modulator we have demonstrated the workflow process chain with a new material. More importantly, a new manufacturing technique and second completely different 3D printer were successfully validated, which presents one more step towards establishing rapid prototyping as a viable option for patient-specific modulators.

The presented results are indicative of the potential of the 3D RM approach, as we have successfully demonstrated a complete workflow loop for a

potential clinical implementation of a 3D RM. However, the patient does not consist of water and the 3D RM concept should be further investigated and validated for the more complex case of a realistic heterogeneous tissue composition. As the basic mathematical and physics principles are not different the authors are confident that the 3D RM concept should work fairly well also in this case. Moreover, the utilization of more sophisticated and advanced optimization algorithms for both the pin geometry and the scan spot optimization is expected to further improve the dose homogeneity and conformity. For example, we have used a 'forward' approach, where a pre-defined and pre-optimized pin databank was used to create the 3D RM. This is in contrast to an alternative approach, where a treatment planning system (TPS) with more advanced algorithms could be used for the 'inverse' optimization of an objective function (dose, dose rate, LET, etc). The obtained scan spot map with the corresponding iso-energy layers and weights can then be subsequently converted to a set of individual pin profiles to create the 3D RM. As this approach might result in more arbitrary pin geometries, a special emphasis should be put on optimizing 'printer-friendly' structures that can be also realistically manufactured.

Finally, the goal of the modulator concept is the very fast dose application for moving targets and/or FLASH. In our particular case with a synchrotron accelerator (MIT) it took  $\sim 6$  s. to irradiate the target with a monoenergetic raster plan. Using an accelerator with higher intensity capabilities (e.g. an isochronous cyclotron), it should definitely be possible to further decrease the treatment time significantly, down to less than a second. By implementing an automated measurement concept with a multi ionization-chamber array and taking advantage of the very short irradiation time, a full high-resolution 3D dose distribution can be reconstructed, paving the way for a practical dose verification QA routine in a time-constrained clinical environment.

## 5. Conclusion

This work extended the concept of the 3D range-modulator to a complex target contour. Additionally, a complete process chain, including the mathematical pin development, MC simulations, scan spot optimization, high-quality manufacturing and fast, high-resolution automated dose measurements, was demonstrated and successfully validated.

The 3D range-modulator concept combines a high degree of dose homogeneity and conformity with very short irradiation times, promising clinically applicable dose distributions for lung and/or FLASH treatment, potentially comparable and competitive to those from conventional irradiation techniques. Recent increased research interest on the potential of the 3D RM, among other things from some of the major players in

the particle therapy community, make us cautiously optimistic and hopeful for the transition of the RM concept from a purely research topic into a clinically feasible option.

## Acknowledgments

The project was supported by the Federal Ministry of Education and Research within the scope of the grant 'Physikalische Modellierung für die individualisierte Partikel-Strahlentherapie und Magnetresonanztomographie', (MiPS, grant number 13FH726IX6). The authors acknowledge the financial support of Zentrales Innovationsprogramm Mittelstand (ZIM) from the German Ministry of Economics, grant number 4223906BA7 and also from the Hessian Ministry of Higher Education, Research, Science and the Arts for the beam time.

We acknowledge Mr Holger Krause (PORTEC GmbH, Germany) for the manufacturing of the aluminum modulator and the continuous support and valuable technical expertise provided throughout the whole project.

We express our appreciation to MIT, Matthias Witt and Yannick Senger for the technical support during measurements and the beam time provided.

## Data availability statement

The data that support the findings of this study are available upon reasonable request from the authors.

## ORCID iDs

Yuri Simeonov  <https://orcid.org/0000-0001-5758-5781>

Veronika Flatten  <https://orcid.org/0000-0003-4963-6838>

Klemens Zink  <https://orcid.org/0000-0001-5785-4101>

## References

- Adrian G, Konradsson E, Lempart M, Bäck S, Ceberg C and Petersson K 2019 The FLASH effect depends on oxygen concentration *Br. J. Radiol.* **93** 20190702
- Andersen V et al 2004 The fluka code for space applications: recent developments *Adv. Space Res.* **34** 1302–10
- Battistoni G et al 2016 The FLUKA code: an accurate simulation tool for particle therapy *Front. Oncol.* **6** 116
- Battistoni G, Cerutti F, Engel R, Fasso A, Gadioli E, Garzelli M V, Ranft J, Roesler S and Sala P R 2006 Recent developments in the FLUKA nuclear reaction models *Proc. 11th Int. Conf. Nucl. React. Mech.* **13** 1–13 ([http://www0.mi.infn.it/~gadioli/Varenna2006/Proceedings/Ferrari\\_A.pdf](http://www0.mi.infn.it/~gadioli/Varenna2006/Proceedings/Ferrari_A.pdf))
- Bert C, Grözinger S O and Rietzel E 2008 Quantification of interplay effects of scanned particle beams and moving targets *Phys. Med. Biol.* **53** 2253
- Böhlen T T, Cerutti F, Chin M P W, Fassò A, Ferrari A, Ortega P G, Mairani A, Sala P R, Smirnov G and Vlachoudis V 2014 The FLUKA code: developments and challenges for high energy and medical applications *Nucl. Data Sheets* **120** 211–4

- Bradt H L and Peters B 1950 The heavy nuclei of the primary cosmic radiation *Phys. Rev.* **77** 54–70
- Cerutti F, Battistoni G, Capezzali G, Colleoni P, Ferrari A, Gadioli E, Mairani A and Pepe A 2006 *Low Energy Nucleus–Nucleus Reactions: The Bme Approach And Its Interface With Fluka* **1** 1–8 (<https://semanticscholar.org/paper/LOW-ENERGY-NUCLEUS%E2%80%93NUCLEUS-REACTIONS%3A-THE-BME-AND-Cerutti-Battistoni/b8735a2bbf34680bd88d39e294b71c25358121cb>)
- Diffenderfer E S et al 2020 Design, implementation, and *in vivo* validation of a novel proton FLASH radiation therapy system *Int. J. Radiat. Oncol. • Biol. • Phys.* **106** 440–8
- Durante M, Bräuer-Krisch E and Hill M 2018 Faster and safer? FLASH ultra-high dose rate in radiotherapy *Br. J. Radiol.* **91** 1–4
- Durante M and Cucinotta F A 2011 Physical basis of radiation protection in space travel *Rev. Mod. Phys.* **83** 1245–81
- Favaudon V et al 2014 Ultrahigh dose-rate FLASH irradiation increases the differential response between normal and tumor tissue in mice *Sci. Transl. Med.* **6** 245ra93–45ra93
- Ferrari A, Sala P R, Fassò A and Ranft J 2005 *FLUKA: A Multi-Particle Transport Code (Program Version 2005)* (Geneva: CERN) (<https://doi.org/10.2172/877507>)
- FLUKA 2021 The official FLUKA site: FLUKAOnline Manual Online ([http://fluka.org/fluka.php?id=man\\_onl&sub=20](http://fluka.org/fluka.php?id=man_onl&sub=20))
- Holm K M, Weber U, Simeonov Y, Krauss A, Jäkel O and Greulich S 2020 2D range modulator for high-precision water calorimetry in scanned carbon-ion beams *Phys. Med. Biol.* **65** 215003
- Jolly S, Owen H, Schippers M and Welsch C 2020 Technical challenges for FLASH proton therapy *Phys. Med.* **78** 71–82
- Ju S G, Kim M K, Hong C-S, Kim J S, Han Y, Choi D H, Shin D and Lee S B 2014 New technique for developing a proton range compensator with use of a 3-dimensional printer *Int. J. Radiat. Oncol.* **88** 453–8
- Konda Gokuldoss P, Kolla S and Eckert J 2017 Additive manufacturing processes: selective laser melting, electron beam melting and binder jetting—selection guidelines *Materials* **10** 672
- Kruth J, Mercelis P, Van Vaerenbergh J, Froyen L and Rombouts M 2005 Binding mechanisms in selective laser sintering and selective laser melting *Rapid Prototyp* **11** 26–36
- Lambert J, Suchowerska N, McKenzie D R and Jackson M 2005 Intrafractional motion during proton beam scanning *Phys. Med. Biol.* **50** 4853
- Lindsay C, Kumlin J, Jirasek A, Lee R, Martinez D M, Schaffer P and Hoehr C 2015 3D printed plastics for beam modulation in proton therapy *Phys. Med. Biol.* **60** N231
- Lindsay C, Kumlin J, Martinez D M, Jirasek A and Hoehr C 2016 Design and application of 3D-printed stepless beam modulators in proton therapy *Phys. Med. Biol.* **61** N276
- Ringbæk T P et al 2015 Fluence inhomogeneities due to a ripple filter induced Moiré effect *Phys. Med. Biol.* **60** N59
- Schuy C, Simeonov Y, Durante M, Zink K and Weber U 2020 Technical note: vendor-agnostic water phantom for 3D dosimetry of complex fields in particle therapy *J. Appl. Clin. Med. Phys.* **21** 227–232
- Simeonov Y, Weber U, Penchev P, Ringbæk T P, Schuy C, Brons S, Engenhardt-Cabillic R, Bliedtner J and Zink K 2017 3D range-modulator for scanned particle therapy: development, Monte Carlo simulations and experimental evaluation *Phys. Med. Biol.* **62** 7075–96
- Simeonov Y, Weber U, Schuy C, Engenhardt-Cabillic R, Penchev P, Durante M and Zink K 2021 Monte Carlo simulations and dose measurements of 2D range-modulators for scanned particle therapy *Z. Für Med. Phys.* **31** 203–14
- Tommasino F et al 2019 A new facility for proton radiobiology at the Trento proton therapy centre: design and implementation *Phys. Med.* **58** 99–106
- Trevisan F, Calignano F, Lorusso M, Pakkanen J, Aversa A, Ambrosio E P, Lombardi M, Fino P and Manfredi D 2017 On the selective laser melting (SLM) of the AlSi10Mg Alloy: process, microstructure, and mechanical properties *Materials* **10** 76
- Vozenin M-C et al 2019a The Advantage of FLASH radiotherapy confirmed in mini-pig and cat-cancer patients *Clin. Cancer Res.* **25** 35–42
- Vozenin M-C, Hendry J H and Limoli C L 2019b Biological benefits of ultra-high dose rate FLASH radiotherapy: sleeping beauty awoken *Clin. Oncol.* **31** 407–15
- Weber U A, Scifoni E and Durante M 2021 FLASH radiotherapy with carbon ion beams *Med. Phys.* **1–19**
- Wieser H-P et al 2017 Development of the open-source dose calculation and optimization toolkit matRad *Med. Phys.* **44** 2556–68

PAPER • OPEN ACCESS

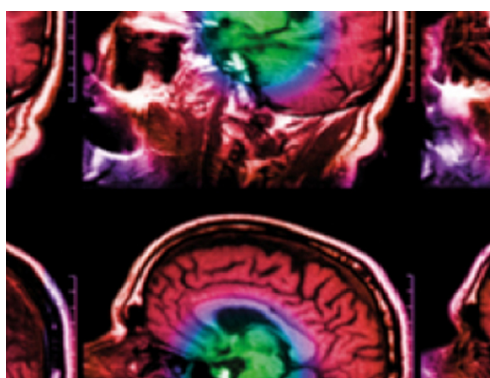
## 2D range modulator for high-precision water calorimetry in scanned carbon-ion beams

To cite this article: Kim Marina Holm *et al* 2020 *Phys. Med. Biol.* **65** 215003

View the [article online](#) for updates and enhancements.

### Recent citations

- [Monte Carlo simulations and dose measurements of 2D range-modulators for scanned particle therapy](#)  
Yuri Simeonov *et al*



**IPEM | IOP**

Series in Physics and Engineering in Medicine and Biology

Your publishing choice in medical physics,  
biomedical engineering and related subjects.

Start exploring the collection—download the  
first chapter of every title for free.

# 2D range modulator for high-precision water calorimetry in scanned carbon-ion beams



## OPEN ACCESS

RECEIVED  
27 November 2019


REVISED  
9 July 2020

ACCEPTED FOR PUBLICATION  
16 July 2020

PUBLISHED  
19 October 2020

Original Content from this work may be used under the terms of the [Creative Commons Attribution 3.0 licence](https://creativecommons.org/licenses/by/4.0/). Any further distribution of this work must maintain attribution to the author(s) and the title of the work, journal citation and DOI.



Kim Marina Holm<sup>1,2,3,4</sup>, Ulrich Weber<sup>5</sup>, Yuri Simeonov<sup>6</sup>, Achim Krauss<sup>1</sup>, Oliver Jäkel<sup>2,3,7</sup>  and Steffen Greilich<sup>2,3</sup>

<sup>1</sup> Department of Dosimetry for Radiation Therapy and Diagnostic Radiology, Physikalisch-Technische Bundesanstalt (PTB), Bundesallee 100, D-38116 Braunschweig, Germany

<sup>2</sup> Department of Medical Physics in Radiation Oncology, German Cancer Research Center (DKFZ), Im Neuenheimer Feld 280, D-69120 Heidelberg, Germany

<sup>3</sup> Heidelberg Institute for Radiation Oncology (HIRO), Heidelberg, Germany

<sup>4</sup> Department of Physics and Astronomy, University of Heidelberg, Im Neuenheimer Feld 226, D-69120 Heidelberg, Germany

<sup>5</sup> Department for Biophysics, GSI Helmholtzzentrum für Schwerionenforschung GmbH, Planckstraße 1, D-64291 Darmstadt, Germany

<sup>6</sup> Institute for Medical Physics and Radiation Protection, Technische Hochschule Mittelhessen, Gießen, Germany

<sup>7</sup> Heidelberg Ion Beam Therapy Center (HIT), University Hospital Heidelberg, Im Neuenheimer Feld 450, D-69120 Heidelberg, Germany

E-mail: [kim.holm@ptb.de](mailto:kim.holm@ptb.de)

**Keywords:** carbon-ion beams, 2D range modulator, spread-out Bragg peak, water calorimetry

## Abstract

Ionization chamber-based dosimetry for carbon-ion beams still shows a significantly higher standard uncertainty than high-energy photon dosimetry. This is mainly caused by the high standard uncertainty of the correction factor for beam quality  $k_{Q,Q_0}$ . Due to a lack of experimental data, the given values for  $k_{Q,Q_0}$  are based on theoretical calculations. To reduce this standard uncertainty,  $k_{Q,Q_0}$  factors for different irradiation conditions and ionization chambers (ICs) can be determined experimentally by means of water calorimetry. To perform such measurements in a spread-out Bragg peak (SOBP) for a scanned carbon-ion beam, we describe the process of creating an almost cubic dose distribution of about  $6 \times 6 \times 6 \text{ cm}^3$  using a 2D range modulator. The aim is to achieve a field homogeneity with a standard deviation of measured dose values in the middle of the SOBP (over a lateral range and a depth of about 4 cm) below 2% within a scanning time of under 100 s, applying a dose larger than 1 Gy. This paper describes the optimization and characterization of the dose distribution in detail.

## 1. Introduction

Over the last several years, radiation therapy with carbon-ion beams has become an attractive tool for cancer treatment (Karger *et al* 2010, Lodge *et al* 2007, Amaldi and Kraft 2005). However, dosimetry for carbon-ion beams is not yet as accurate as for conventional high-energy photon beams. The standard uncertainty for dosimetry in terms of the absorbed dose to water in clinical photon beams by means of calibrated ionization chambers (ICs) is at about 1% (Andreo *et al* 2006, Mitch *et al* 2006, Van Dyk *et al* 2013), whereas the standard uncertainty for carbon-ion beams is about three times higher (Andreo *et al* 2006). This is mainly due to the high standard uncertainty of the correction factor  $k_{Q,Q_0}$  (Karger *et al* 2010).

The absorbed dose to water for a given beam quality  $Q$  is determined via

$$D_{w,Q} = M_Q * N_{D,w,Q_0} * k_{Q,Q_0}, \quad (1)$$

with the corrected IC reading  $M_Q$  in the beam quality  $Q$ , the chamber-specific calibration factor  $N_{D,w,Q_0}$  for the beam quality  $Q_0$  in which the chamber was calibrated (usually  $^{60}\text{Co}$ ) (Andreo *et al* 2006, Palmans *et al* 2002). The correction factor  $k_{Q,Q_0}$  corrects for the different response of the IC to the beam qualities  $Q$  (here:  $^{12}\text{C}$ ) and  $Q_0$  ( $^{60}\text{Co}$ ).  $k_{Q,Q_0}$  is defined as the ratio of the chamber calibration factors for beam quality  $Q$  and  $Q_0$  (Andreo 1992). It can be experimentally determined by measuring the absorbed dose to water and the

corresponding reading  $M_Q$  of the IC under the same irradiation conditions:

$$k_{Q,Q_0} = \frac{N_{D,w,Q}}{N_{D,w,Q_0}} = \frac{D_{w,Q}/M_Q}{N_{D,w,Q_0}}. \quad (2)$$

Due to a lack of experimental data,  $k_{Q,Q_0}$  values are based primarily on theoretical calculations using equation (3), which is given, for example, in the International Code of Practice for the Dosimetry of External Radiotherapy Beams TRS-398 (Andreo *et al* 2006):

$$k_{Q,Q_0} = \frac{(s_{w,air})_Q (W_{air})_Q p_Q}{(s_{w,air})_{Q_0} (W_{air})_{Q_0} p_{Q_0}}. \quad (3)$$

In the TRS-398, constant values are assumed for the stopping power ratio  $(s_{w,air})_Q$ , the mean excitation energy per ion pair  $(W_{air})_Q$  and the perturbation factor  $p_Q$  for the beam quality  $Q$ . The resulting relative standard uncertainty of 2.8% for  $k_{Q,Q_0}$  factors leads to a high overall standard uncertainty in carbon-ion dosimetry. The German dosimetry protocol DIN 6801-1 (DIN-Normenausschuss Radiologie NAR 2019) calculates  $(s_{w,air})_Q$  as a function of the particle's residual range and assumes constant values for  $(W_{air})_Q$  and  $p_Q$ , leading to a relative standard uncertainty for  $k_{Q,Q_0}$  of 2.2%.

Within the scope of an ongoing project,  $k_{Q,Q_0}$  factors for different irradiation conditions and ICs are being determined experimentally using the water calorimeter designed at Physikalisch-Technische Bundesanstalt (PTB) (Krauss 2006, Krauss *et al* 2012) to reduce their standard uncertainty. This was done previously for the entrance channel of a monoenergetic carbon-ion beam for two Farmer-type ICs, achieving a standard uncertainty of 0.8% (Osinga-Blättermann *et al* 2017). This region is characterized by a shallow depth, a monoenergetic field and relatively low LET. Based on this,  $k_{Q,Q_0}$  factors for a further eight different cylindrical ICs and three different plane-parallel ICs were determined by means of cross-calibration, showing a standard uncertainty of 1.1% (Osinga-Blättermann and Krauss 2018). As a continuation of this work,  $k_{Q,Q_0}$  factors are determined in the spread-out Bragg peak (SOBP) of a carbon-ion beam. Here, the goal is to achieve a relative standard uncertainty for  $k_{Q,Q_0}$  in the same order as it is given for  $k_{Q,Q_0}$  factors in photon beams, as it was also achieved for the entrance channel of a carbon-ion beam.

To this end, a homogeneous irradiation field of reasonable size and dose irradiated in a short time is needed. The irradiation field parameters that shall be achieved are presented in detail in the following.

**Total dose and field size:** As the radiation induced temperature rise to be measured within the calorimetric experiment only amounts to about 0.24 mK Gy<sup>-1</sup> (Krauss 2006), doses larger than 1 Gy are typically applied in water calorimetry (Krauss 2006, Sassowsky and Pedroni 2005) for a reliable signal to noise ratio. The field size chosen had to be a compromise between irradiation time (as described below), the dose that can be applied within this time and the field size's influence on the heat conduction. As a dose > 1 Gy should be applied, a large field size (as e.g. the reference field size of 10 × 10 cm<sup>2</sup> according to TRS-398 (Andreo *et al* 2006)) would require a long irradiation time. A very small irradiation field would directly influence heat conduction effects making greater corrections necessary and thereby also increasing their uncertainty (Krauss 2006, Krauss and Kapsch 2014). Also taking the characteristic of the beam delivery system at HIT (e.g. irradiation time) into account, a field size between 5 × 5 cm<sup>2</sup> and 7 × 7 cm<sup>2</sup> seems to be appropriate for the  $k_{Q,Q_0}$  determination in this investigation. Therefore, we chose a size of 6 × 6 cm<sup>2</sup>, as it was also done in Osinga-Blättermann *et al* (2017), fully covering the sensitive parts of the calorimetric detector as well as the ICs used. The SOBP should have a depth of 6 cm resulting in a dose cube of 6 × 6 × 6 cm<sup>3</sup>.

**Irradiation time:** To determine the  $k_{Q,Q_0}$  factors by means of water calorimetry, a number of correction factors are required, e.g. heat conduction corrections. The heat conduction corrections are particularly dependent on the duration of irradiation, as heat conduction effects lead to the initially induced heat dissolving with time (Krauss 2006), making water calorimetric measurements rather time-critical. Medin *et al* (2006) obtained  $k_{Q,Q_0}$  factors in monoenergetic proton beams with a reasonably low standard uncertainty of 0.7% for an irradiation time of 2 min; Osinga-Blättermann *et al* (2017) achieved a standard uncertainty in the same order of magnitude for the entrance channel of a carbon ion beam for an irradiation time of about 95 s. Based on that, an irradiation time of less than 100 s should be achieved within this study.

A full three-dimensional active scanning of the irradiation field, as is usually done in carbon-ion therapy (Haberer *et al* 2004, Kamada *et al* 2015) would take several minutes (about 8 min for a 6 × 6 × 6 cm<sup>3</sup> volume of 1 Gy), leading to a high uncertainty for the heat conduction and thus to a high overall uncertainty for  $k_{Q,Q_0}$  factors determined. Therefore, a passive modulation of the SOBP in terms of depth is needed that allows the irradiation to take place within less than 100 s. Using pencil beam scanning, a passive modulation with a moving range modulator (e.g. a modulator wheel) is possible only to a very limited extent. Here, we used a static 2D range modulator (Simeonov *et al* 2017), which is comparable to a ridge filter (Kostjuchenko *et al* 2001).

*Reproducibility and homogeneity:* To determine the correction factors needed for the water calorimetric and ionometric measurements correcting for example for a positioning uncertainty of the whole setup, the off-axis position of the thermistor probes inside the calorimetric detector (Krauss 2006) or an IC's volume effect (Osinga-Blättermann *et al* 2017), a detailed knowledge of the irradiation field is needed. To achieve a low uncertainty in these factors, and thus a low overall uncertainty in the resulting  $k_{Q,Q_0}$  factors, the irradiation field must be reproducible and homogeneous (Sassowsky and Pedroni 2005). As criteria for the reproducibility, Osinga-Blättermann *et al* (2017) determined the relative standard deviation of dose distributions from each other, which were repeatedly measured over a period of seven months; this amounted to 0.3%. A maximum deviation of measured dose values within the  $40 \times 40 \text{ mm}^2$  lateral dose distribution at the measurement depth of 3% was found. Because we evaluated a 3D dose distribution in contrast to the 2D distribution considered by Osinga-Blättermann *et al*, we *a priori* had to anticipate larger margins for field homogeneity and reproducibility. So, we choose a reproducibility of with a standard deviation of the repeated measurements below 0.5% and a field homogeneity with a standard deviation of dose values with a maximum distance of 20 mm from the center below 2%, for which the influence on several correction factors like for heat conduction correction or correction for IC's volume effect should still be small enough to be used for a  $k_{Q,Q_0}$  determination with a standard uncertainty in the order of about 1%. The range of 20 mm is motivated by the off-axis measurement position of the thermistor probes inside the calorimetric detector (Krauss 2006) and the ICs' volume to be generously covered.

This paper describes the application of a 2D range modulator to create a suitable irradiation technique for water calorimetry in a  $^{12}\text{C}$ -SOBP to fulfill the criteria mentioned above. A detailed field characterization is presented that includes repeated three-dimensional measurements of the irradiation field as well as Monte Carlo simulations to investigate the particle spectra.

## 2. Material and methods

### 2.1. 2D range modulator

The spread-out Bragg peak (SOBP) is generated by a so-called 2D range modulator (2DRM) consisting of pyramid-shaped pins (Simeonov *et al* 2017, Tommasino *et al* 2019). The pyramid shape is not linear; the pins have a well-defined profile with different gradients at different heights. The pins' shape was optimized for a 60 mm wide SOBP generated by carbon ions with an energy of 278 MeV/u. The designing methods for the range modulator are described in detail in Simeonov *et al* (2017). There, Simeonov *et al* describe a 3D range modulator for which each pin creates an individual depth dose distribution to achieve a certain 3D dose distribution, like for example a sphere as given in the reference. In contrast here, we use a 2D range modulator for which the pin's shape and thereby also the created depth dose distribution is constant over the modulator's lateral area.

To fully cover the desired irradiation field, the 2DRM has a total area of  $10 \times 10 \text{ cm}^2$ ; each pin has a height of 57 mm (figure 1). We worked with different pin base areas (period of the pin distance) of  $2 \times 2 \text{ mm}^2$ ,  $3 \times 3 \text{ mm}^2$  and  $4 \times 4 \text{ mm}^2$ , testing their impact on the resulting irradiation field. The 2DRMs were produced using rapid prototyping with a Stratasys Objet30 Pro PolyJet 3D printer, the printing material was RIGUR RGD450.

Two identical 2DRMs were printed using the same 3D printer (as was also done by Simeonov *et al* (2017)) to investigate the reproducibility of the manufacturing process. Systematic deviations of the 3D printer can be taken into account by a corrected design of the 2DRM. But in this case we did not correct for such deviations, as a satisfying shape of the dose distribution for the purpose of water calorimetry was already achieved with the original design.

For all measurements, the back of the 2DRM was positioned at the isocenter, as was later done for the calorimetric measurements. The pins were pointing towards the beam nozzle. The 2DRMs were placed on a positioning table that allows a relative accuracy of  $5 \mu\text{m}$  in x- and y-direction and  $1 \mu\text{m}$  in z-direction, as well as a defined tilting around each spatial axis ( $0.1^\circ$  around x- and y-axis, less than  $0.006^\circ$  around z-axis). Also taking the positioning accuracy using the wall-mounted laser system of 0.5 mm (Jäkel *et al* 2000) into account, this gives an alignment accuracy of the 2DRM of 0.5 mm in each direction and less than  $0.3^\circ$  around each spatial axis.

### 2.2. Irradiation

All measurements were performed at the Heidelberg Ion Beam Therapy Center (HIT) (Haberer *et al* 2004) using pencil beam scanning (Haberer *et al* 1993).

As the SOBP is generated by passive scattering, only one iso-energy slice, e.g. a monoenergetic field, is needed. Its energy is defined by the structure of the calorimeter, as shown in Osinga-Blättermann *et al* (2017), and by the desired measurement depth in water. Choosing a measurement depth of 10 cm in water

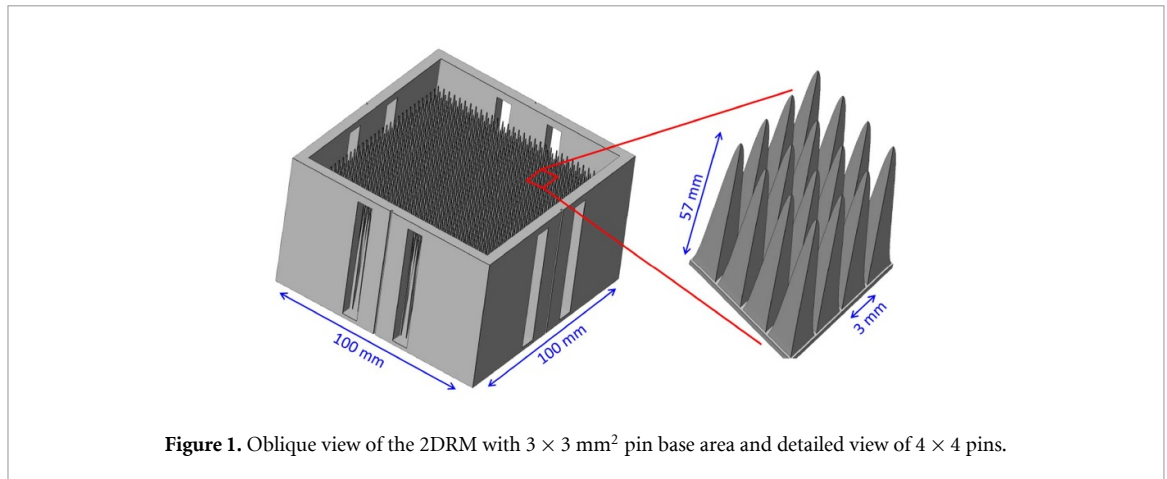


**Figure 1.** Oblique view of the 2DRM with  $3 \times 3 \text{ mm}^2$  pin base area and detailed view of  $4 \times 4$  pins.

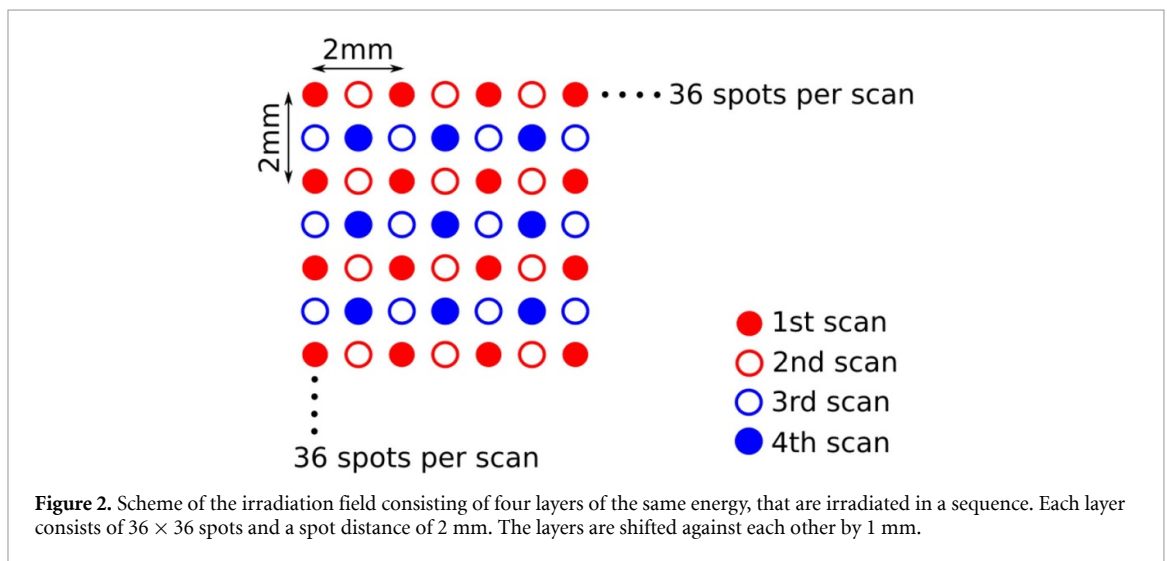


**Figure 2.** Scheme of the irradiation field consisting of four layers of the same energy, that are irradiated in a sequence. Each layer consists of  $36 \times 36$  spots and a spot distance of 2 mm. The layers are shifted against each other by 1 mm.

inside the calorimeter (11.41 cm water equivalent path length), an energy of 278.29 MeV/u is needed. The irradiation field was optimized for homogeneity in terms of the physical dose. The best results concerning field homogeneity were achieved for four monoenergetic layers irradiated in sequence. These layers had a spot distance of 2 mm and were shifted against each other by 1 mm in the x-, y- or xy-direction. Each layer consists of  $36 \times 36$  spots with a focus size of 8.2 mm full width of half maximum (FWHM). Using the 2DRM, this leads to a dose cube of  $6 \times 6 \times 6 \text{ cm}^3$ . The pattern of the irradiation field is shown in figure 2.

For a short irradiation, the highest clinically used particle flux of  $8 \times 10^7$  ions per second was chosen, allowing a scan of the whole irradiation field within 90 s for a dose of 1.5 Gy.

### 2.3. Peakfinder

The PTW Peakfinder Water Column (Freiburg 2019) was used to measure depth dose distributions. It consists of one reference detector fixed at the entrance window and one measuring detector between two water-containing bellows that are adjustable in length. In this way, the depth of the measuring detector can be adjusted. A plane-parallel Bragg peak type 34 080 chamber is used as a measuring detector, while a type 34 082 chamber is used as a reference detector. The measuring detector has a circular sensitive area with a radius of 41 mm. The Peakfinder allows depth dose distributions to be measured with a spatial resolution of  $10 \mu\text{m}$  and positioning accuracy of  $100 \mu\text{m}$ . Its movement is synchronized with the synchrotron's spill signal. Both chambers were operated at 400 V using a PTW-TANDEM XDR dual channel electrometer.

For all Peakfinder measurements, the Peakfinder's front window was positioned at the isocenter due to spatial constraints, while the 2DRM was positioned 65.5 cm in front of it. The Peakfinder's offset of 19.5 mm was taken into account for all measurements.

### 2.4. IC array and water phantom

To measure the lateral dose distribution, a prototype IC array (PTW Octavius 1000P) was used. The Octavius 1000P consists of 977 ICs arranged in an  $11 \times 11 \text{ cm}^2$  rectangle. Compared to the Octavius



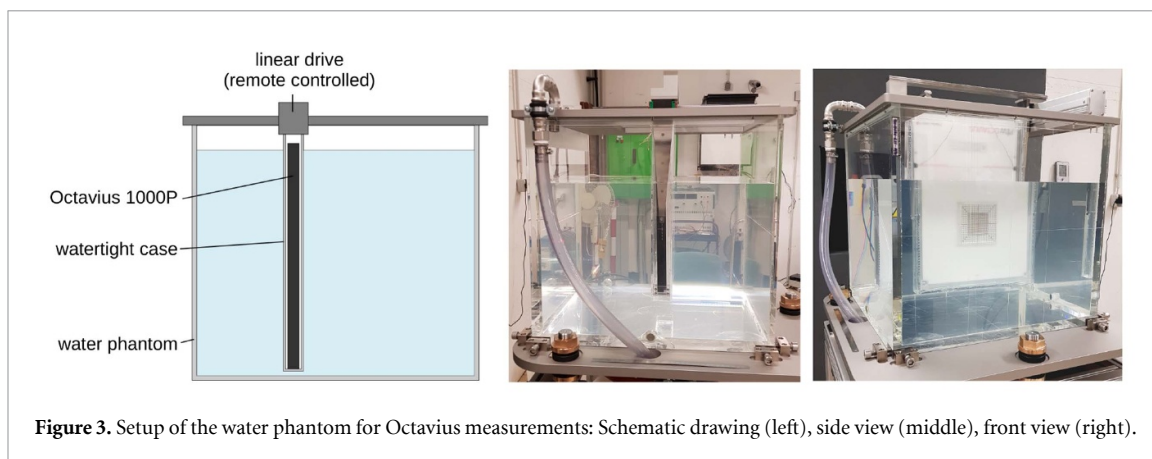


**Figure 3.** Setup of the water phantom for Octavius measurements: Schematic drawing (left), side view (middle), front view (right).

1000SRS (Freiburg 2019), the 1000P is adapted for particle-beam applications whose ICs are filled with air instead of liquid to avoid recombination effects. The ICs have a distance of 2.5 mm in the inner  $5 \times 5 \text{ cm}^2$  and 5 mm in the outer part of the detecting area. Each IC has an active area of  $2.3 \times 2.3 \text{ mm}^2$  (Bauer 2018).

As the IC array is only used for relative dose measurements, its signal was not corrected for air density. Therefore, for the comparison of measurements, the dose values were normalized to the mean value of the dose values within a 20 mm radius around the center. The array was calibrated for the relative response of its chambers to each other at a well characterized 6 MV photon field at PTB Braunschweig. A correction factor for each chamber was determined and a standard uncertainty of this correction factor of 0.34% was estimated.

For the field characterization measurements, the array was positioned in a water phantom inside a waterproof case made of PMMA (based on the procedure developed by Schuy *et al* (2019)). At its upper edge, this case is attached to a linear drive at one side and to a smooth-running rail at the other side. This allows the depth of the array to be adjusted via remote control inside the water phantom with a depth positioning accuracy of 0.1 mm. This setup is shown in figure 3.

The water phantom was positioned 65.6 cm behind the 2DRM, i.e. the later position of the water calorimeter. A polystyrol block was positioned in front of the phantom to mime the calorimeter's insulation layer.

The data measured with the IC array inside the water phantom was compared with the Peakfinder measurements by taking the measurement position relative to the isocenter, the phantom's and array case's PMMA wall thicknesses, the linear drive's offset and the Octavius' measurement depth, in total 51 mm, into account. All depth indications in the measurement data are given as water equivalent path lengths from the isocenter. To compare the depth dose distribution measured with the Octavius water phantom setup with the Peakfinder results, the Octavius signals of the inner chambers within a radius of 41 mm were averaged, roughly corresponding to the active area of the Peakfinder's measurement chamber.

## 2.5. Film measurements

A prerequisite for using the IC array for field characterization measurements is a sufficient spatial resolution; it is necessary to ensure that the decomposed spectrum of the irradiation field does not contain high spatial frequencies that are missed by the array. To this end, simultaneous film and IC array measurements were performed to verify the array's spatial resolution. To take the dimensions of a single IC of the array into account, the plotted one-dimensional film signal was averaged over seven rows of pixels, which correspond to a width of 2.5 mm.

In addition, film measurements were performed to investigate the blurring out of the pattern in the irradiation field introduced by the 2DRM. For this purpose, EBT3 film segments were positioned at different depths inside a phantom that mimes the calorimeter:

- in front of the calorimeter, 65.5 cm in air behind the 2DRM (0.7 mm WET),
- at a 5 cm depth in water inside the calorimeter (60.7 mm WET),
- at a 10 cm depth in water (including the calorimetric detector's glass wall) inside the calorimeter (111.3 mm WET); this position corresponds to the calorimetric measurement depth.

The values given in parentheses are the sums of water equivalent thicknesses (WETs) of the material in the beam path between the back of the 2DRM and the measurement position. The phantom to mime the calorimeter was a modified version of the one used by Osinga-Blättermann *et al* (2017); in particular, we

added additional solid water (RW-3, PTW, Germany) slabs of corresponding water equivalent thickness to reach a measurement depth of maximum 10 cm in water whereas Osinga-Blättermann *et al* used the phantom for a maximum depth of 5 cm. The 2DRM was positioned with its back in the isocenter; the distance between the 2DRM and the phantom was 65.5 cm, as is also the case for the calorimeter setup.

For all film measurements, Gafchromic EBT3 film (lot number 10 031 801) was used. All film segments were scanned on a flatbed Epson Expression 10 000XL scanner in transmission mode and evaluated using the triple channel analysis defined by Micke *et al* (2011). We only evaluated relative film signals taken from single, fixed depths perpendicular to the beam and limited to the central region of the field for which the particle spectrum is uniform and therefore the LET-dependent film response is the constant (Martisikova and Jäkel 2010, Castriconi *et al* 2017).

## 2.6. Monte carlo FLUKA transport code

We performed Monte Carlo simulations using the FLUKA code version 2 011.2x.5 (Ferrari *et al* 2014) to investigate the particle and LET spectra. The simulations were performed both for a passively modulated SOBP using the 2DRM as well as for a SOBP created by several layers of different energies, e.g. active scanning. The actively scanned irradiation field consists of 22 layers with energies ranging from 196.23 MeV/u to 272.77 MeV/u to create a 6 cm SOBP with a distal edge at 14.41 cm WET, comparable to the 2DRM-modulated SOBP.

The particle spectra at the calorimetric measurement position in the middle of both SOBP were compared. This was done to provide a rationale for transferring the results concerning new  $k_{Q,Q_0}$  factors for a passively modulated SOBP to active scanning irradiation conditions, as is prevalent in ion beam radiotherapy (Kamada *et al* 2015). As  $k_{Q,Q_0}$  corrects for the different response of an IC to given beam qualities defined by its particle and LET spectrum,  $k_{Q,Q_0}$  will be identical for irradiation fields with comparable spectra.

For all simulations, the settings for precise simulations (PRECISIO) were used. A 278.29 MeV/u carbon-ion beam was simulated. We used a rectangular beam shape with an area of  $11 \times 11 \text{ mm}^2$  to fully cover the area of the 2DRM implemented.

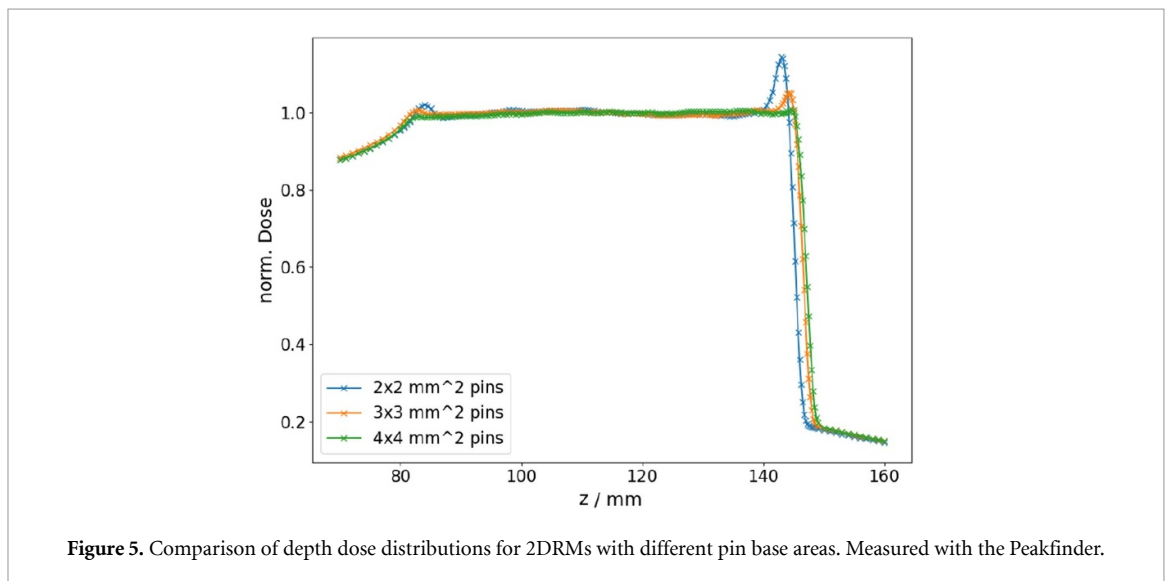
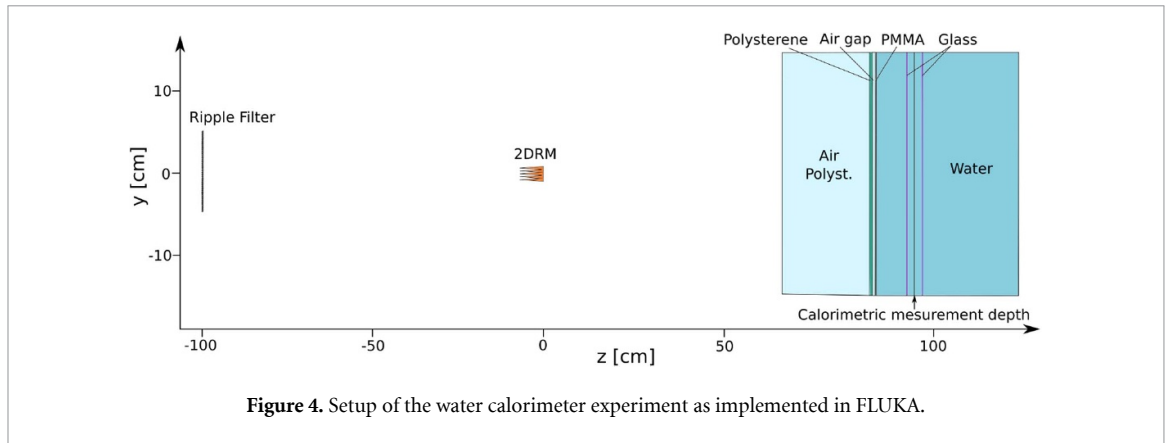
The 3 mm ripple filter was implemented by means of several rectangular parallelepipeds and infinite half-spaces crossing the parallelepipeds. The ripple filter material was set to water. The calorimeter was simulated by means of rectangular material slabs mimicking the different calorimeter materials in the beam path. The whole setup can be seen in figure 4. The beam application and monitoring system (BAMS) of the accelerator was not implemented in the simulation. As its WET is already considered in the Peakfinder's offset, it was not taken into account for the simulation to be able to compare both depth dose distributions as a proof of concept for the simulation setup.

### 2.6.1. Implementation of the 2DRM

The 2DRM was implemented as voxel geometry. We tested different resolutions ranging from  $59 \times 59 \times 56$  voxel per pin (vx/pin) to  $160 \times 160 \times 152$  vx/pin to simulate a pin with a  $3 \times 3 \text{ mm}^2$  base area and a 57 mm height. We used an online voxelizer program (Westerdie 2019) to convert the pin STL-file (data file containing the geometric information for 3D printing) into a text file containing the voxel coordinates. After reshaping, the voxel text file was converted into a FLUKA voxel geometry file using the FORTRAN routine writegolem (Ferrari *et al* 2014). The voxel geometry file was implemented in FLUKA using the VOXELS card. The voxel's size was scaled with the water equivalent thickness (WET) of the 2DRM's material and the voxel's material was set to water, as the exact composition of the 3D printing material is not given by the manufacturer. The WET was experimentally determined beforehand using the Peakfinder. Due to a limitation of the voxel geometry within the FLUKA code, we only simulated a section of the 2DRM of  $5 \times 5$  pins. For this reason, the full irradiation plan could not be simulated. Instead, we used one single spot beam with an initial energy of 278 MeV/u and a rectangular shape with an area of  $11 \times 11 \text{ mm}^2$  to fully cover the 2DRM implemented.

### 2.6.2. Scoring

The absorbed dose was estimated using the USRBIN DOSE card. The fluence, fluence-weighted LET and dose-weighted LET were determined using the USRBIN ALL-PART card and an independently written FORTRAN routine implemented in the FLUKA simulation. The particle spectra for particles with atomic number  $Z = 1$  to  $Z = 6$  were determined for each quantity using the AUXSCORE card. Each USRBIN detector implemented had a total size of  $5 \times 5 \times 20 \text{ cm}^3$  (xyz), with one detecting bin in the x- and y-directions and 400 bins in the z-direction to estimate distributions in depth.



### 3. Results and discussion

#### 3.1. Characterization of the dose distribution from the 2DRM

The 2DRM's properties such as resulting dose distributions and their sensitivity to tilting were investigated. The 2DRM was optimized in terms of field homogeneity.

##### 3.1.1. Depth dose distribution

Figure 5 shows depth dose distributions for a 278.29 MeV/u  $^{12}\text{C}$  beam in water after passing a 2DRM with a  $2 \times 2 \text{ mm}^2$  (blue),  $3 \times 3 \text{ mm}^2$  (orange) and  $4 \times 4 \text{ mm}^2$  (green) pin base area.

A clear formation of a SOBP can be observed for all 2DRMs. For the  $2 \times 2 \text{ mm}^2$  pin 2DRM, the SOBP shows a peak at the beginning and at the end of the plateau region (region of flat dose distribution,  $z = 85 \dots 141 \text{ mm}$ ), which become smaller for  $3 \times 3 \text{ mm}^2$  pins and disappear for  $4 \times 4 \text{ mm}^2$  pins. These artifacts can be explained by an inaccuracy during the 3D printing process, namely a bending of the pins' tips and a filling of the grooves between the pins, which slightly changes the weights for contribution of the highest and lowest energy of the SOBP superposition, respectively. With a bigger pin base area, the printed structures become less fine and the relative printing inaccuracies, and thus also the artifacts, become smaller.

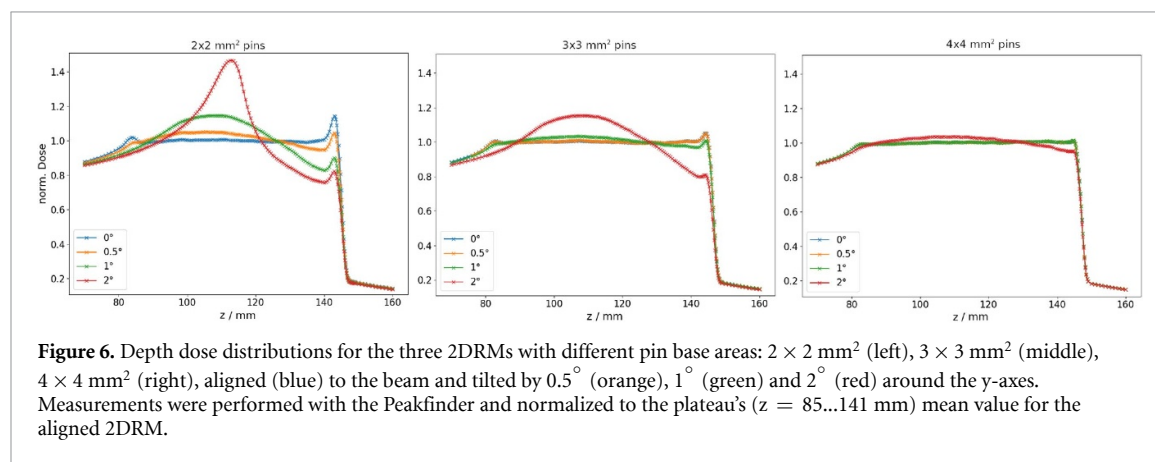
Table 1 gives the relative standard deviations and the relative maximum deviations of the dose values measured within the plateau region of the SOBP (without peaks) for the three 2DRMs with different pin base areas. The standard deviation becomes smaller, which means the plateau becomes more homogeneous the larger the pin base area is.

##### 3.1.2. Sensitivity to tilting

The sensitivity of the dose distribution to the alignment accuracy of the 2DRM was investigated. Three 2DRMs with different pin base areas were tested. Measurements of the depth dose distribution for a single spot as well as measurements of the lateral dose distribution in the middle of the SOBP of the whole

**Table 1.** Relative standard deviation and maximum relative deviation of doses measured within the plateau region of the SOBP for each 2DRM.

2DRM	Rel. std. dev. / %	Max. dev. / %
$2 \times 2 \text{ mm}^2$ pins	0.53	2.08
$3 \times 3 \text{ mm}^2$ pins	0.44	1.54
$4 \times 4 \text{ mm}^2$ pins	0.31	1.34



irradiation plan, as described in 2.2, were performed. Each 2DRM was first accurately aligned to the beam and then tilted by  $0.5^\circ$ ,  $1^\circ$  and  $2^\circ$  around the  $y$ -axis (with the beam in the  $z$ -direction). For each setup, a Peakfinder and a Octavius measurement (with the Octavius inside the water phantom) were performed. Figure 6 shows the depth dose distributions for each 2DRM for the different tilting angles.

For every 2DRM, the measured distribution differs more from the aligned 2DRM's distribution the larger the tilting angle is; an influence of a misalignment of the 2DRM can be clearly observed. This effect is greater the smaller the pin base area is. For the  $4 \times 4 \text{ mm}^2$  pin 2DRM, nearly no difference in the distributions can be observed up to a tilting angle of  $1^\circ$ , the maximum deviation of the distributions in the plateau region for aligned 2DRM and tilted around  $1^\circ$  is at 0.5%. In contrast, even a tilting angle of  $0.5^\circ$  clearly changes the distribution when using the 2DRM with  $2 \times 2 \text{ mm}^2$  pins.

The lateral dose distribution also changes when tilting the 2DRM. Across the  $x$ -axis, an increase in the dose towards negative values can be observed. Across the  $y$ -axis, the dose distribution stays constant, but the absolute dose rises the larger the tilting angle is. Here, too, the effects observed are greater the smaller the pin base area is. Later simulations of this effect showed that only tilting the 2DRM does not lead to an oblique lateral profile. The effect observed can be explained by a slight misalignment of the IC array with which the shown data was measured. This misalignment leads to a visible effect in the profile measured only in regions with high gradients as given for the depth dose distributions of the tilted 2DRMs (see figure 6). Therefore, the dose profile for a perfectly aligned 2DRM in the flat plateau region of the SOBP is not influenced by this misalignment.

### 3.1.3. Film measurements of the lateral dose distribution

The pattern of the 2DRM's pins introduces a pattern in the resulting dose distribution, which becomes increasingly blurred the greater the distance from the 2DRM is. To investigate this effect, EBT3 film segments were positioned at different depths inside a phantom, as described in section 2.5. The results are shown in figure 7.

A clear pin pattern can be seen in the lateral dose distributions in front of the calorimeter (65.5 cm air between 2DRM and film) for both 2DRMs. For the  $3 \times 3 \text{ mm}^2$  pin 2DRM, this pattern is completely blurred and becomes invisible at a 5 cm depth in water. In contrast, the pattern is clearly visible for the  $4 \times 4 \text{ mm}^2$  pin 2DRM at this position. Even at a 10 cm depth in water for the  $4 \times 4 \text{ mm}^2$  pin 2DRM, the pattern can still be recognized. This means that the distance between the 2DRM and the measurement is not large enough for a homogeneous dose distribution for this 2DRM.

The relative standard deviations for the dose values within the inner  $100 \times 100 \text{ px}$  ( $= 35 \times 35 \text{ mm}^2$ ) of the film segment at a 10 cm depth in water for both 2DRMs were calculated. For the  $3 \times 3 \text{ mm}^2$  pin 2DRM, this was 1.32% and 1.51% for the  $4 \times 4 \text{ mm}^2$  pin 2DRM. This indicates a better homogeneity of the lateral dose distribution for a 2DRM if the pin base area is small.

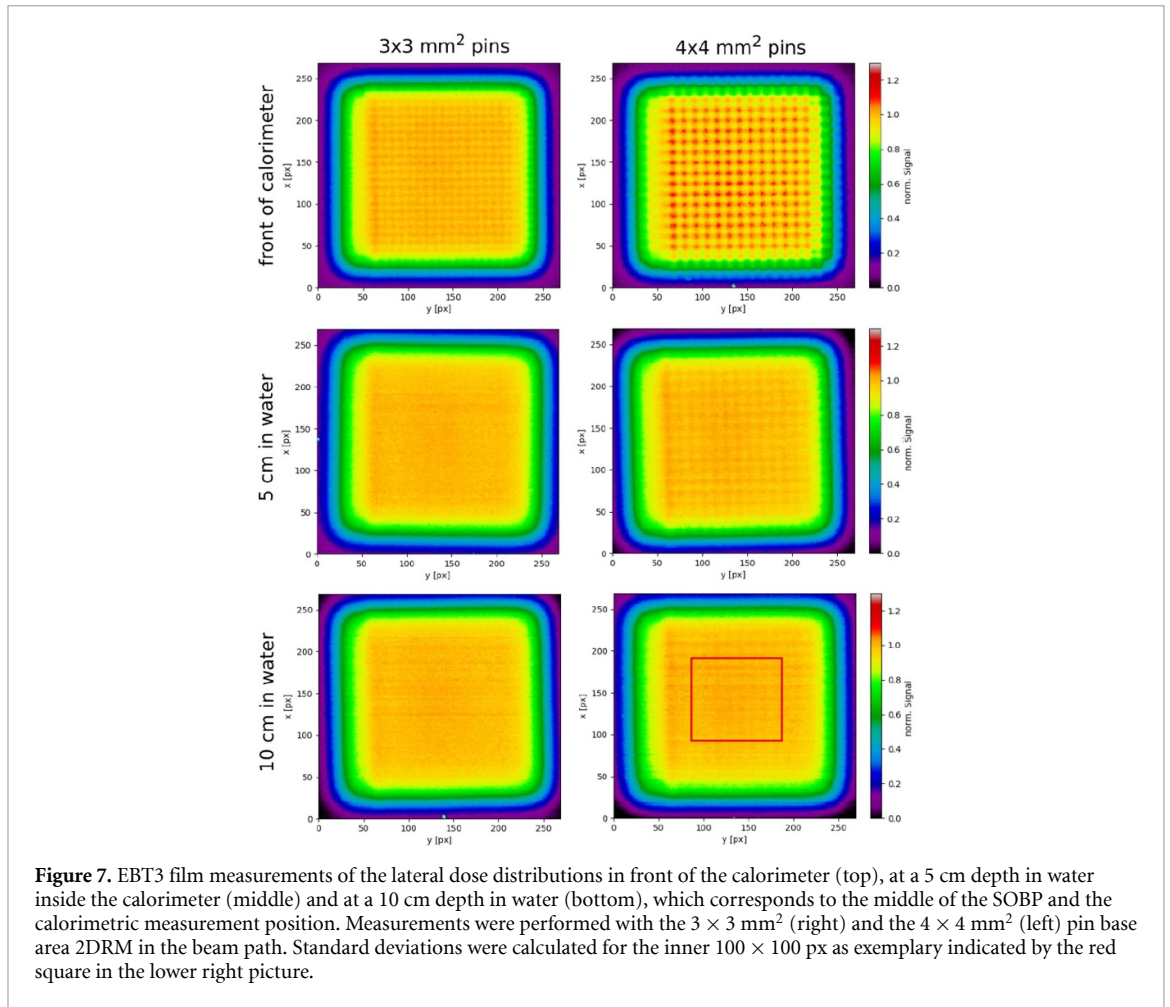


**Table 2.** Relative standard deviation in percentage of measured doses within the plateau region of the SOBP in terms of depth (taken from Peakfinder measurement) and within a certain radius around the center of the lateral 2D dose distribution in the middle of the SOBP (taken from Octavius measurement) for the two versions of the 2DRM with a  $3 \times 3 \text{ mm}^2$  pin base area.

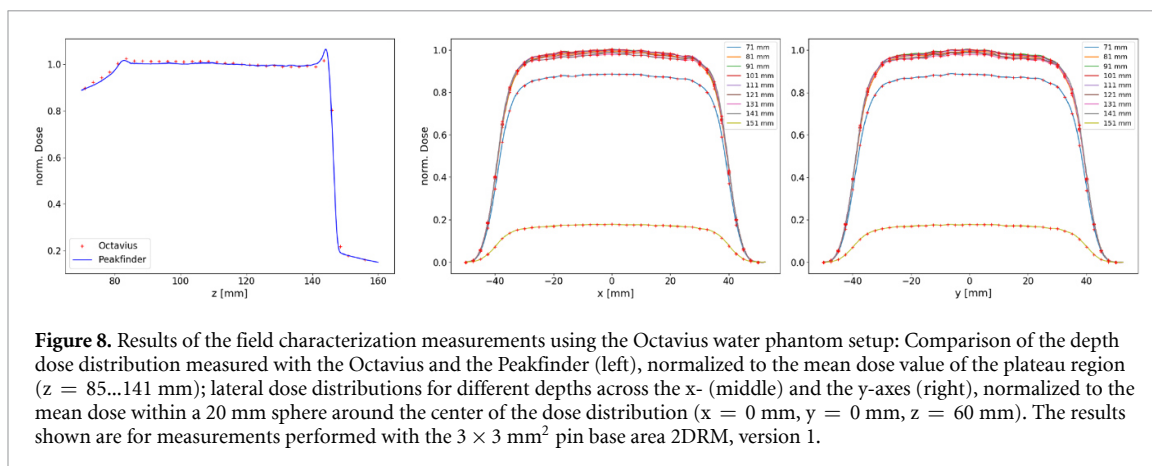
Rel. standard deviation / %	Modulator version 1	Modulator version 2
in terms of depth	0.44	0.42
laterally (15 mm radius)	1.13	1.00
laterally (20 mm radius)	1.35	1.34

### 3.1.4. Selection of the 2DRM type for further measurements

Finally, we selected the 2DRM with a  $3 \times 3 \text{ mm}^2$  pin base area for further investigation. This is a good compromise between axial and lateral field homogeneity; in addition, for this 2DRM, the pin pattern induced in the irradiation field is completely blurred in the SOBP region.

As a backup for this 2DRM, via which all subsequent measurements were performed, a second, identical 2DRM was produced. By comparing these two versions of the  $3 \times 3 \text{ mm}^2$  pin 2DRM, the reproducibility of the manufacturing process was investigated. To clarify the difference between both 2DRM versions, table 2 gives the standard deviations calculated for both 2DRMs in terms of depth within the plateau region (figure 5 ( $3 \times 3 \text{ mm}^2$  pins) between  $z = 85 \text{ mm}$  and  $141 \text{ mm}$ ) and laterally within a radius around the center of the dose distribution. Here, we used both a 15 mm and a 20 mm radius. The 20 mm radius from the central beam axis was chosen because the corresponding area is comparable to the area that was investigated in terms of field homogeneity by Osinga-Blättermann *et al* (2017), based on which we defined the field homogeneity that shall be achieved. For all following evaluations of the irradiation field characterization in the SOBP, a spherical volume with a 20 mm radius was used.

The two versions of the final 2DRM create very similar dose distributions in terms of depth as well as laterally, even though there are small differences. For comparison, the differences between the single normalized measurement points of the distributions created with the versions of the 2DRM were calculated, these are below 0.4% for the lateral dose distribution and below 1.1% for the depth dose distribution (within



the plateau region). The standard deviations for the measured values in the plateau region in terms of depth and laterally are also of the same order, although they differ slightly. From these results, it can be concluded that both 2DRMs can be used for calorimetric measurements as well, although they must be characterized individually.

### 3.2. Field characterization

Repeated measurements of the three-dimensional dose distribution around the later calorimetric measurement position were performed. To this end, the Octavius was moved in terms of depth inside a water phantom.

#### 3.2.1. Comparison of film data with IC array data

To verify the spatial resolution of the Octavius before using it for all subsequent field characterization measurements, simultaneous EBT3 film measurements were performed. The film signal measured was corrected using the triple channel analysis, normalized to its maximum and compared to the relative Octavius signal. For each data set, the measurement was performed four times.

Both distributions agree very well. The film data has a standard deviation of the measured data points in the inner  $100 \times 100$  px ( $35 \times 35$  mm<sup>2</sup>) of 1.3%; for the Octavius data, the standard deviation in the inner  $35 \times 35$  mm<sup>2</sup> is 0.8% and thus in the same magnitude as the film data's standard deviation. This shows that the Octavius resolution is sufficient and that no higher spatial frequencies have been missed. Therefore, all subsequent measurements are performed using only the Octavius.

#### 3.2.2. Homogeneity and reproducibility of the irradiation field

For the field characterization measurements, the depth of the Octavius in water was adjusted in steps of 2.5 mm over a width of 80 mm to fully cover the SOBP. For each 2DRM ( $3 \times 3$  mm<sup>2</sup> pin base area, two identical versions), seven measurements were performed over a period of time of 10 weeks. The results for version 1 of the 2DRM can be seen in figure 8.

As can be seen in figure 8 (left), the data points agree with the Peakfinder signal very well. On the right, the one-dimensional lateral dose distributions across the x- and y-axes (in each case in the middle of the field) are shown for different depths.

As a value for the field's homogeneity, the standard deviation of the dose values measured within a sphere with a 20 mm radius around the center of the 3D dose distribution (5164 data points) was calculated. The values for each measurement are given in table 3. The relative standard deviations are all below 1.1%, indicating a very flat and homogeneous irradiation field around the calorimetric measurement position.

As a criterion for the reproducibility of the relative dose distribution, the standard deviation between the signals of the repeated measurements from each was calculated for every single measurement point within the 20 mm sphere. Therefore the data was normalized before, as mentioned in section 2.4. On average this calculated standard deviation amounts to 0.26% for both versions of the 2DRM, which means that the field is also quite stable over the given period of time.

### 3.3. Monte Carlo simulations

For all FLUKA simulations, a pin base area of  $3 \times 3$  mm<sup>2</sup> was used, as this is the pin base area of the selected 2DRM. For all results shown, 200 000 particles were simulated in each case.

**Table 3.** Relative standard deviations of doses measured within a sphere with a 20 mm radius around the calorimetric measurement position for each field characterization measurement.

Measurement	Modulator vers.	Rel. std. dev. / %
05-19-19	1	0.78
05-21-19	1	0.97
05-21-19	1	0.83
05-23-19	1	1.03
05-31-19	1	1.05
06-25-19	1	0.78
07-31-19	1	0.91
05-19-19	2	0.71
05-21-19	2	0.92
05-23-19	2	1.00
05-23-19	2	0.98
05-31-19	2	1.02
06-25-19	2	0.86
07-31-19	2	0.85

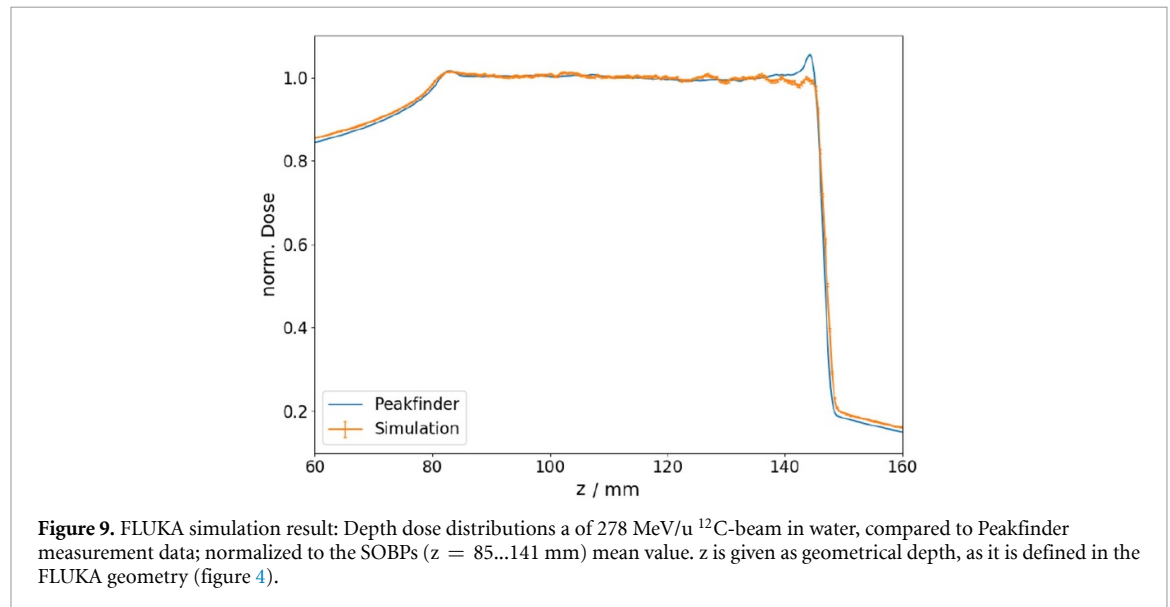
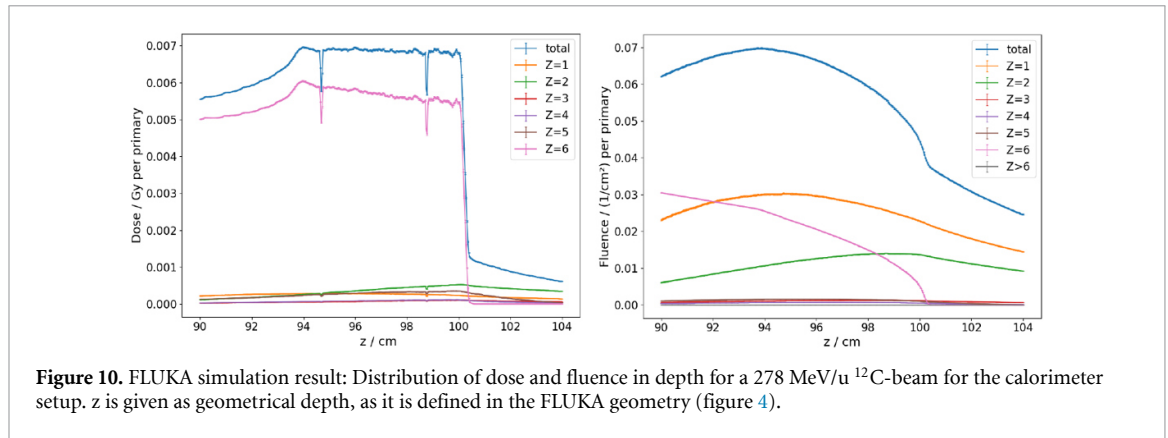
**Figure 9.** FLUKA simulation result: Depth dose distributions of a 278 MeV/u  $^{12}\text{C}$ -beam in water, compared to Peakfinder measurement data; normalized to the SOBPs ( $z = 85\dots141$  mm) mean value.  $z$  is given as geometrical depth, as it is defined in the FLUKA geometry (figure 4).

Figure 9 shows the resulting depth dose distribution of this simulation setup for a beam in water compared to the depth dose distribution measured with the Peakfinder for the real 2DRM with a  $3 \times 3 \text{ mm}^2$  pin base area.

The simulated data is slightly noisier towards the end of the SOBP. The peak at the end of the SOBP given in the experimental data cannot be observed in the simulation, as the 2DRM's inaccuracies are not implemented in the simulation. However, both data sets agree very well, especially in the region that is of interest for calorimetric measurements, the middle of the SOBP. This result shows that the implemented setup sufficiently maps the real setup when looking at the middle of the SOBP, even though simplifications had to be made due to computational constraints.

We tested the impact of the pins' voxel resolution on the resulting depth dose distribution. For the smallest resolution ( $59 \times 59 \times 56$  vx/pin), the distribution within the plateau region was very noisy, but becomes flatter with increasing resolution. Because the computational time increases as the pins' voxel resolution increases, and due to a limitation of the voxel geometry within the FLUKA code, we were limited to a maximum resolution of  $160 \times 160 \times 152$  vx/pin. We tested the resolution's impact on the particle spectra obtained as a measure of the reliability of the results with a limited resolution. Comparing the particle spectra for the pins with  $59 \times 59 \times 56$  vx/pin resolution to pins with a resolution of  $127 \times 127 \times 121$  vx/pin, all discrepancies concerning dose, fluence and LET are below 1.5% for  $Z \leq 6$ . When the results for a resolution of  $127 \times 127 \times 121$  vx/pin are compared to the highest resolution tested ( $160 \times 160 \times 152$  vx/pin), even smaller deviations (below 1%) are given. This shows that even a resolution higher than  $160 \times 160 \times 152$  vx/pin would not change the result significantly.



**Figure 10.** FLUKA simulation result: Distribution of dose and fluence in depth for a 278 MeV/u  $^{12}\text{C}$ -beam for the calorimeter setup.  $z$  is given as geometrical depth, as it is defined in the FLUKA geometry (figure 4).

**Table 4.** Mean values for percentage of fluence and dose, and track-weighted LET per particle type at the measurement position for the 2DRM-modulated SOBP and for the active scanned SOBP in parentheses.

$Z$	$N_i / \sum N_i / \%$	$D_i / D_{all} / \%$	$\overline{LET} / \text{keV}/\mu\text{m}$
1	44.77 (47.66)	4.08 (4.49)	0.98 (1.00)
2	20.55 (19.37)	5.77 (5.72)	3.01 (3.12)
3	1.98 (1.83)	1.18 (1.16)	6.41 (6.68)
4	1.10 (1.00)	1.32 (1.22)	12.52 (12.90)
5	2.48 (2.07)	4.57 (3.91)	19.85 (19.96)
6	28.98 (27.97)	82.97 (83.39)	30.81 (31.56)
rest		0.11 (0.13)	

As the result changes only slightly between a resolution of  $127 \times 127 \times 121$  vx/pin and  $160 \times 160 \times 152$  vx/pin, while the computational time dramatically increases, we decided to use a pin resolution of  $127 \times 127 \times 121$  vx/pin for the simulation to obtain particle spectra for the whole calorimeter setup. The resulting absorbed dose to matter and fluence particle spectra are shown in figure 10. The dose distribution shows two very significant drops that appear at the calorimetric detector's glass walls. They can be explained by a difference in the mass stopping power of glass compared to water. They will be taken into account when performing heat transport calculations to correct for heat conduction effects in the upcoming calorimetric measurements as described in Krauss (2006).

The dose, fluence and LET per particle type at the measurement position ( $96.7 \text{ mm} \leq z \leq 96.8 \text{ mm}$  in figure 10) are given in table 4. For most of the particles at the measurement position,  $Z = 1$  (protons, deuterons and tritons); only 30% of the fluence is carbon ions. Nevertheless, due to the difference in LET, the dose is mainly deposited by carbon ions (83%), whereas particles with  $Z = 1$  only provide 4% of the total dose. Helium ions ( $Z = 2$ ) make up 20% of the fluence, but only 6% of the dose. The percentage of lithium ( $Z = 3$ ), beryllium ( $Z = 4$ ), and boron ( $Z = 5$ ) within the spectrum is below 2.5% each, together making up about 7% of the dose. Target fragments with  $Z > 6$  are only 0.1% of the delivered dose.

We compared the results of this simulation setup with a simulation in which the SOBP is created by irradiating layers of different energies (i.e. by means of active scanning). The simulation showed only slight differences in the particle spectra of the actively scanned SOBP compared to the 2DRM-SOBP. The percentage of fluence for particles with  $Z = 1$  was 3% higher; for the other particles, it was between 0.2% and 1.2% lower for the actively scanned SOBP; particles with  $Z = 1$  and  $Z = 6$  contributed 0.4% more to the total dose for the actively scanned SOBP. The maximum difference in LET was about 3%. The values for percentage of dose and fluence and for LET per particle type at the measurement position for the active scanned SOBP are given in parentheses in table 4.

## 4. Conclusion

The objective of this study was to develop and optimize an irradiation technique for water calorimetry in a SOBP for scanned carbon-ion beams, resulting in irradiation field parameters fulfilling certain requirements. To this end, we investigated the applicability of a 2D range modulator produced using rapid prototyping with a 3D printer. The 2DRM is very well suited to passively create a  $^{12}\text{C}$ -SOBP for time-critical applications. A 1.5 Gy dose cube of  $6 \times 6 \times 6 \text{ cm}^3$  was produced within 90 s. A relative standard deviation of  $\leq 1.1\%$  for the measured values of the 3D dose distribution with a maximum distance of 20 mm from the calorimetric



measurement position was achieved. A deviation of 0.26% of these values for repeated measurements over a period of 10 weeks was found, which shows that the relative dose distribution is stable over time.

Even for the identical design, the two versions of the 2DRM tested showed slight differences due to the limitation of the printing accuracy of the fine structures. It was therefore necessary to characterize each 2DRM individually.

The very low deviation in the simulated particle spectra for the passively modulated 2DRM-SOBP and an actively scanned SOBPs gives a good rationale for also transferring the results concerning new  $k_{Q,Q_0}$  factors to irradiation fields created by active scanning. The next step will be to perform the calorimetric measurements under the given field parameters to determine experimental  $k_{Q,Q_0}$  factors in the passively realized SOBPs of a  $^{12}\text{C}$  beam.

## Acknowledgments

We are grateful to Stephan Brons and his colleagues from HIT for their help with technical issues during the irradiations. We would like to thank the PTB mechanical workshop for building the Octavius water phantom setup and Andreas Schlesner for processing the software for the linear drive.

## ORCID iD

Oliver Jäkel  <https://orcid.org/0000-0002-6056-9747>

## References

- Amaldi U and Kraft G 2005 Radiotherapy with beams of carbon ions *Rep. Prog. Phys.* **68** 1861
- Andreo P 1992 Absorbed dose beam quality factors for the dosimetry of high-energy photon beams *Phys. Med. Biol.* **37** 2189
- Andreo P, Burns D, Hohlfeld K, Saiful Huq M, Kanai T, Laitano F, Smyth V, and Vynckier S 2006 *Absorbed Dose Determination in External Beam Radiotherapy: an International Code of Practice for Dosimetry Based on Standards of Absorbed Dose to Water (IAEA TRS-398, V.12)* (Vienna: International Atomic Energy Agency)
- Bauer D 2018 Study of the Octavius ionization chamber array as a film replacement for clinical ion beam quality assurance *Master's thesis* Department of Physics, University of Heidelberg
- Castriconi R *et al* 2017 Dose-response of EBT3 radiochromic films to proton and carbon ion clinical beams *Phys. Med. Biol.* **62** 377
- DIN-Normenausschuss Radiologie (NAR) 2019 Dosismessverfahren nach der Sondenmethode für Protonen- und Ionenstrahlung- Teil 1: Ionisationskammern *DIN 6801-1: 2019-09*
- Ferrari A, Sala P R, Fasso A, and Ranft J 2014 Fluka: a multi-particle transport code (Program version)
- Freiburg PTW Particle Therapy QA Tools <https://www.ptwdosimetry.com/en/products/peakfinder/> (Accessed: 8 August 2019)
- Freiburg PTW Octavius 1000 SRS [www.ptw.de/2287.html](http://www.ptw.de/2287.html) (Accessed: 4 April 2019)
- Haberer T, Becher W, Schardt D and Kraft G 1993 Magnetic scanning system for heavy ion therapy *Nucl. Instrum. Methods Phys. Res. A* **330** 296
- Haberer T, Debus J, Eickoff H, Jäkel O, Schulz-Ertner D and Weber U 2004 The Heidelberg ion therapy center *Radiother. Oncol.* **73** S186
- Jäkel O, Hartmann G H, Karger C P, Heeg P and Rassow J 2000 Quality assurance for a treatment planning system in scanned ion beam therapy *Med. Phys.* **27** 1588
- Kamada T *et al* 2015 Carbon ion radiotherapy in Japan: an assessment of 20 years of clinical experience *Lancet Oncol.* **16** e93
- Karger C, Jäkel O, Palmans H and Kanai T 2010 Dosimetry for ion beam radiotherapy *Phys. Med. Biol.* **55** R193
- Kostjuchenko V, Nichiporov D and Luckjashin V 2001 A compact ridge filter for spread out Bragg peak production in pulsed proton clinical beams *Med. Phys.* **28** 1427
- Krauss A 2006 The PTB water calorimeter for the absolute determination of absorbed dose to water in  $^{60}\text{Co}$  radiation *Metrologia* **43** 259
- Krauss A 2006 Heat conduction effects during the calorimetric determination of absorbed dose to water in radiotherapy beams *Thermo. Acta* **445** 126
- Krauss A, Buermann L, Kramer H-M and Selbach H-J 2012 Calorimetric determination of the absorbed dose to water for medium-energy x-rays with generating voltages from 70 to 280 kV *Phys. Med. Biol.* **57** 2523
- Krauss A and Kapsch R 2014 Experimental determination of kQ factors for cylindrical ionization chambers in 10 cm × 10 cm and 3 cm × 3 cm photon beams from 4 MV to 25 MV *Phys. Med. Biol.* **59** 2523
- Lodge M, Pijls-Johannesma M, Stirk L, Munro A, De Ruyscher D and Jefferson T 2007 A systematic literature review of the clinical and cost-effectiveness of hadron therapy in cancer *Radiother. Oncol.* **83** 110
- Martíšíková M and Jäkel O 2010 Dosimetric properties of Gafchromic® EBT films in medical carbon ion beams *Phys. Med. Biol.* **55** 5557
- Medin J, Ross C K, Klassen N V, Palmans H, Grusell E and Grindborg J-E 2006 Experimental determination of beam quality factors, kQ, for two types of Farmer chamber in a 10 MV photon and a 175 MeV proton beam *Phys. Med. Biol.* **51** 1503
- Micke A, Lewis D and Yu X 2011 Multichannel film dosimetry with nonuniformity correction *Med. Phys.* **38** 523
- Mitch M, DeWerd L, Minniti R and Williamson J 2009 Treatment of Uncertainties in Radiation Dosimetry *Clinical Dosimetry Measurements in Radiotherapy (Aapm)* Chapter 22 p 737
- Osinga-Blättermann J-M, Brons S, Greilich S, Jäkel O and Krauss A 2017 Direct determination of kQ for Farmer-type ionization chambers in a clinical scanned carbon ion beam using water calorimetry *Phys. Med. Biol.* **62** 2033
- Osinga-Blättermann J-M and Krauss A 2018 Determination of kQ factors for cylindrical and plane-parallel ionization chambers in a scanned carbon ion beam by means of cross calibration *Phys. Med. Biol.* **64** 015009
- Palmans H *et al* 2002 Absorbed dose to water based dosimetry versus air kerma based dosimetry for high-energy photon beams: an experimental study *Phys. Med. Biol.* **47** 421
- Sassowsky M and Pedroni E 2005 On the feasibility of water calorimetry with scanned proton radiation *Med. Phys. Biol.* **50** 5381

- Schuy C, Simeonov Y, Zink K, Durante M and Weber U 2019 Technical note: Vendor-agnostic water phantom for 3D dosimetry of complex fields in particle therapy *Med. Phys.* (<https://doi.org/10.1002/acm2.12996>)
- Simeonov Y, Weber U, Penchev P, Ringbaek T, Schuy C, Brons S, Engenhardt-Cabillic R, Bliedtner J and Zink K 2017 3D range-modulator for scanned particle therapy: development, Monte Carlo simulations and experimental evaluation *Phys. Med. Biol.* **62** 7075
- Tommasino F *et al* 2019 A new facility for proton radiobiology at the Trento proton therapy centre: design and implementation *Phys. Medica* **58** 99
- Van Dyk J, Battista J and Baumann G 2013 Accuracy and uncertainty considerations in modern radiation oncology *The Modern Technology of Radiation Oncology* Chapter 11, vol 3 (Madison, WI: Medical Physics Publishing) p 378
- Westerdiep A Online Voxelizer <http://drububu.com/miscellaneous/voxelizer/> (Accessed: 7 August 2019)

## **APPENDIX**

### **Verzeichnis der akademischen Lehrenden**

#### **In Marburg:**

Rita Engenhardt-Cabillic

#### **An der GSI:**

Uli Weber

#### **In Gießen:**

Joachim Breckow

Franz Cemic

Vera Dammann

Martin Fiebich

Bernd Heimrich

Ulrich Kirschbaum

Rudolf Kleinöder

Jürgen Koch

Klaus-Jürgen Kügler

Horst Prehn

Albert Schneider

Hans-Martin Seipp

Jörg Subke

Werner Trampisch

Klemens Zink

## **Danksagung**

An dieser Stelle möchte ich mich bei meinen Betreuern Prof. Dr. Klemens Zink und Prof. Dr. Rita Engenhardt-Cabillic bedanken, die diese Arbeit ermöglicht haben und mich richtungsweisend und mit viel Engagement begleitet haben.

Ein ganz besonderer Dank geht an Prof. Dr. Klemens Zink und Prof. Dr. Uli Weber für ihre exzellente Kompetenz und sehr gute Betreuung dieser, aber auch früherer Arbeiten. Sie haben mir nicht nur fachlich, sondern auch menschlich viel beigebracht und hatten immer ein offenes Ohr. Die spannenden Nachtmessungen an den Partikeltherapieanlagen, die ich mit Prof. Dr. Klemens Zink, Prof. Dr. Uli Weber und Dr. Christoph Schuy durchgeführt habe und die kompromisslose submillimeter-genaue Ausrichtung und Fixierung der Modulatoren und Detektoren werden unvergesslich bleiben.

Die originelle Idee für die Entwicklung und 3D Druck von 3D Modulatoren habe ich Prof. Dr. Uli Weber zu verdanken.

Des Weiteren möchte ich mich bei meinem Kollegen, Co-Autor und sehr guten Freund M.Sc. Petar Penchev bedanken: für die programmiertechnische Unterstützung, die innovativen Ideen bei schwierigen Problemen und die anregenden Diskussionen bis in die späten Abendstunden.

Meinen herzlichen Dank geht an meinen ehemaligen Kollegen und heutigen Freunden Toke Printz Ringbæk, Alina Santiago und Gheorghe Iancu, die mir vor vielen Jahren den Einstieg in die Forschungswelt erleichtert haben und im Rückblick betrachtet auf eine fast schicksalhafte Weise kleine Puzzleteile ergänzt haben, ohne die diese Arbeit nicht zustande gekommen wäre.

Ich möchte mich auch bei Dr. Christina Zinecker bedanken, die nicht nur die 3D-Druck Forschung an der THM vorangetrieben hat, sondern auch als sehr kompetenter Ansprechpartner einen wichtigen Beitrag bei der Antragstellung und Finanzierung von Projekten geleistet hat.

Mein Dank gilt auch allen Kollegen des Instituts für Medizinische Physik und Strahlenschutz (IMPS) für die wertvollen Kommentare und Anregungen.

Ich bedanke mich auch für die finanzielle Unterstützung durch den Strategischen Forschungsfonds der THM, die mir einige Konferenzteilnahmen ermöglicht hat.